Micro Structured Sensors for Neutron Detection

D. S. McGregor
Kansas State University, mcgregor@ksu.edu

S. L. Bellinger
Radiation Detection Technologies, Inc

J. C. Boyington
Kansas State University

Y. Cheng
Kansas State University

R. G. Fronk
Idaho National Laboratory

See next page for additional authors

Presenter Information

D. S. McGregor, S. L. Bellinger, J. C. Boyington, Y. Cheng, R. G. Fronk, W. Fu, L. C. Henson, J. D. Hewitt, C. W. Hilger, R. M. Hutchins, K. E. Kellogg, J. A. Medina, D. M. Nichols, T. R. Ochs, M. A. Reichenberger, J. A. Roberts, S. R. Stevenson, T. M. Swope, and T. C. Unruh

College of Engineering
Mechanical and Nuclear Engineering

Microstructured Sensors for Neutron Detection

Douglas S. McGregor[1], Steven L. Bellinger[4], J.C. Boyington[1], Anthony Caruso[6],Y. Cheng[2], Ryan G. Fronk[5], Wenkai Fu[2], Luke C. Henson[4], David Huddleston[3], Robyn M. Hutchins[1], Daniel Nichols[1], Taylor R. Ochs[1], Michael Reichenberger[5], Jeremy A. Roberts[2], J. Kenneth Shultis[1], Tim Sobering[3], Sarah Stevenson[1], T.M. Swope[1], Russell Taylor[3], Troy Unruh[5]

[1]Semiconductor Materials and Radiological Technologies Laboratory (SMART) Laboratory
Department of Mechanical and Nuclear Engineering, Kansas State University
Manhattan, KS 66506

[2]CORPS, Department of Mechanical and Nuclear Engineering, Kansas State University
Manhattan, KS 66506

[3]Electronics Design Laboratory, Kansas State University
Manhattan, KS 66506

[4]Radiation Detection Technologies, Inc.
Manhattan, KS 66502

[5]Idaho National Laboratory, Idaho Falls, Idaho 83415

[6]Dept. of Physics, University of Missouri – Kansas City
Kansas City, MO 64110

KANSAS STATE UNIVERSITY

Semiconductor Materials And Radiological Technologies

Two alternative neutron reactions popular for thermal neutron detection are the $^{10}B(n,\alpha)^{7}Li$ reaction and the $^{6}Li(n,t)^{4}He$ reaction.

σ_{th} = 3840 barns

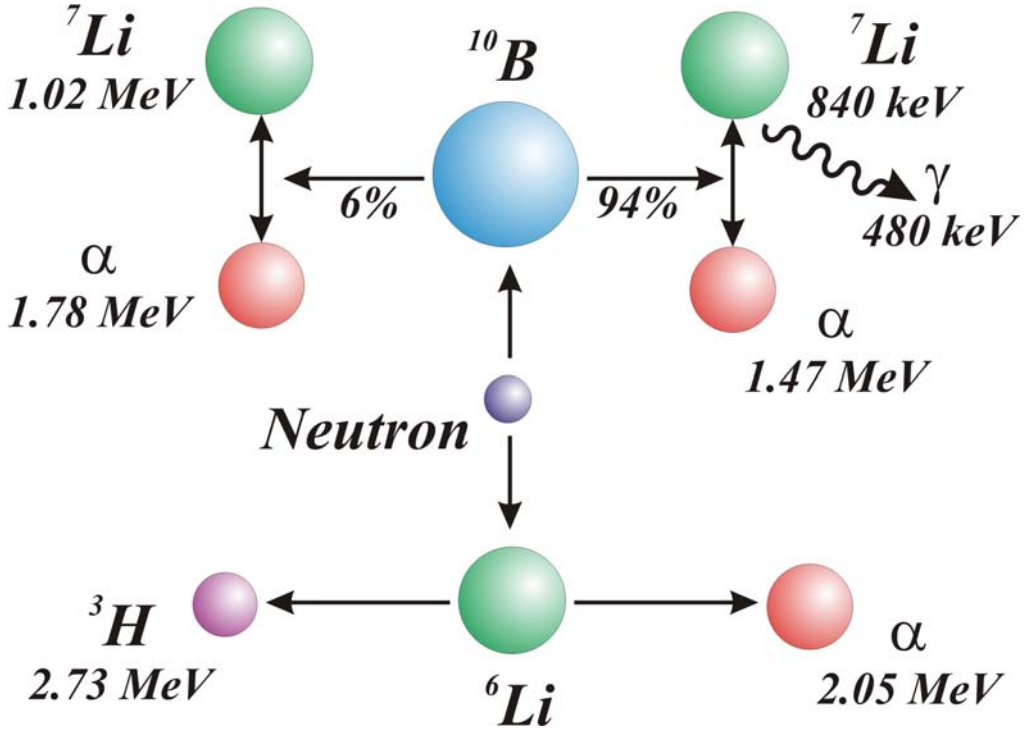

σ_{th} = 940 barns

Neutron Absorption Cross Sections - 1/v

$$\sigma_\gamma(E_c) = \pi\lambda_1^2 g\left(\frac{E_1}{E_c}\right)^{1/2} \frac{\Gamma_n\Gamma_\gamma}{(E_c - E_1)^2 + \Gamma^2/4} \cong \frac{K}{v_c}$$

Radiative capture (Breit-Wigner)

$$\sigma_{a,b} = \left(\frac{E_b}{E_a}\right)^{1/2} H(E_a) \cong \frac{K}{v_a};\ \text{for reaction } X(a,b)Y$$

Charged particle capture

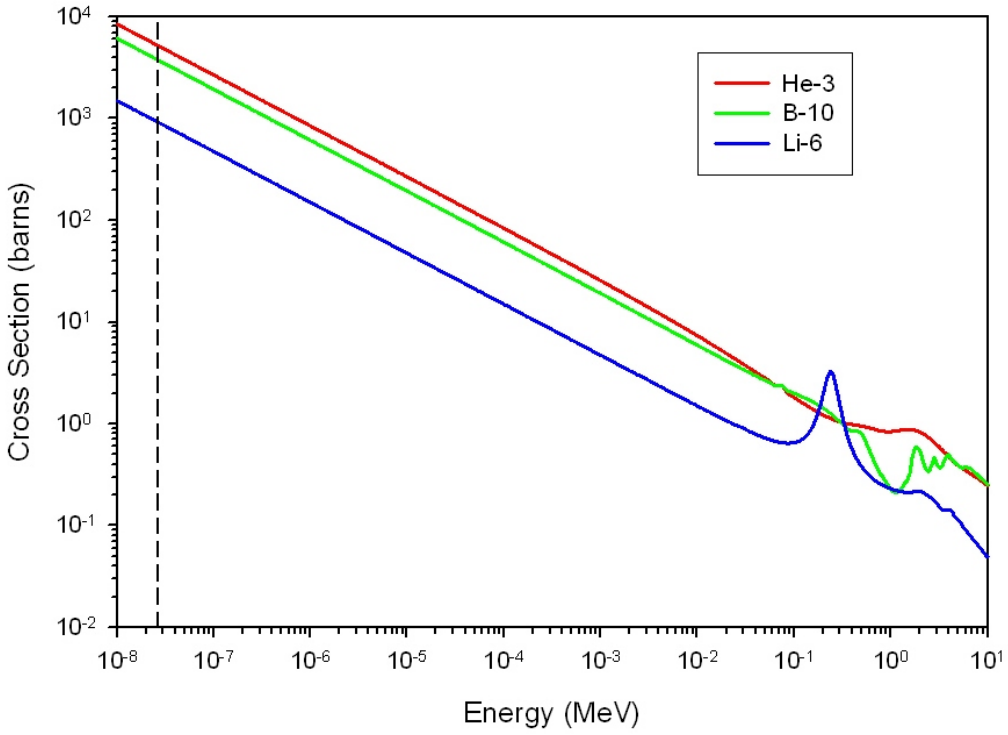

Thin-Film-Coated Device Concept: Ranges and Energy Deposition

Bragg Ionization Curves in Boron

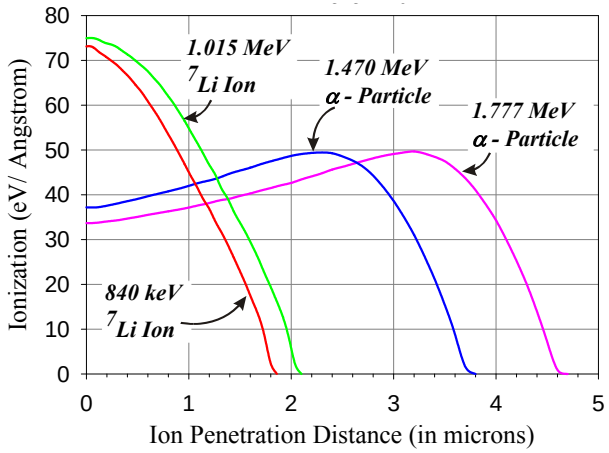

Bragg Ionization Curves in LiF

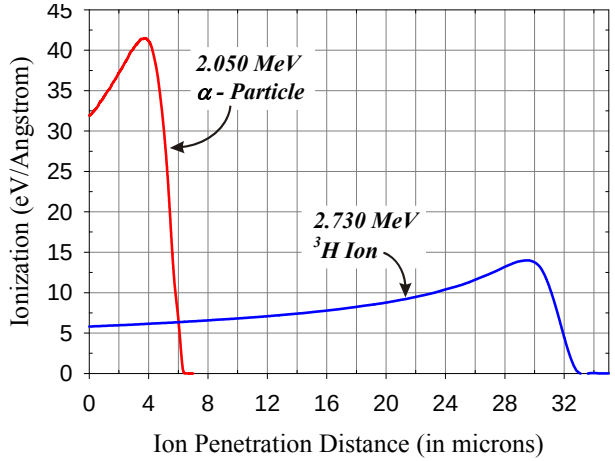

Residual Energy in Boron

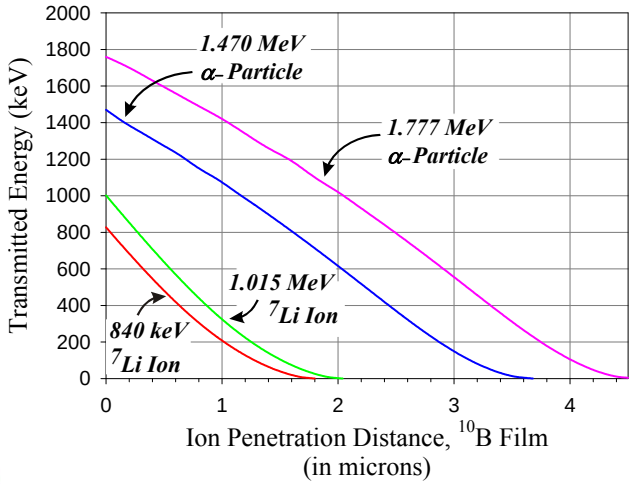

Residual Energy in LiF

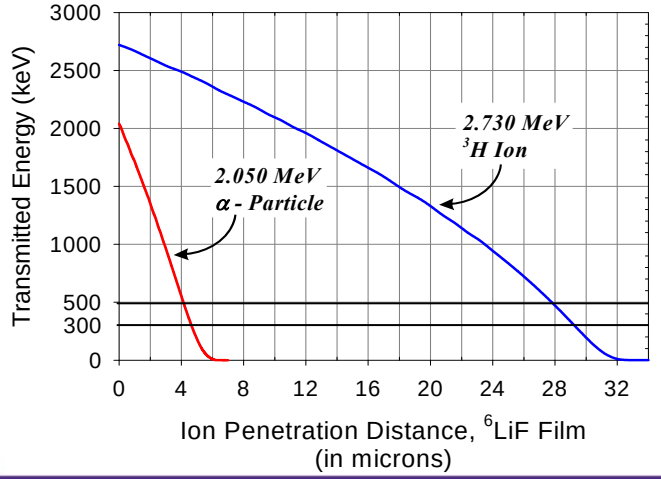

D.S. McGregor, M.D. Hammig, H.K. Gersch, Y-H. Yang, and R.T. Klann, Nuclear Instrum. and Meth., A500 (2003) p. 272.

Coated Neutron Detectors

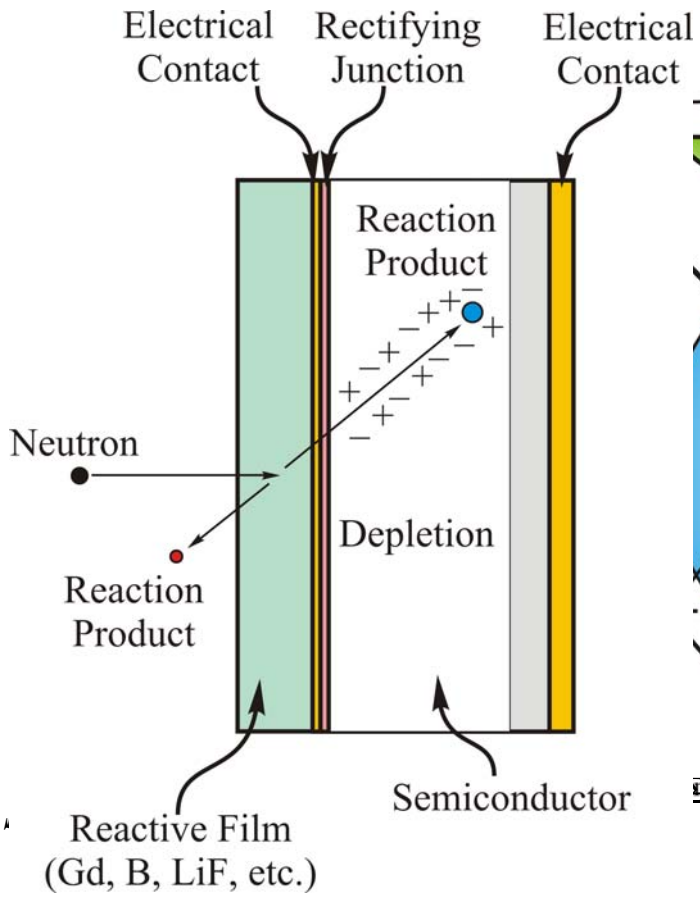

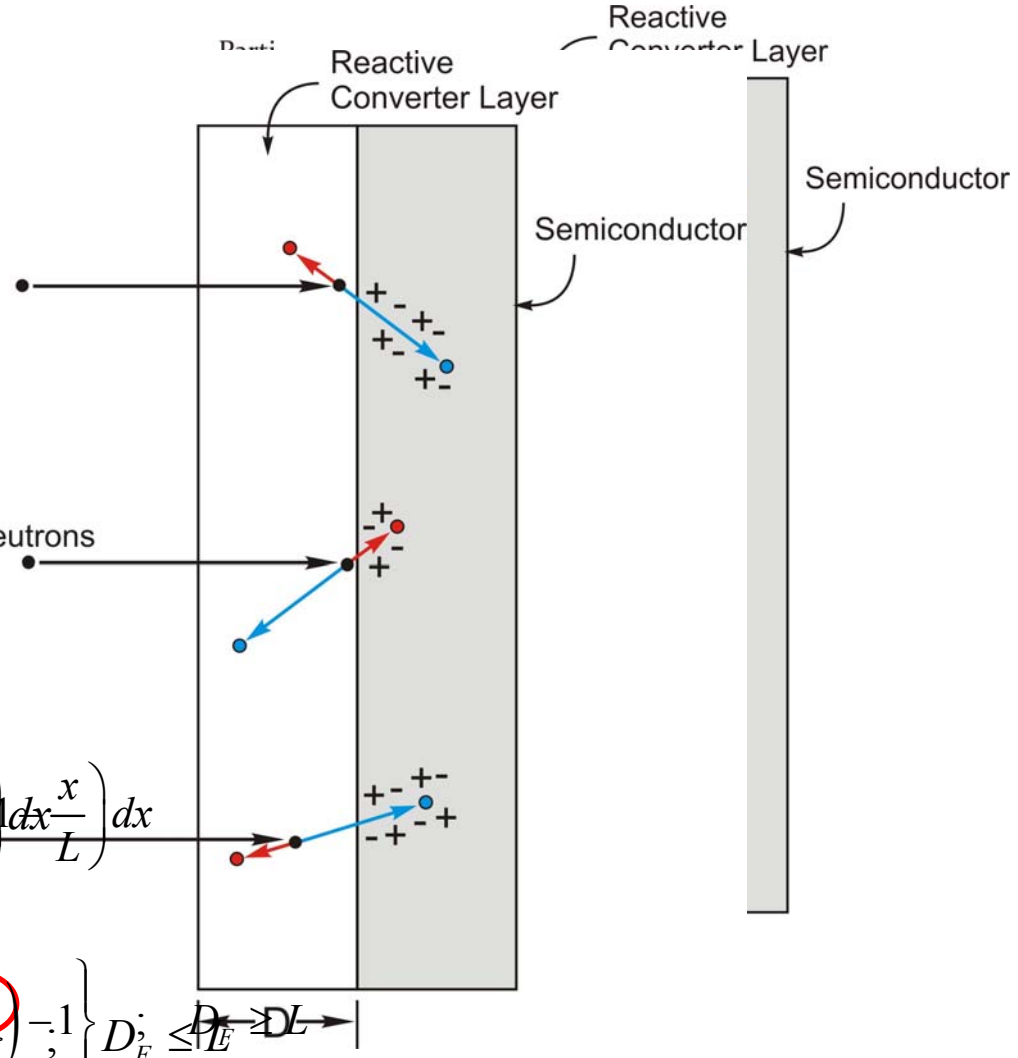

$$\int_0^{D_F} \left(1 - \frac{x}{L}\right) dx$$

$$= 0.5 F_p e^{-\left\{\left(1 + \frac{\Sigma_F (D_F + L)}{\Sigma_F L}\right)\left(\left(1 + \frac{1}{\Sigma_F L}\right)\left(1 - e^{-\frac{D_F}{L}}\right) - 1\right)\right\}}; \quad D_F \le L$$

D.S. McGregor, M.D. Hammig, H.K. Gersch, Y-H. Yang, and R.T. Klann, Nuclear Instrum. and Meth., A500 (2003) p. 272.

Thin-Film-Coated Device Concept

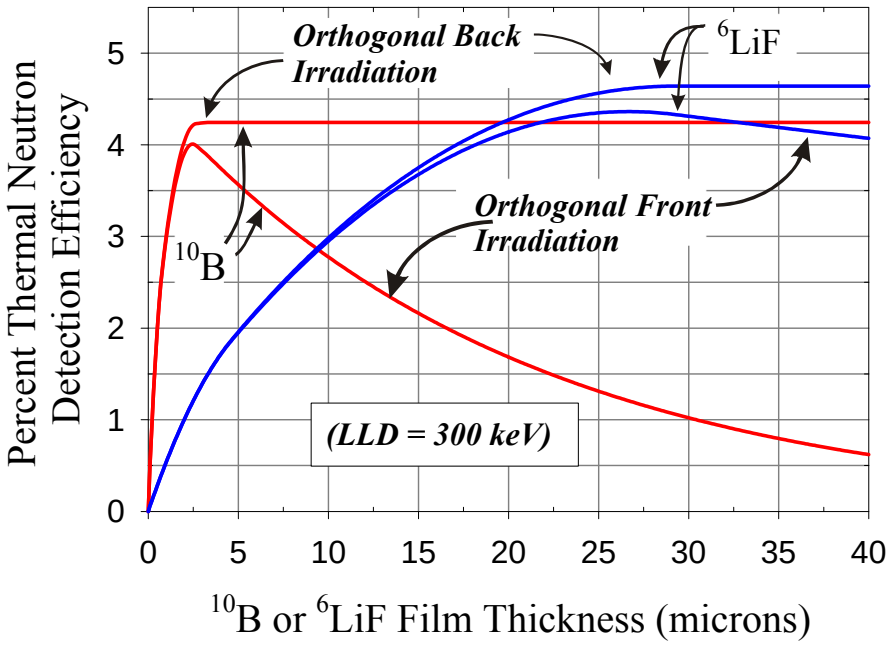

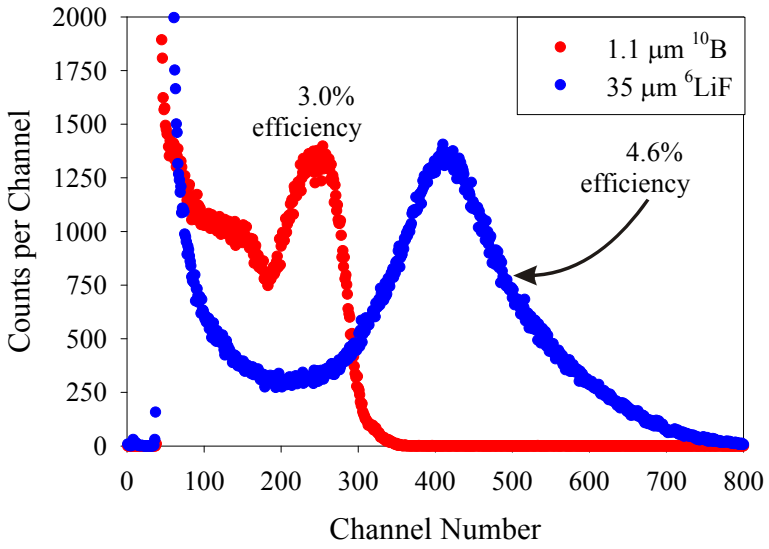

With the *LLD* set at 300 keV equivalent, maximum efficiencies range from 4% to 4.6% depending on the film and the irradiation direction. Hence, both ^{10}B and ^{6}LiF thin film devices have similar performance.

^{10}B-coated devices require less material for optimum performance.

^{6}LiF-coated devices have improved gamma ray discrimination.

D.S. McGregor, M.D. Hammig, H.K. Gersch, Y-H. Yang, and R.T. Klann, Nuclear Instrum. and Meth., A500 (2003) p. 272.

Basic Microstructure Detector Design

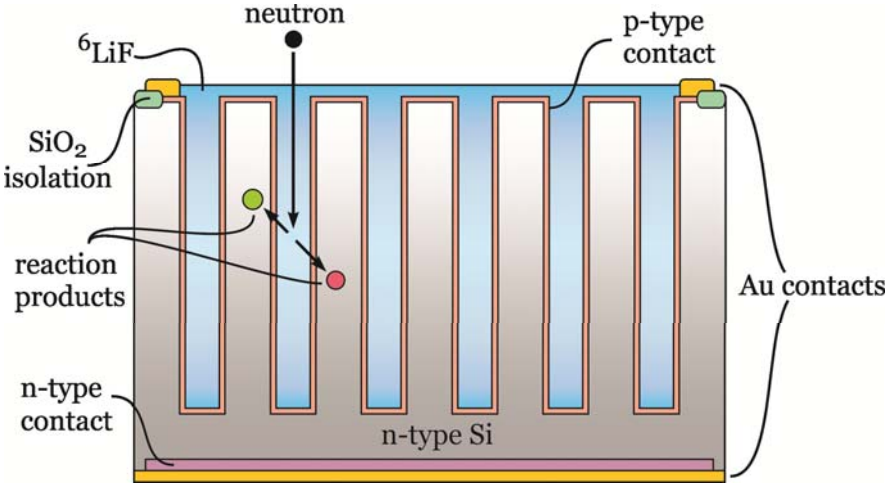

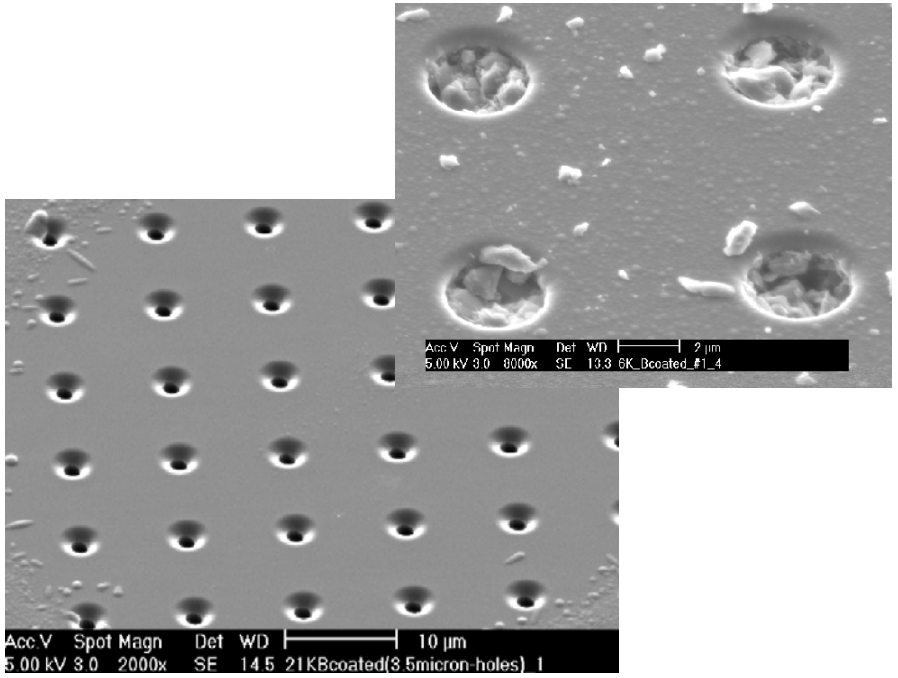

Main Design Considerations:

1. *Neutron reactive backfill materials*
2. *Geometric pattern design*
3. *Substrate material*

3% eff → 3.3% eff

Not much change, but 6σ from average.

D.S. McGregor, R.T. Klann, H.K. Gersch, E. Ariesanti, J.D. Sanders, and B. VanDerElzen, Conf. Rec. of the IEEE Nucl. Sci. Symp., San Diego, California, Nov. 4-9, 2001.

We calculate intrinsic efficiency for a normally incident beam of thermal (2200 m-s^{-1}) neutrons.

Hole

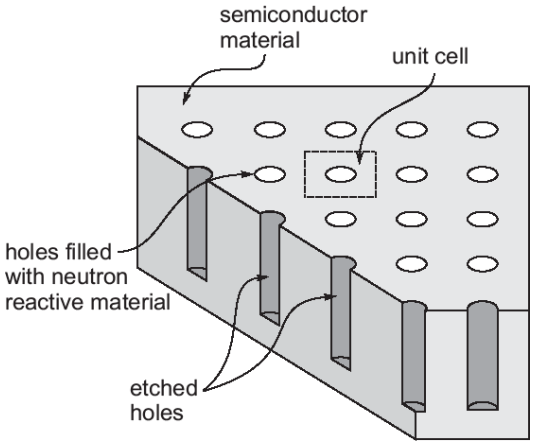

Trench

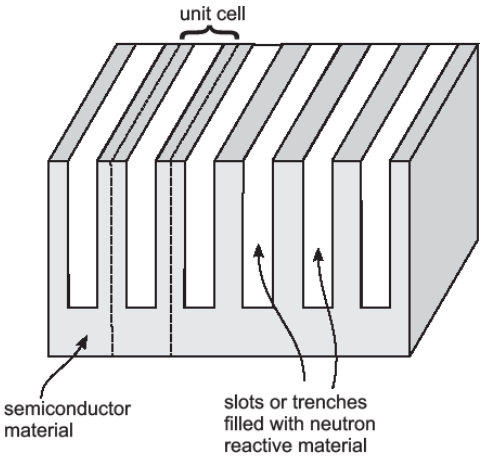

Pillar

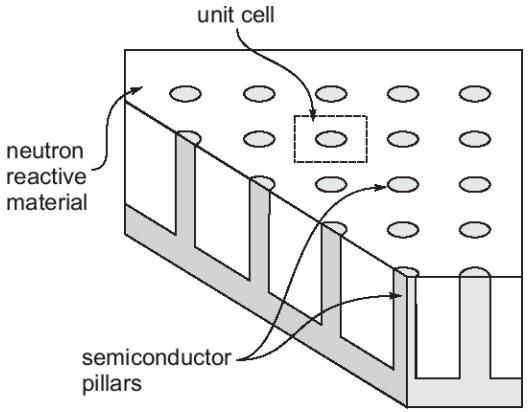

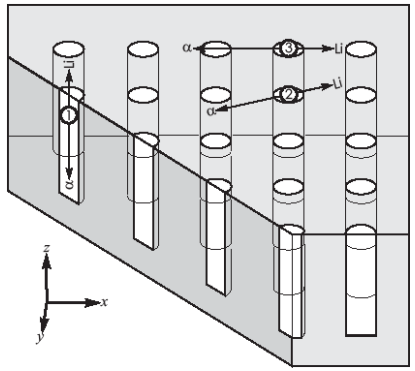

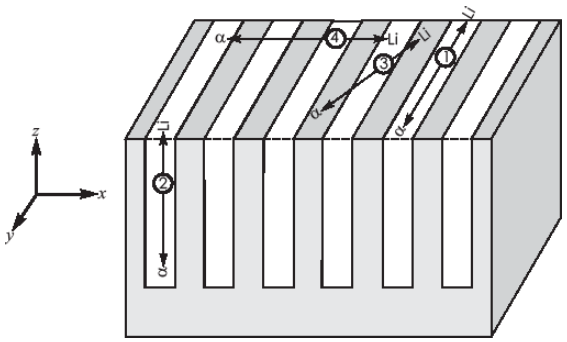

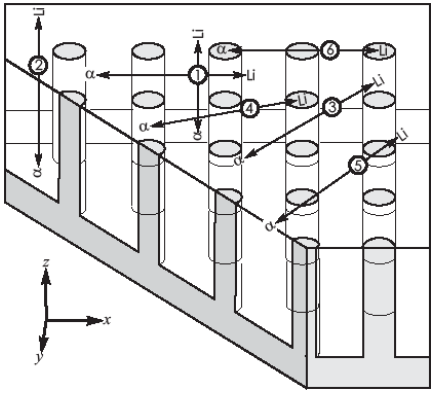

J.K. Shultis and D.S. McGregor, Nuclear Instruments and Methods, A606 (2009) pp. 608-636.

MSND Theoretical Performance
^{6}LiF Backfilled

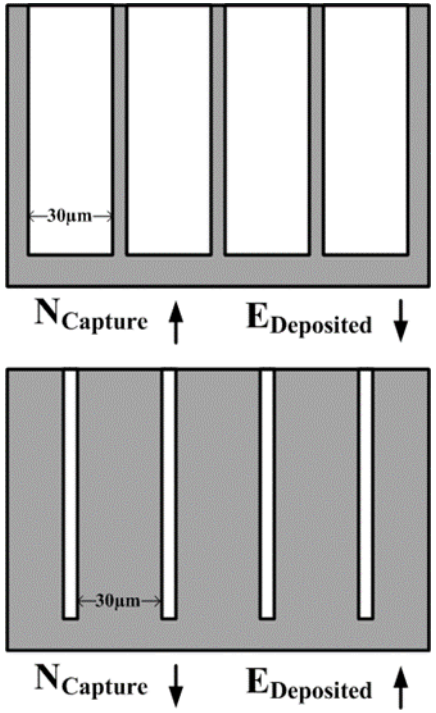

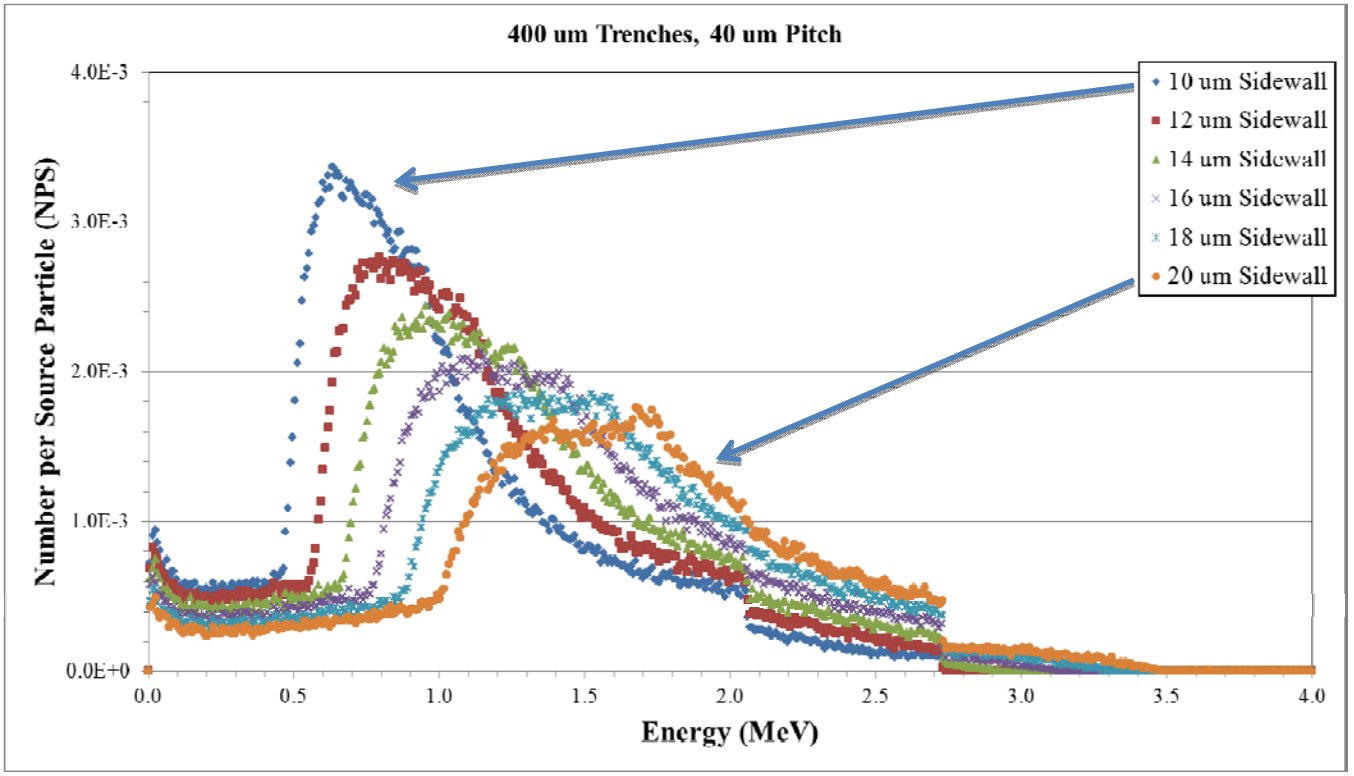

Sidewall Width	10 um	12 um	14 um	16 um	18 um	20 um
Trench Width	30 um	28 um	26 um	24 um	22 um	20 um
Total Eff.	36.33%	35.29%	34.05%	32.61%	30.98%	29.19%
0.3 MeV LLD	34.04%	33.27%	32.27%	31.09%	29.66%	28.07%
0.5 MeV LLD	32.29%	31.94%	31.13%	30.12%	28.82%	27.36%

D.S. McGregor, et al., Rad. Chem. Phys., 116 (2015) pp. 32-37.

MSND Theoretical Performance (LiF-Filled, Cell Dimension = 40 Microns)

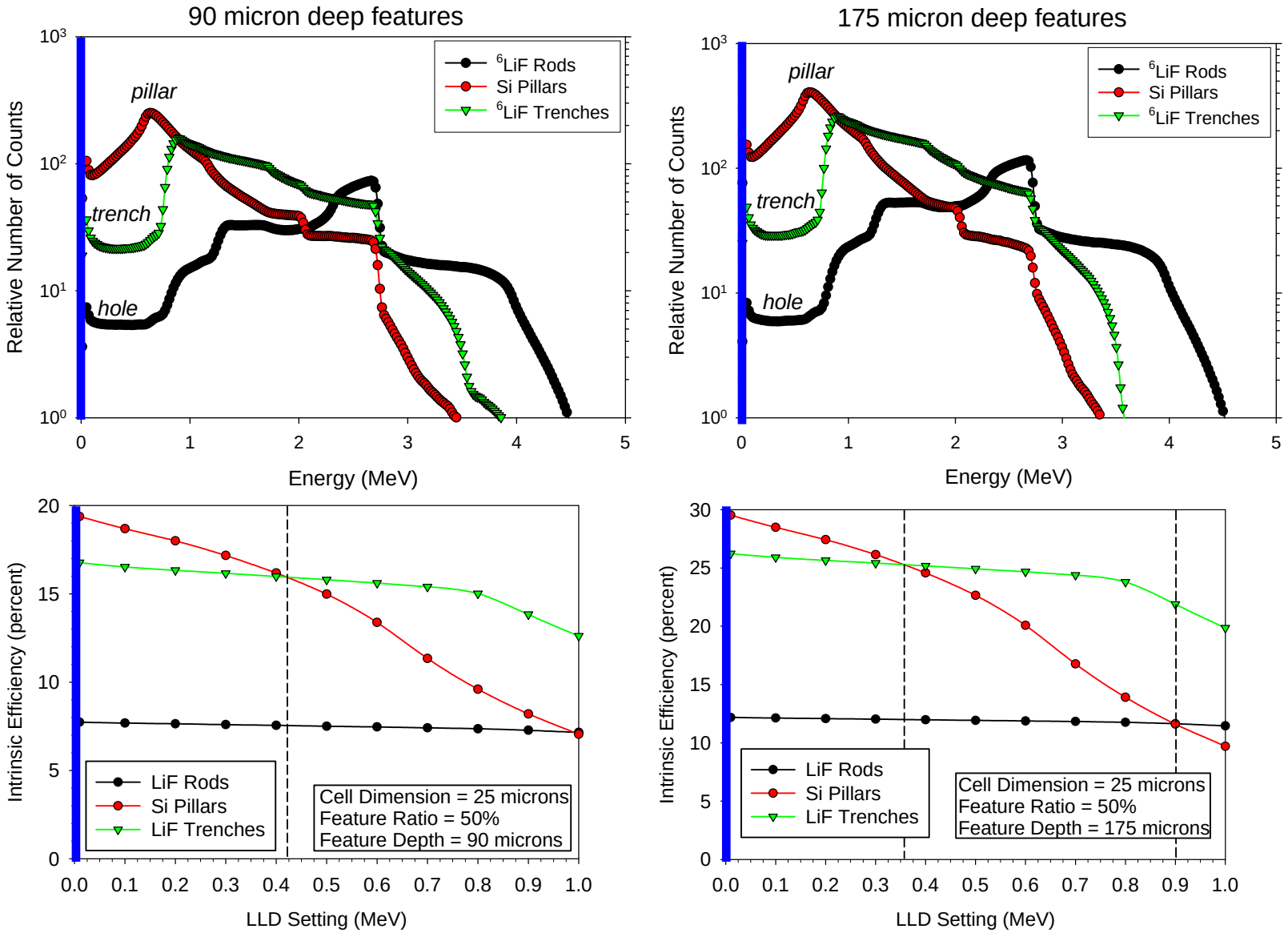

J.K. Shultis, D.S. McGregor, Nucl. Instrum. and Meth. A 606(2009) pp. 608-636.

MSND Device Design

- 52 1-cm^2 active-area, 500-µm thick devices are produced on 4-inch (110)-silicon wafer.
- Up to 50 wafers can be batch-processed.
- Standard VLSI processing techniques
- 1-cm^2 MSNDs mounted in 1.2x1.2x0.2-cm CDBs
- Intrinsic thermal-neutron detection efficiency ~ 30%

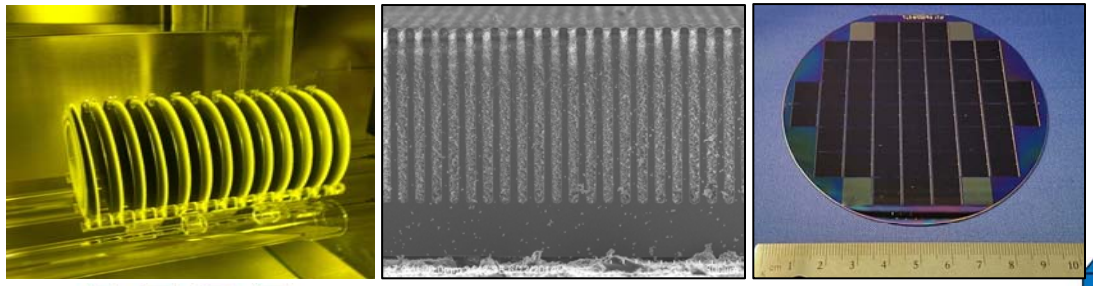

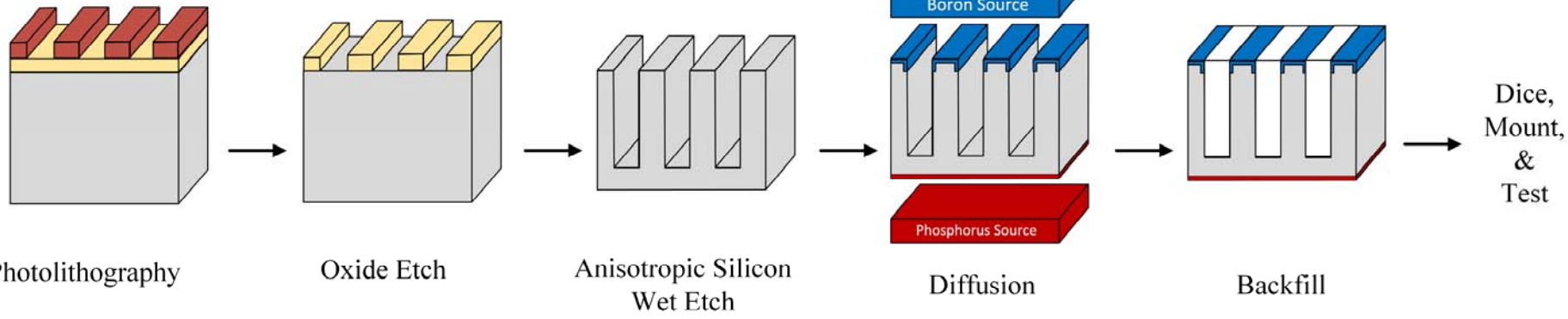

D.S. McGregor, S.L. Bellinger, J.K. Shultis, J. Crys. Growth, 379 (2013) pp. 99-110.

Cavity Backfilling of Microstructured Devices

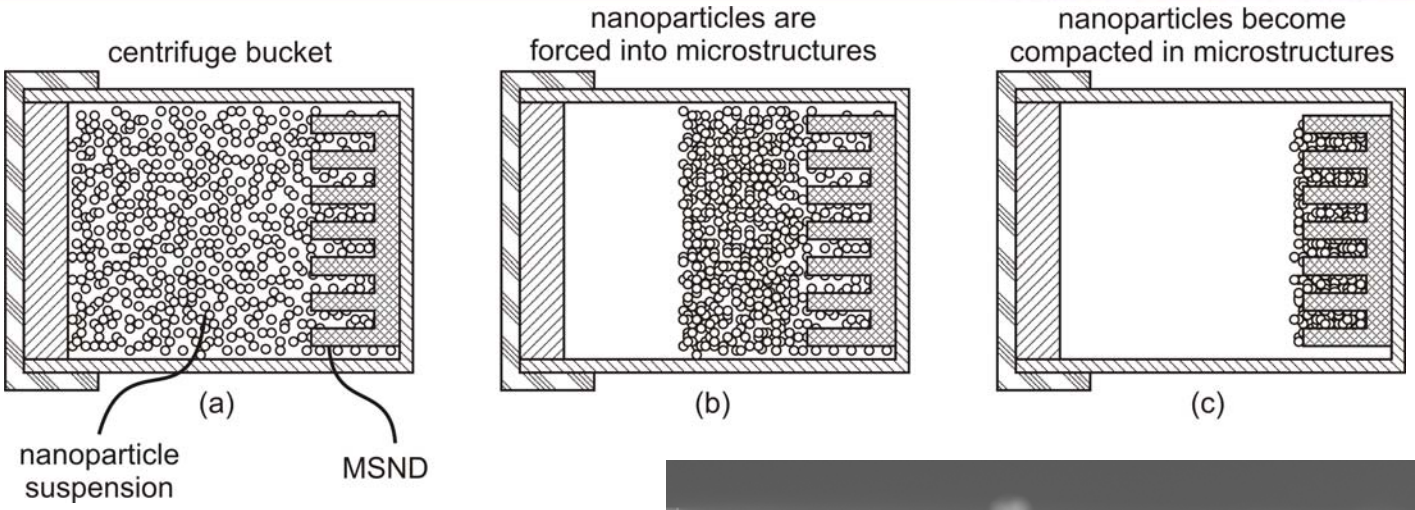

The LiF nanopowder is compacted into the microstructures with a centrifuge.

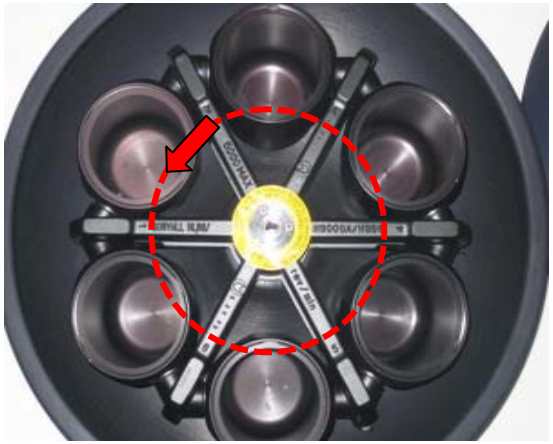

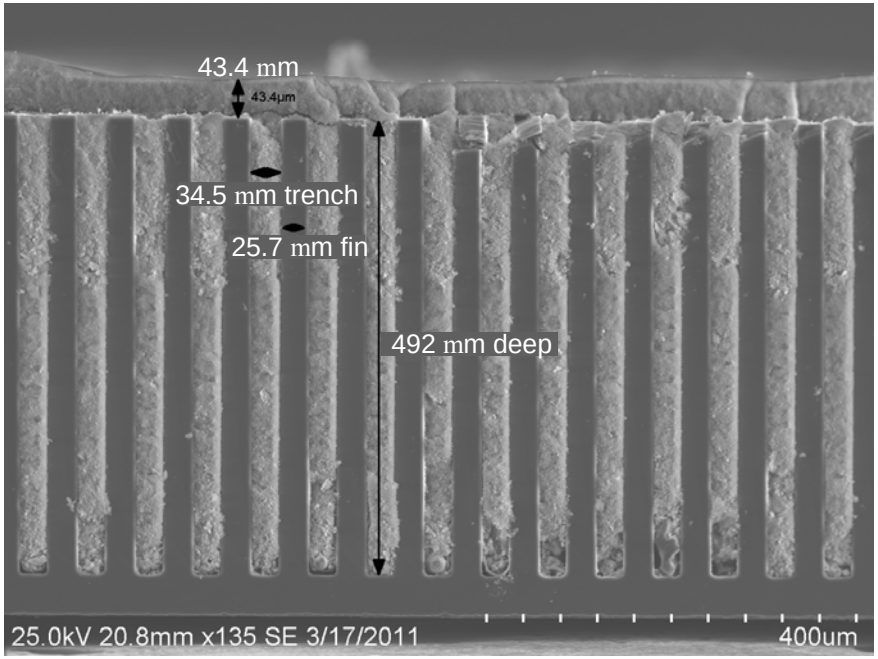

D.S. McGregor, S.L. Bellinger, J.K. Shultis, J. Crys. Growth, 379 (2013) pp. 99-110.

Neutron Efficiency of 4-cm^2 MSND Detector

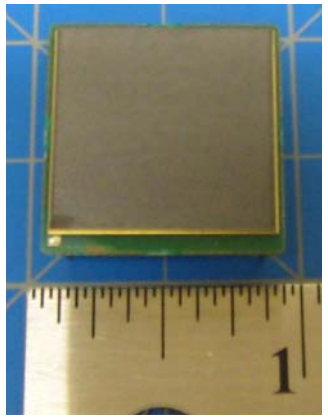

Pulse height spectrum taken with a ^{6}LiF-filled MSND was from a single 4-cm^2 detector.

- The microstructures were **443 microns deep**.
- Intrinsic **thermal** neutron detection efficiency was measured to be:
  - **30.1 ± 0.5%** at a 650 keV LLD (chn 45) with normal beam incidence.
  - **37.6 ± 0.7%** at a 650 keV LLD (chn 45) with 45 deg. beam incidence.

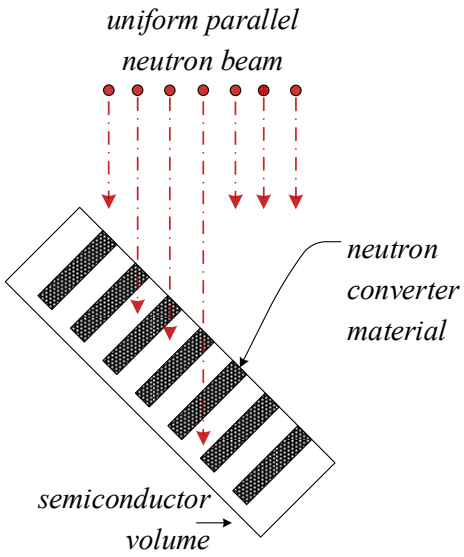

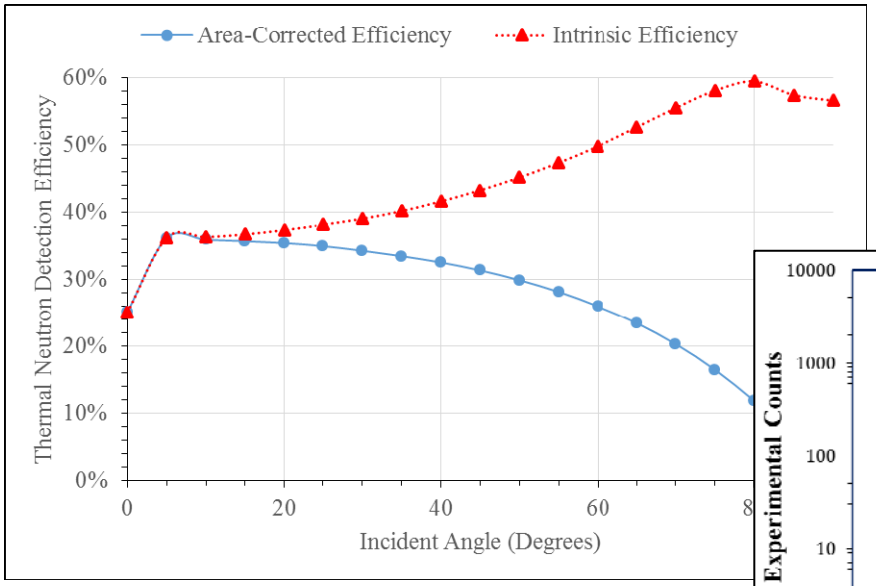

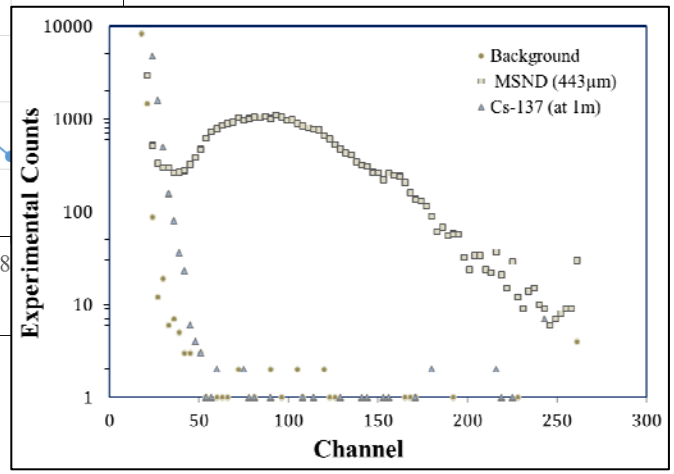

Double-Stacked MSNDs

Double-stacking MSNDs

- Streaming neutrons are incident on conversion material of second MSND.
- Thermal neutron absorption efficiency is improved from 53% to ~93%.
- **42.0±0.25%** intrinsic thermal neutron detection efficiency (300 keV LLD).

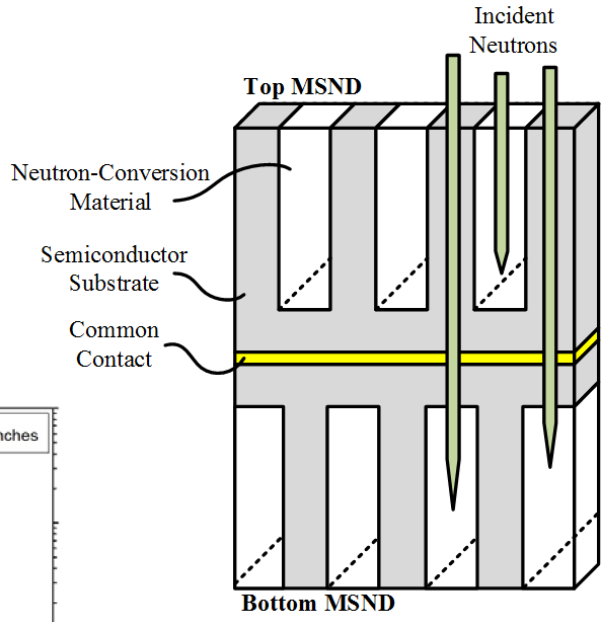

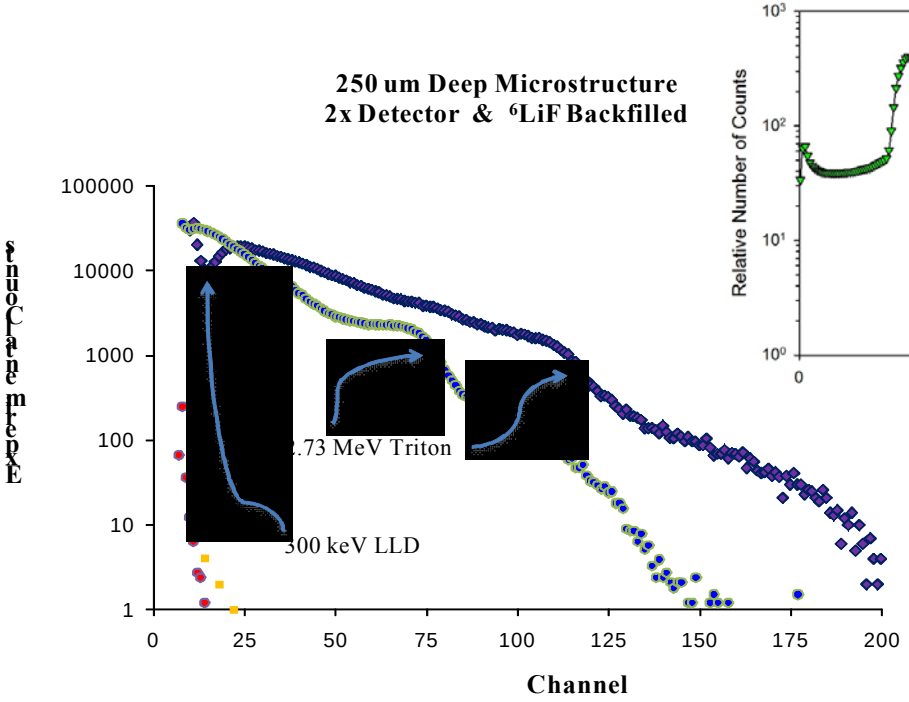

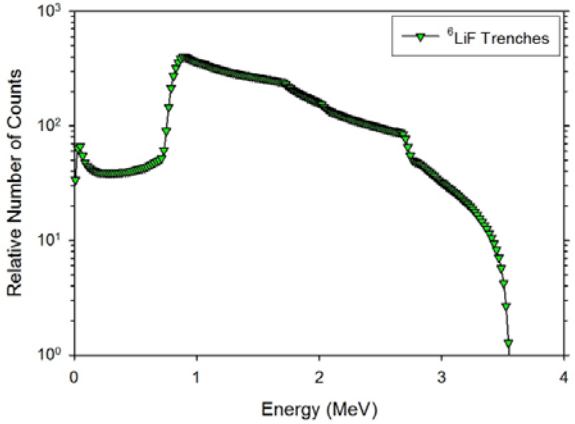

- Difficult to stack (misalignment, off rotationally, etc.).
- Device mismatching causes poor signal integration.
- Double the capacitance.
- Double the leakage current.

S.L. Bellinger, R.G. Fronk, W.J. McNeil, T.J. Sobering, D.S. McGregor, Nucl. Instrum. and Meth. A, 652 (2011) pp. 387-391.

Dual Sided - Microstructured Semiconductor Neutron Detectors (DS-MSND)

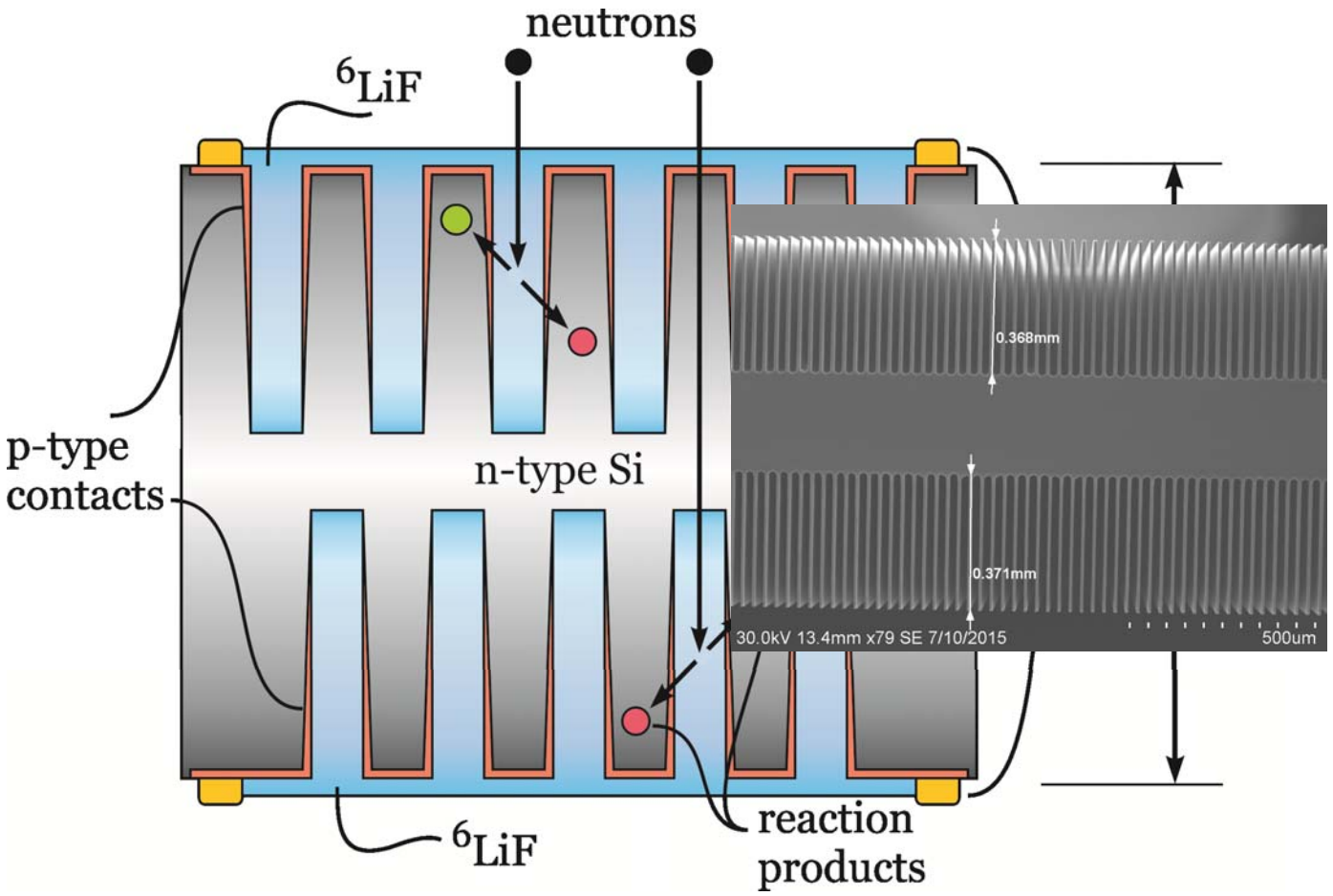

R.G. Fronk, S.L. Bellinger, L.C. Henson, T.R. Ochs, C.T. Smith, J.K. Shultis, D.S. McGregor, Nucl. Instrum. Meth., A804 (2015) pp. 201-206.

Simulation of DSMSND Performance

- Thermal neutron detection efficiency is simulated using MCNP6.
- Pulse-height generation is simulated using TCAD.
- Efficiency is calculated as (LLD = 300 keV):

$$\varepsilon_{th} = \frac{Number\ of\ Neutrons\ 'Counted'}{Number\ of\ Neutrons\ Normally\ Incident\ on\ Detector}$$

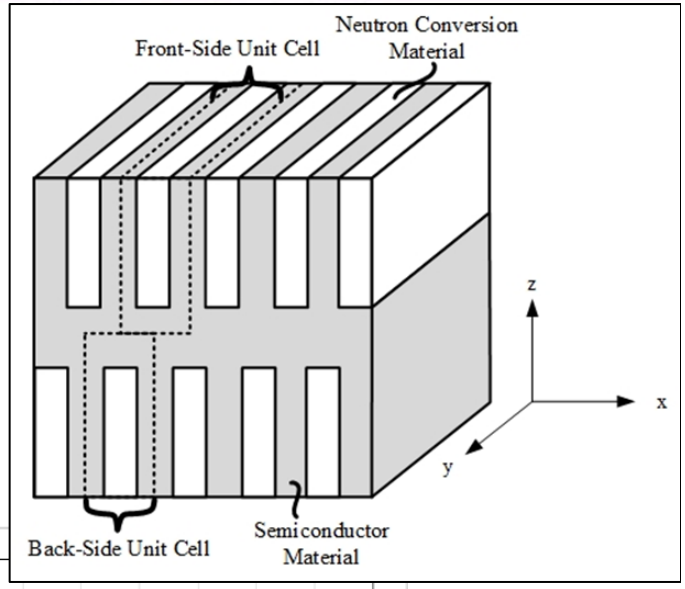

1.0 mm	Trench depth H = 360 um				
T/W_Cell	Cell width W_Cell (um)				
	10	20	30	40	50
0.10	17.0%	16.9%	16.6%	16.3%	16.0%
0.20	33.6%	32.5%	31.5%	30.4%	29.3%
0.30	49.3%	47.1%	44.7%	42.4%	40.1%
0.40	64.6%	60.5%	56.5%	52.4%	48.5%
0.50	79.4%	73.0%	66.7%	60.5%	54.4%
0.60	79.6%	71.4%	63.3%	55.2%	47.2%
0.70	80.2%	70.6%	61.1%	51.5%	42.1%
0.80	76.5%	61.5%	58.1%	47.7%	37.9%
0.90	37.7%	31.4%	29.7%	32.4%	31.3%

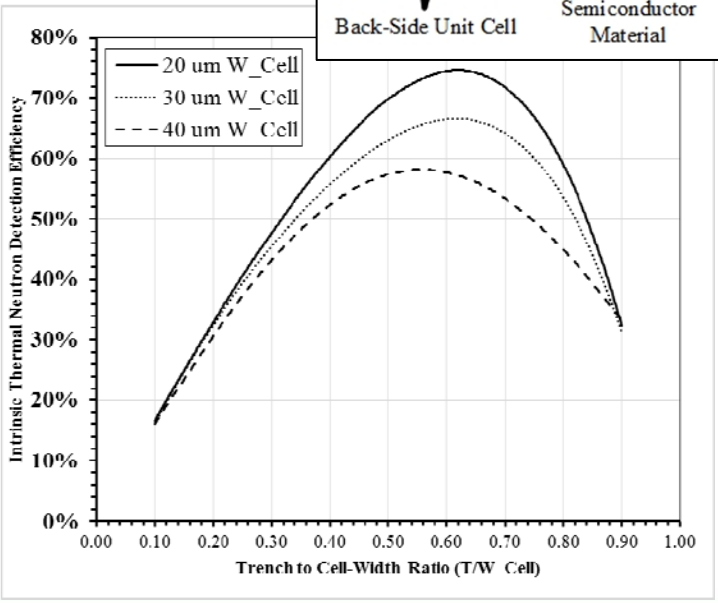

R.G. Fronk, S.L. Bellinger, L.C. Henson, T.R. Ochs, C.T. Smith, J.K. Shultis, D.S. McGregor, Nucl. Instrum. Meth., A804 (2015) pp. 201-206.

Theoretical models indicate that efficiencies greater than 60% can be achieved with a DS-MSND design.

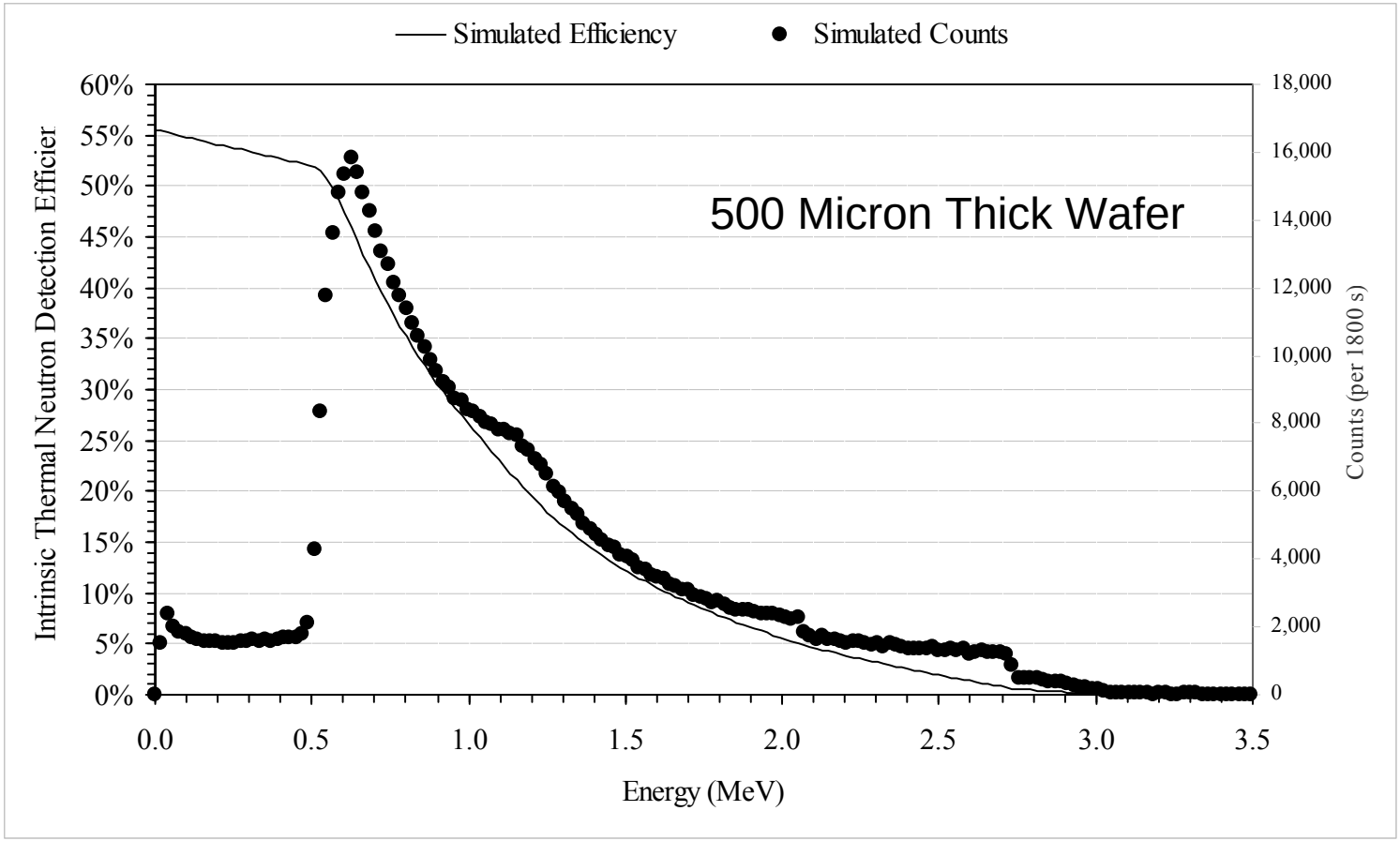

Simulation of DSMSND Performance

- Inside of an instrument, normally-incident detection efficiency is not useful.
- Thermal neutron detection efficiency varies with incident neutron angle.
- Efficiency is calculated as (LLD = 300 keV):

$$\varepsilon_{th} = \frac{Number\ of\ Neutrons\ Counted}{Number\ of\ Neutrons\ Incident\ on\ Detector}$$

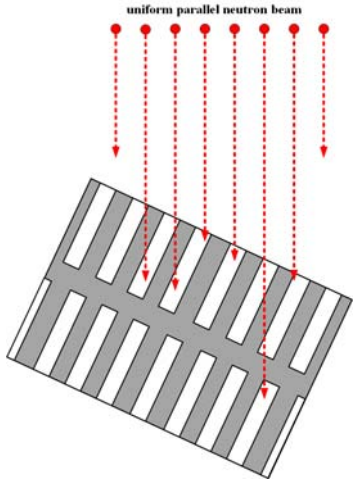

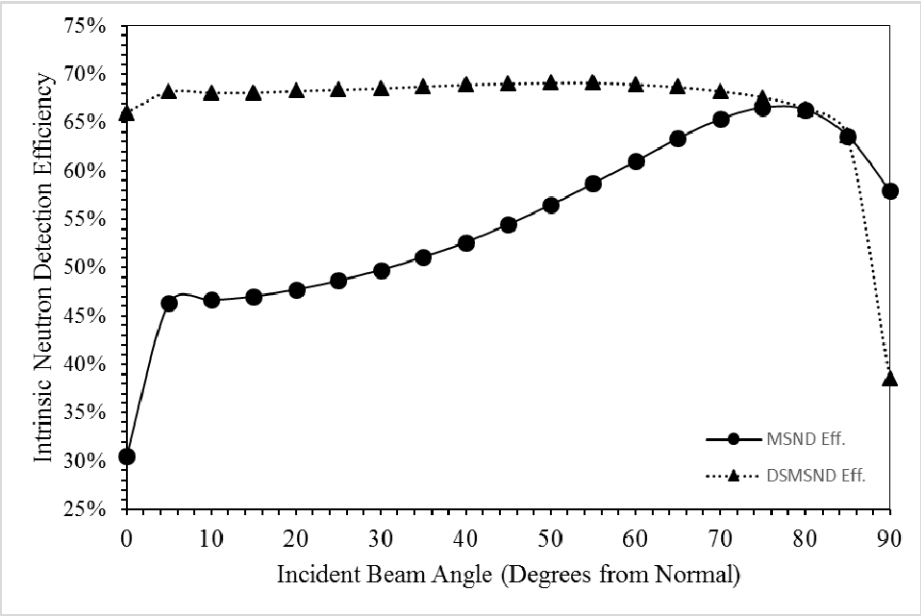

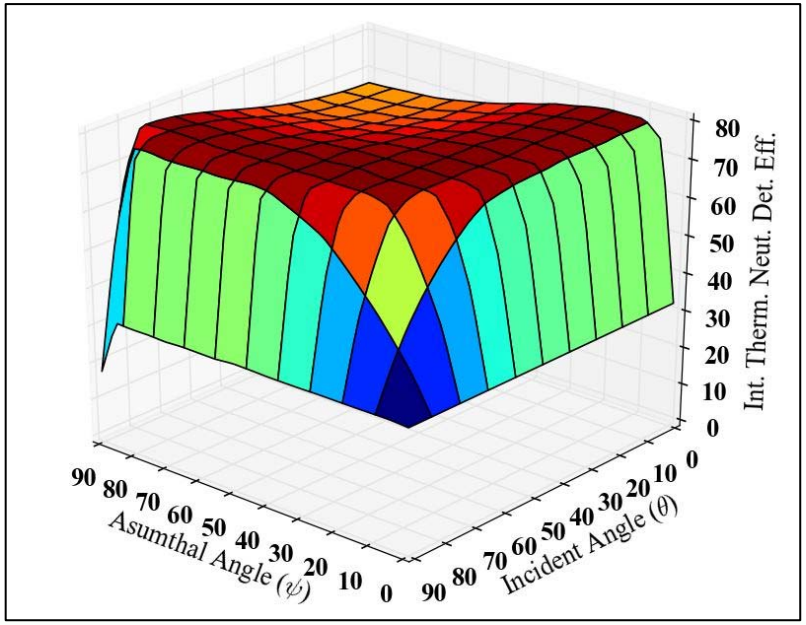

Conversion Material Backfill Density

- Reached a plateau in intrinsic thermal-neutron detection efficiency in 2015-2017 of **50-55%**
- Assumed that LiF backfill density was >90% of crystalline ^{6}LiF.
- Packing fraction was measured by mass, neutron attenuation, and simulation
- The backfill density is actually be closer to **30%** of solid LiF.

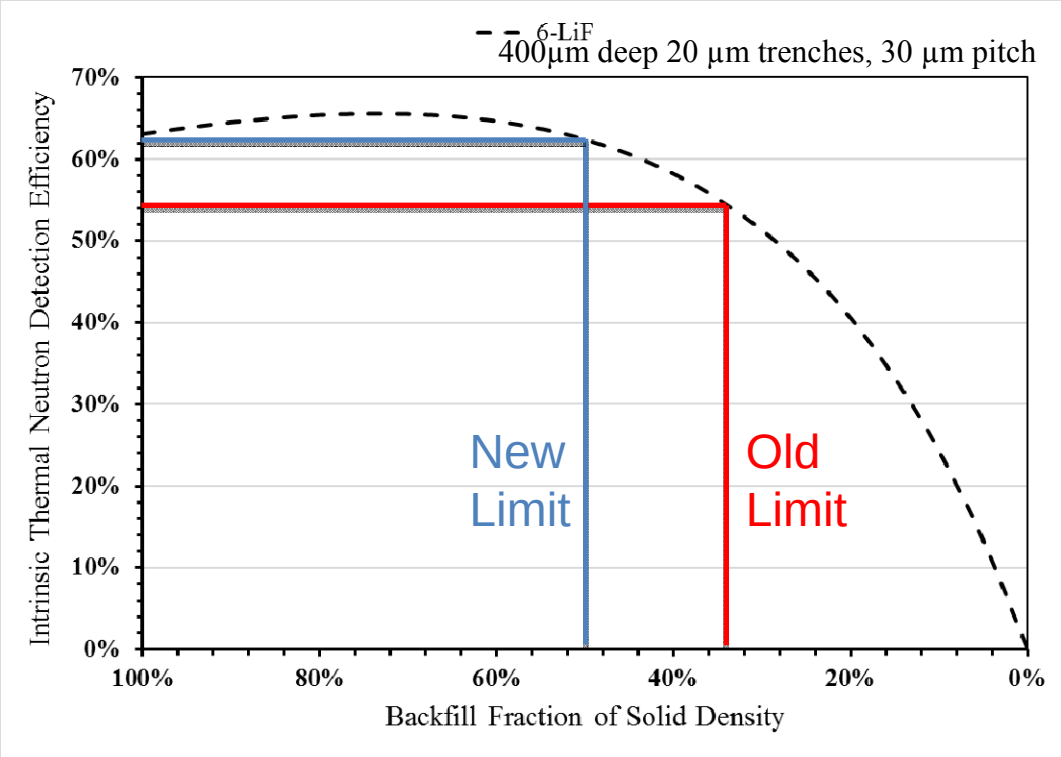

^{6}LiF Density Measured by Mass	
Total Trench Volume (cm^{-3})	2.632
Mass ^{6}LiF (g)	2.015
Density (g/cm^{-3})	**0.766**
Packing Fraction	**30.0%**

^{6}LiF Density Measured by Neutron Attenuation

Configuration	Net Counts	% Reduction
Ref. Detector Only	7,888	
Tape + Ref. Detector.	7,875	0.16%
DS-MSND + Tape + Ref. Detector	3002	**61.94%**
Expected Attenuation	-	**~91%**

Conversion Material Backfill Density

Goal is to increase LiF packing fraction:

- Implement bimodal powder size distribution
  - "Nano-sized" ^{6}LiF fills in gaps between larger particles
- Change backfilling method
  - Use ink roller to press powder into trenches
- Investigate lubricating solutions
- Packing fraction measured by measuring mass of diode before and after backfilling
- Increase packing fraction from 30% to 55%

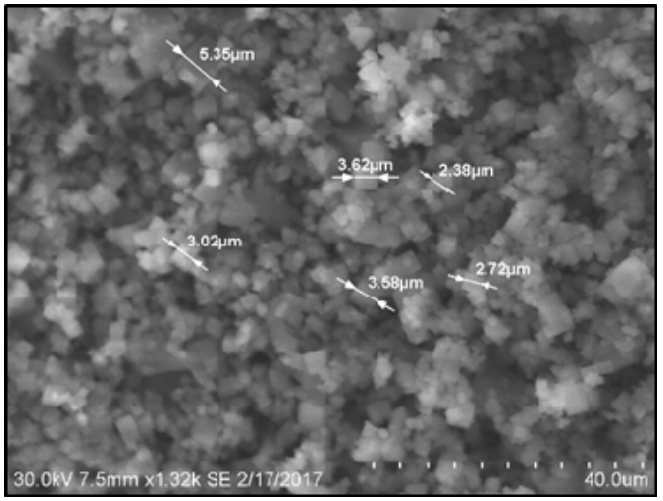

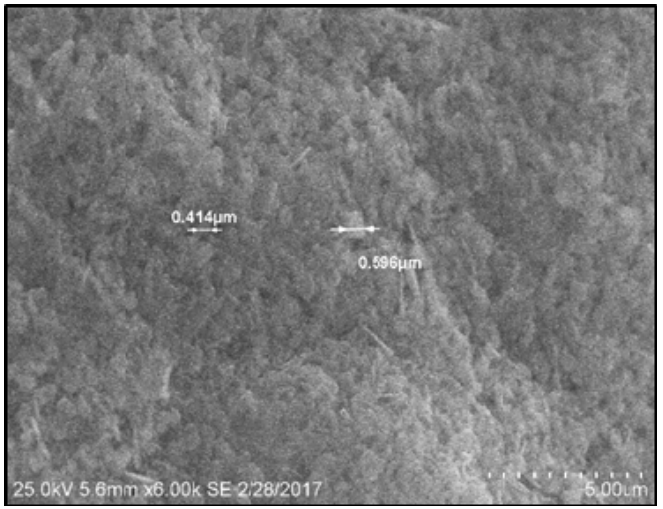

Lubricant Solution	wt% nano-LiF	Packing Fraction
Methanol + Acetic acid	0 %	43.6%
Methanol + Acetic acid	10%	51.7%
Methanol + Acetic acid	20%	55.1%
Methanol	25%	35-45%
Ethylene glycol	25%	45-50%

Adjusting DS-MSND Geometry for Decreased Packing Fraction

- MCNP6 to simulate alternative trench dimensions to see if 70% detection efficiency can be achieved
- Move to 1.5-mm thick wafers allows high efficiency with reduced packing fraction
  - Requires trench depth of 550 µm to 650 µm for 30 µm pitch pattern

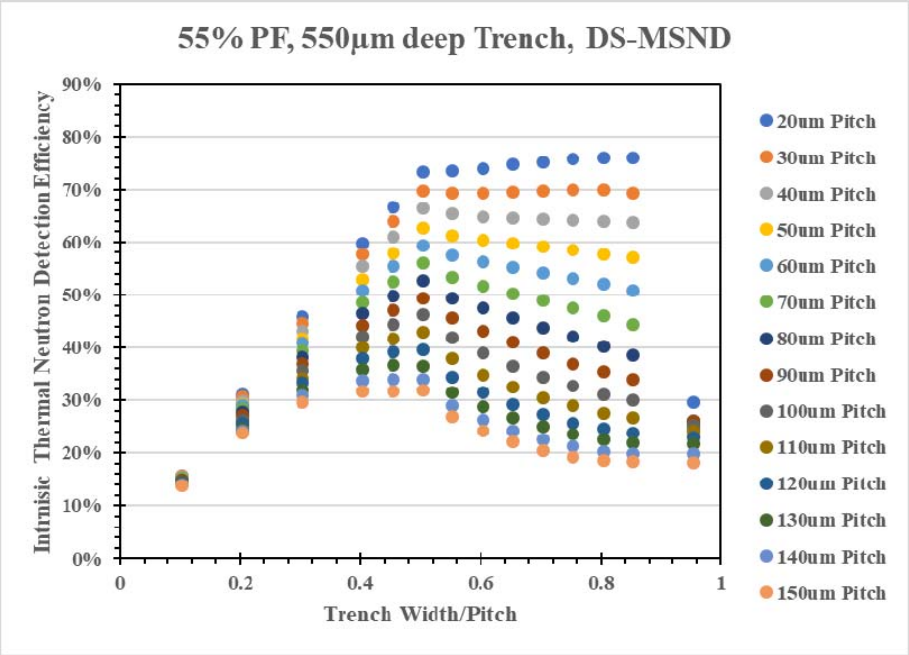

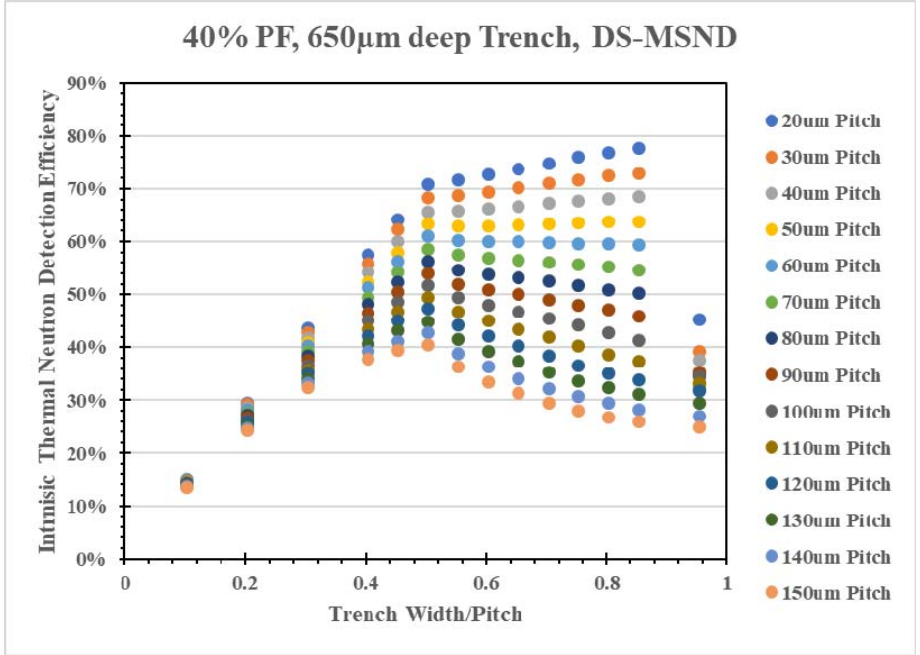

Efficiency Measurements

- Offset DS-MSNDs with 525-μm deep x 20-μm trenches and 30-μm pitch
- Measured efficiency against ^{6}LiF-backfilled DS-MSNDs calibrated in thermal-neutron beam port
- Moderated ^{252}Cf measurement
- **69.2±0.8% Intrinsic Thermal Neutron Detection Efficiency Has Been Achieved.**

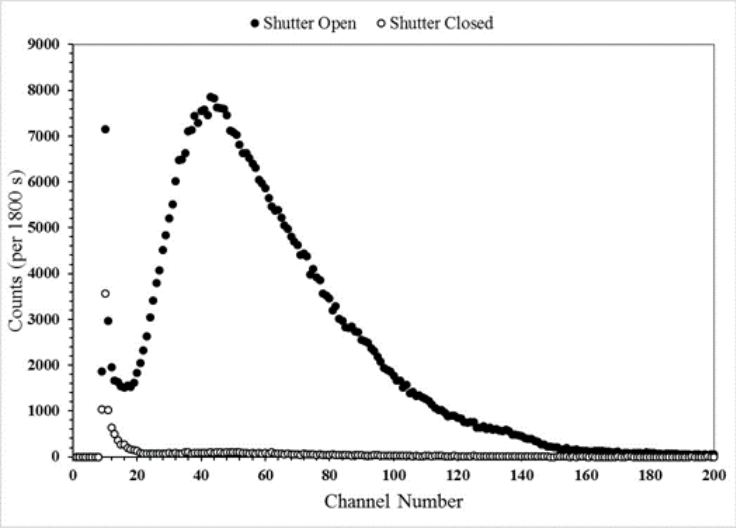

Diode	Detection Efficiency	Err. Det. Eff.
B0802	65.1%	0.7%
B0804	64.0%	0.7%
B0806	66.6%	0.8%
B0811	68.1%	0.8%
B0812	**69.2%**	**0.8%**
B0814	65.1%	0.7%

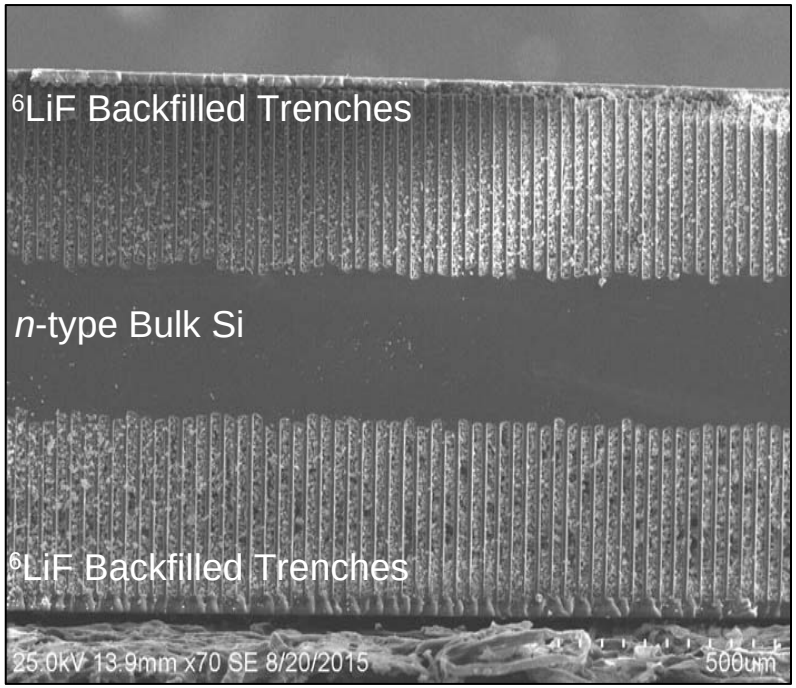

Instrumentation
MSND-based Domino

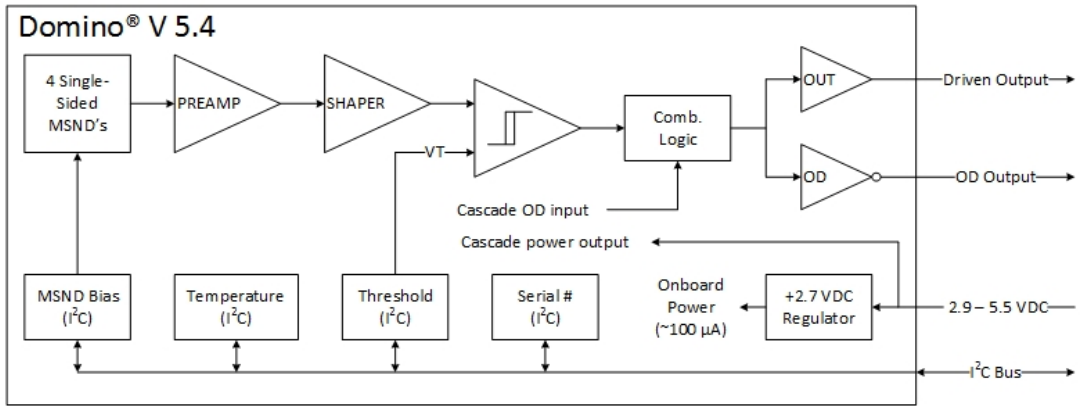

Characteristic	Domino V5.4
Overall Dimensions	1.04" x 1.5"
MSND Area	4 x 1 cm^2
Operating Voltage	2.95–5.5 VDC
Current Draw (max.)	90 µA
Noise (input inferred)	1.61 fC_{RMS}
Bias/Threshold Prog.	I^2C Prog.
Temperature Sensor	Yes
Detection Efficiency	ε_{th} = 30%

- **Mass-produced modular device.**
- **Contains all signal processing electronics for neutron counting.**
- **5-V TTL output pulse.**
- **10 - 50 µs pulse width.**
- **Tiled to 1-m long strings.**

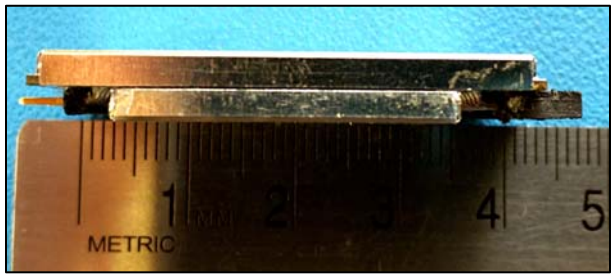

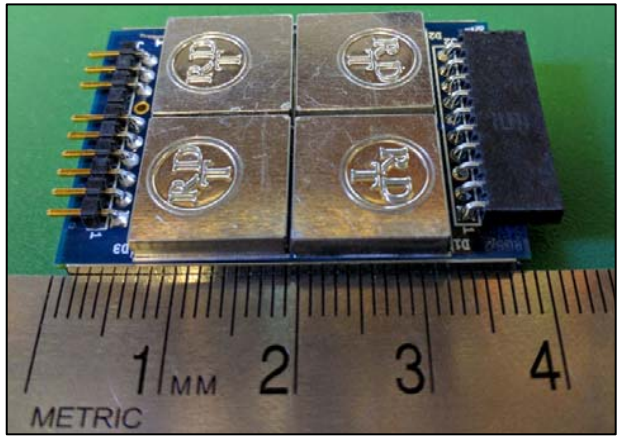

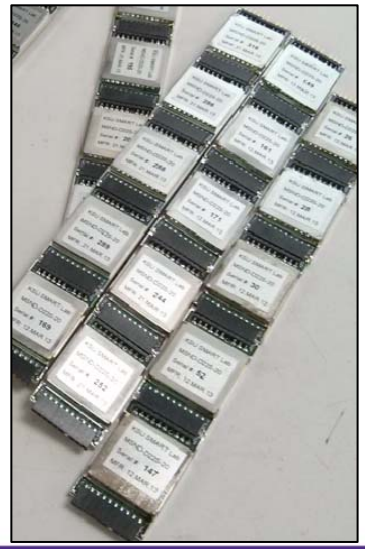

R.G. Fronk, et al., Conf. Proc. IEEE Nucl. Sci. Symp., Strasbourg, France, Oct. 29-Nov. 5, 2016.

Semiconductor Materials And Radiological Technologies ©

^{3}He Replacement (HeRep Mk III, 2015 Model)

- Designed to directly replace a 0.75-in. diameter, 6-atm ^{3}He detector.
- 4.5-in. long by 0.75-in. diameter (2.4-in. active region).
- Populated with *pvp*- dual-sided MSNDs (DSMSNDs).
- Interior moderator can be added between detector strips and case.
- Improved low power operation.

HeRep Mk III (2015) - Specifications	
DSMSND Area	1 cm^2
# of DSMSNDs	12
ε_{th} of DSMSNDs	50% @ 300keV LLD
Voltage	5 V
Power	~ 15 mW
GRR	5x10^{-7} ^{137}Cs @ 50mR/h

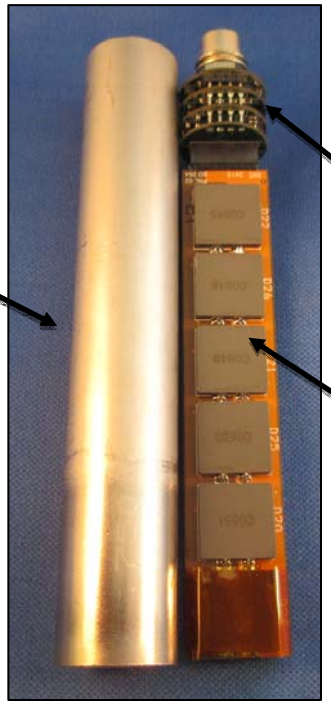

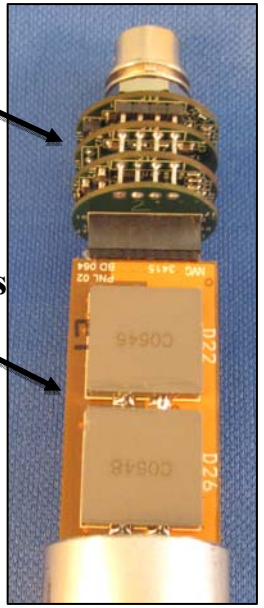

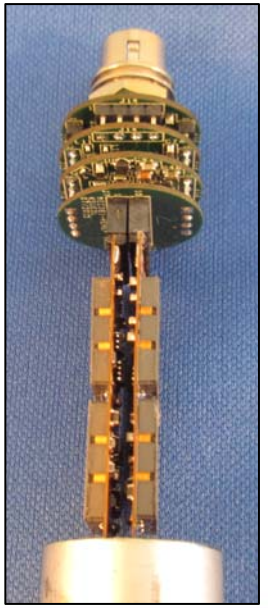

D.S. McGregor, S.L. Bellinger, R.G. Fronk, L. Henson, D. Huddleston, T. Ochs, J.K. Shultis, T.J. Sobering, R.D. Taylor, Rad. Phys. Chem., 116 (2015) pp. 32-37.

^{3}He Replacement (HeRep Mk IV, 2016 Model)

- Designed to directly replace a 0.75-in. diameter, 10-atm ^{3}He detector.
- 3.1-in. long by 0.75-in. by 0.75-in.
- 6.1-in. long by 0.75-in. by 0.75-in.
- Populated with *pvp*- dual-sided MSNDs (DSMSNDs).

HeRep Mk IV (2016) – Specifications	
DSMSND Area	1 cm^2
# of DSMSNDs	15
ε_{th} of DSMSNDs	50% @ 300keV LLD
Voltage	5 V
Power	~ 10 mW
GRR	1.5x10^{-7} ^{137}Cs @ 50 mR/h

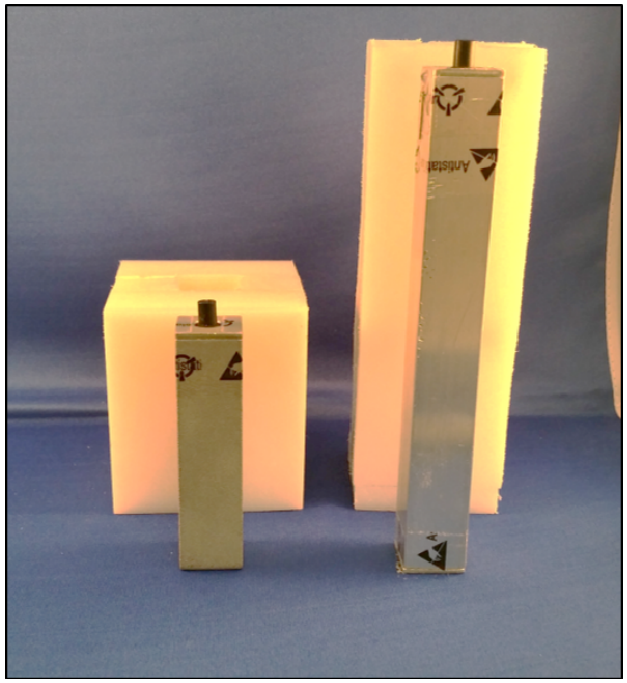

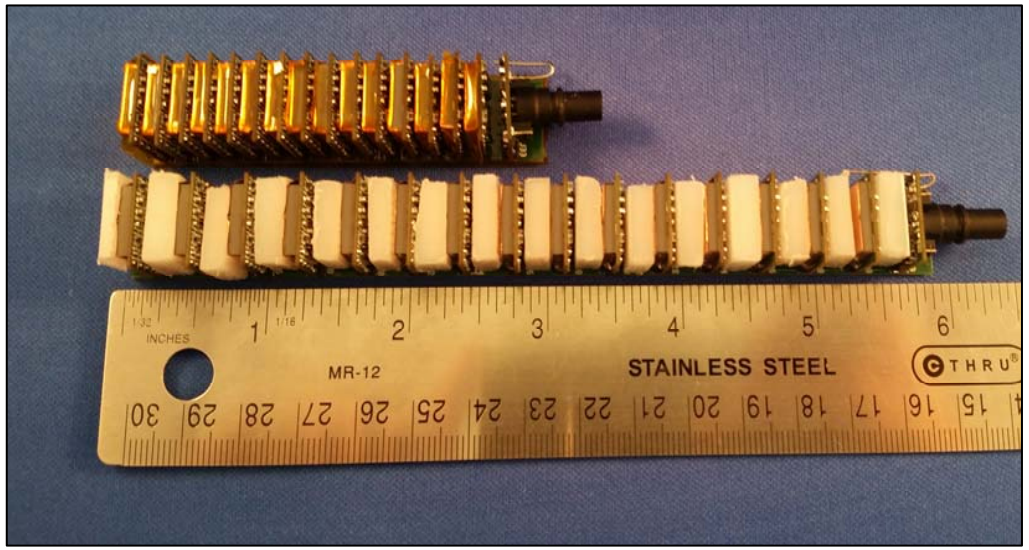

HeRep Mk IV

T.R. Ochs, et al., Conf. Proc. IEEE Nucl. Sci. Symp., Strasbourg, France, Oct. 29-Nov. 5, 2016.

HeRep Mk IV Testing

- Direct comparison to 10-atm ^{3}He detector.
- HeRep Mk IV detectors more sensitive than 10-atm ^{3}He detector to AmBe.
- Internal neutron moderation in HeReps.

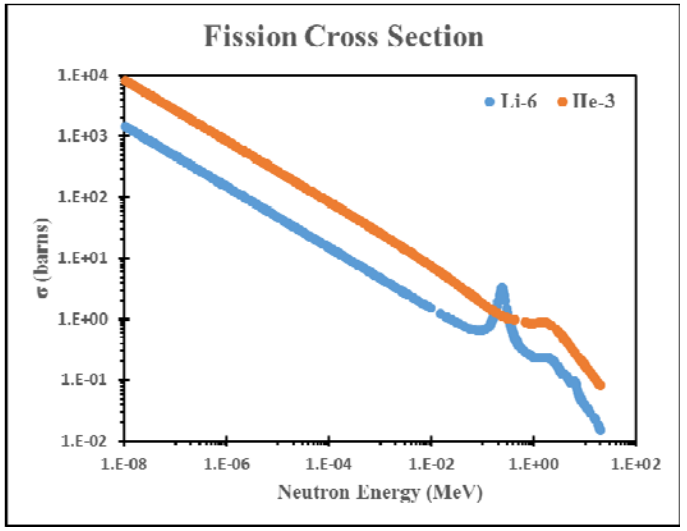

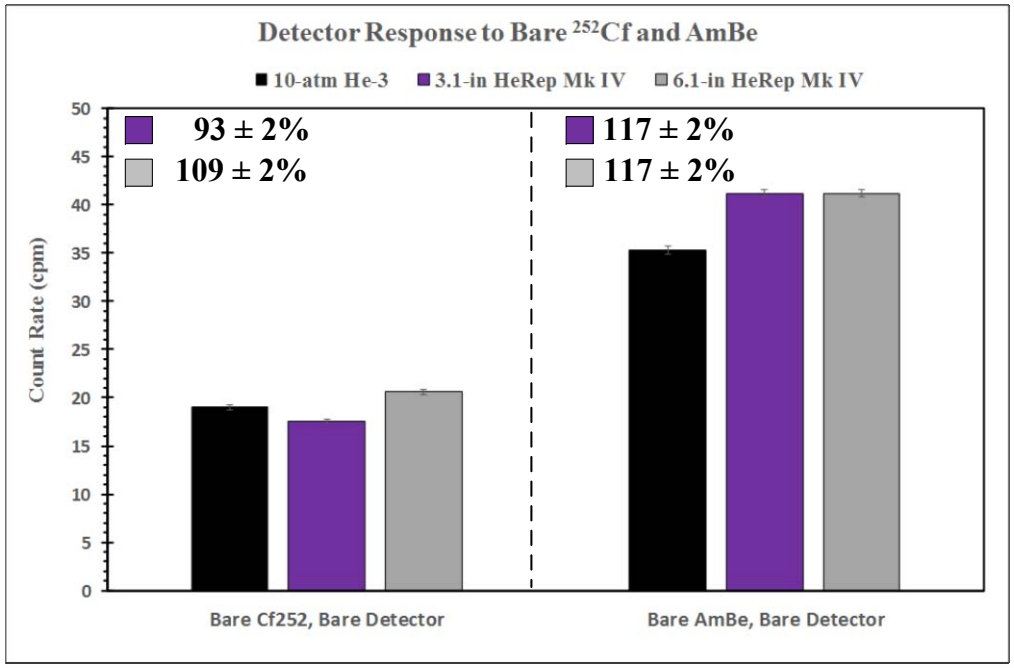

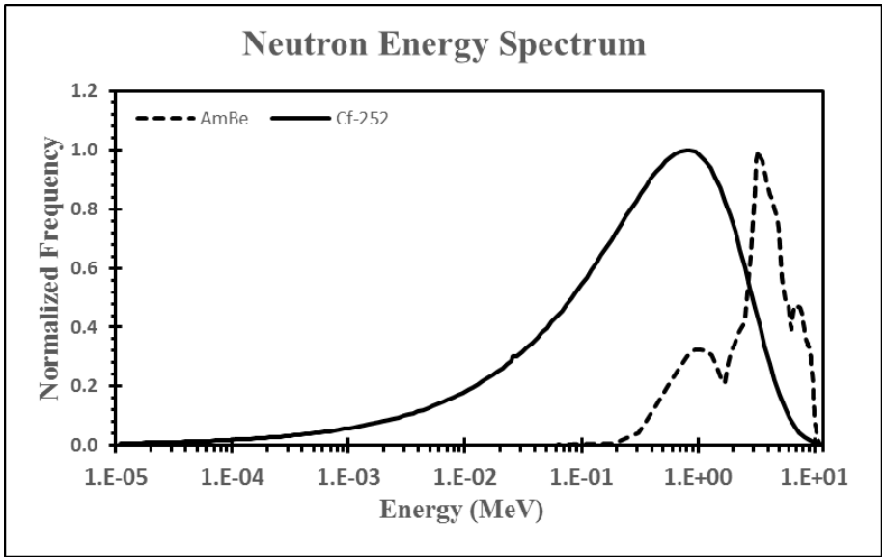

T.R. Ochs, et al., Conf. Proc. IEEE Nucl. Sci. Symp., Strasbourg, France, Oct. 29-Nov. 5, 2016.

HeRep Mk IV Testing (Continued)

- Neutron stand-off testing; angular dependency on neutron response.
- Detector was placed 25-cm from bare 26-ng ^{252}Cf source, 1-m above concrete floor.
- Detector was rotated through 360 degrees in 30-degree increments.

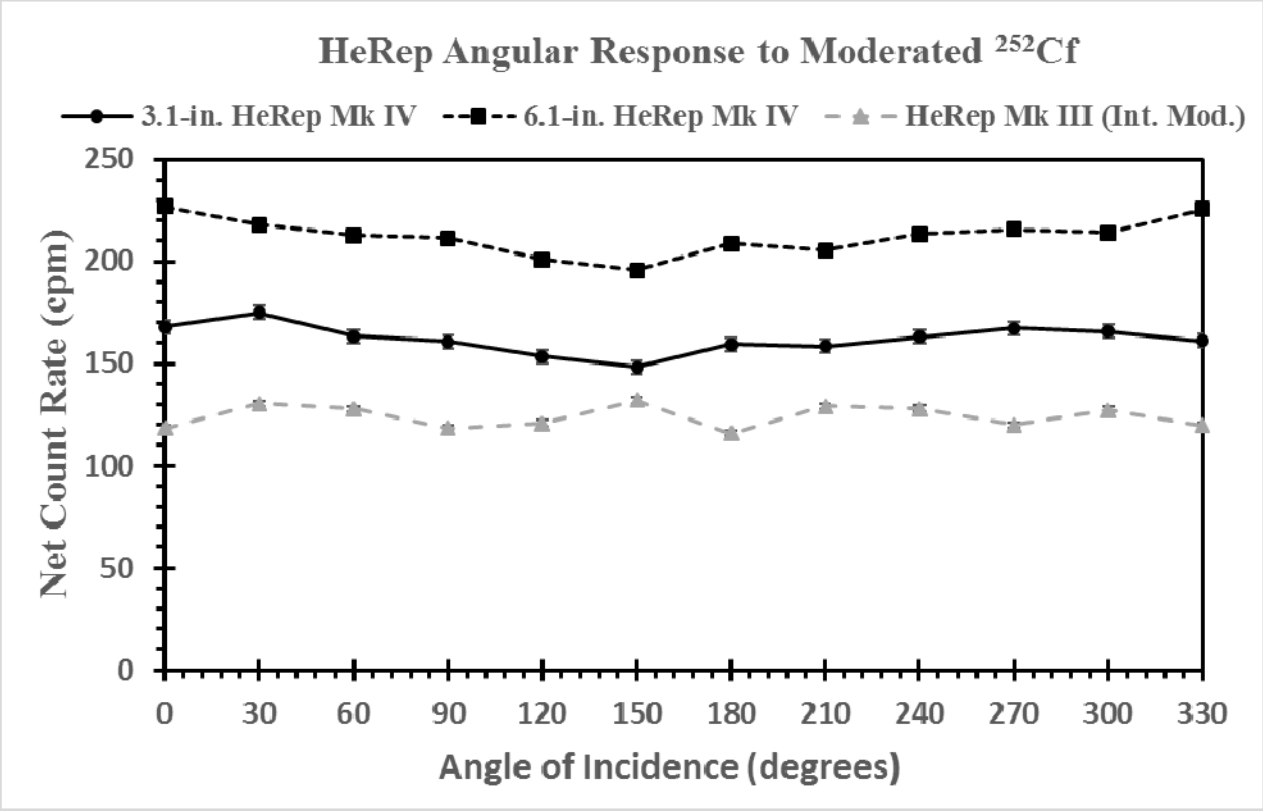

3.1-in HeRep Mk IV

$$\frac{\textit{Minimum Count Rate}}{\textit{Maximum Count Rate}} \approx 0.85$$

6.1-in HeRep Mk IV

$$\frac{\textit{Minimum Count Rate}}{\textit{Maximum Count Rate}} \approx 0.86$$

Arrayed Domino Neutron Detectors

- Dominoes can be connected together into strings of ~**1-m** long.
- Strings can be arrayed laterally; produces an array of Dominoes.

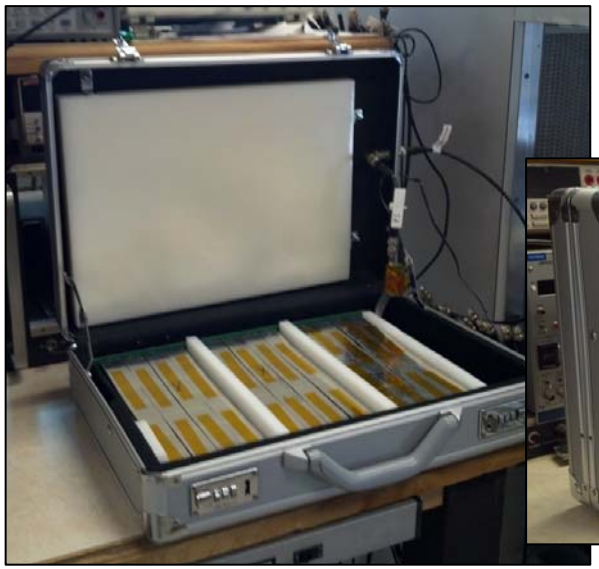

Briefcase Neut. Det.	
Num. Dom.	84
Weight	21 lbs.
Input Volt.	5 V
Power	~0.3 W

Det. Resp. (Cf-252)	
Dist.	**s^{-1} ng^{-1}**
1 m	~0.54±0.02
2 m	~0.27±0.01
5 m	~0.08±0.01

Panel Array Neut. Det.	
Num. Dom.	480
Area	1 m^2
Input Volt.	12 V
Power	~12 W

Det. Resp. (Cf-252)	
Dist.	**s^{-1} ng^{-1}**
2 m	1.45 ± 0.009
5 m	0.45 ± 0.004
10 m	0.111 ± 0.001

D.S. McGregor, S.L. Bellinger, R.G. Fronk, L. Henson, D. Huddleston, T. Ochs, J.K. Shultis, T.J. Sobering, R.D. Taylor, Rad. Phys. Chem., 116 (2015) pp. 32-37.

Domino™ – A standard modular device that is **mass producible** and houses one MSND.

- Individual Dominoes can be connected together, forming strings up to **1 m** long.
- Powered by a **1-3V** input, draws ~**3mW**.
- Weighs **9.5 grams**.

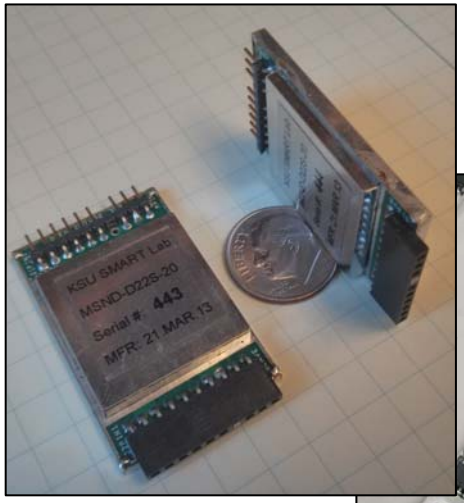

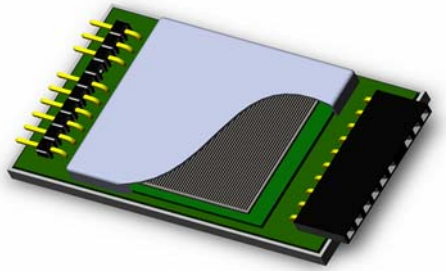

- Manufacturing: MSNDs and Readout Electronics
  - Produced Revised 4x4 MSND array readout electronics that can be tiled together into an 8x8 array, which are then stacked in the moderator.
  - Manufactured 1120 MSNDs in CDB packages for final prototype. Shipped to PCB assembler. Should receive 70 of the 4x4 arrays next week.

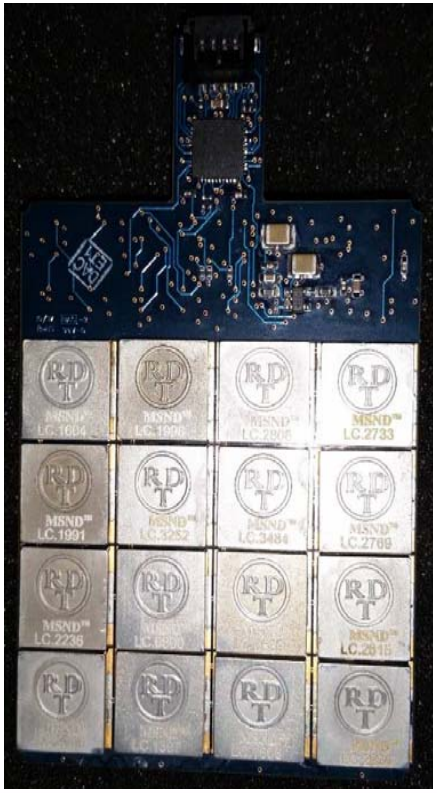

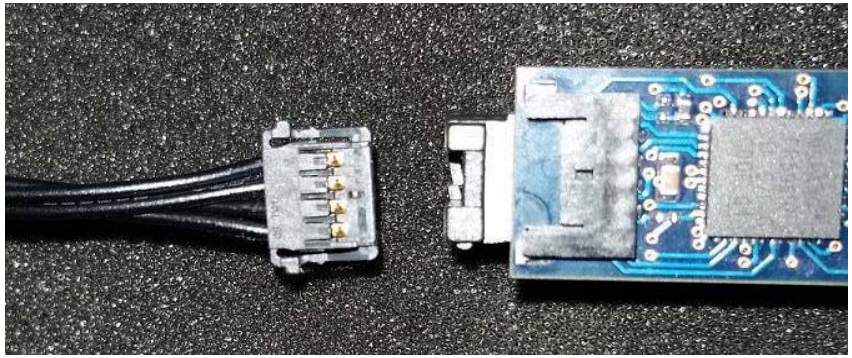

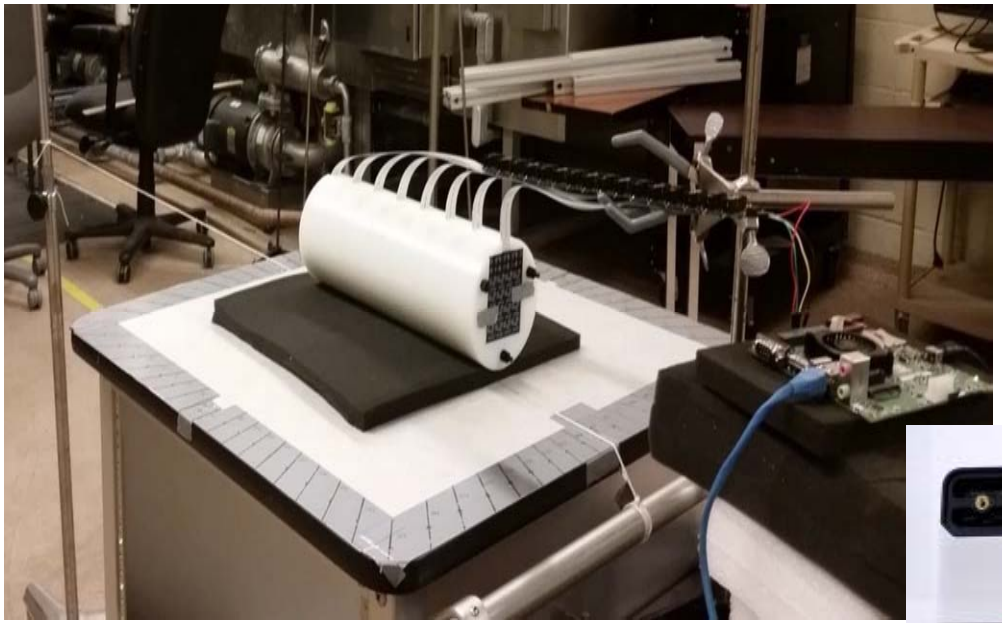

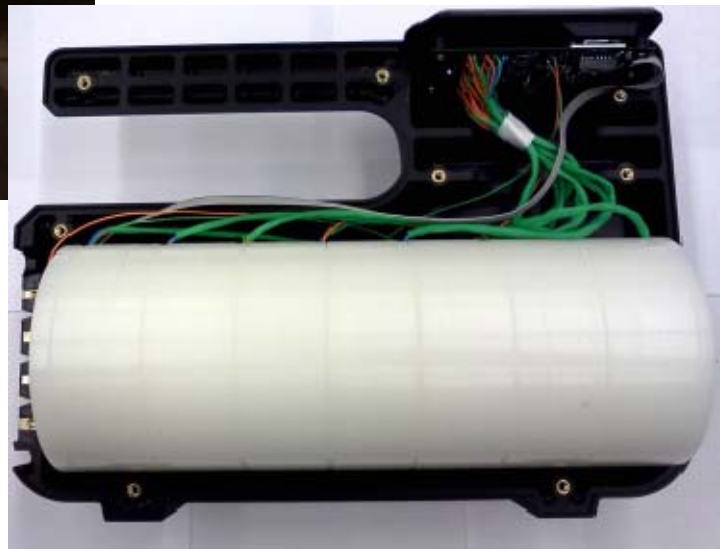

9-12% intrinsic eff.
For ^{252}Cf
(front face incidence)

C.B. Hoshor, et al., Nucl. Instrum. Meth., A803 (2015) pp. 68-81.
C.B. Hoshor, et al., Nucl. Instrum. Meth., A866 (2017) pp. 252-264.

Instrumentation
MSND Neutron Spectrometer

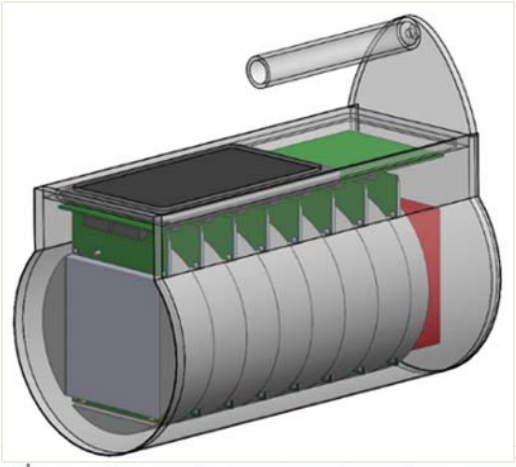

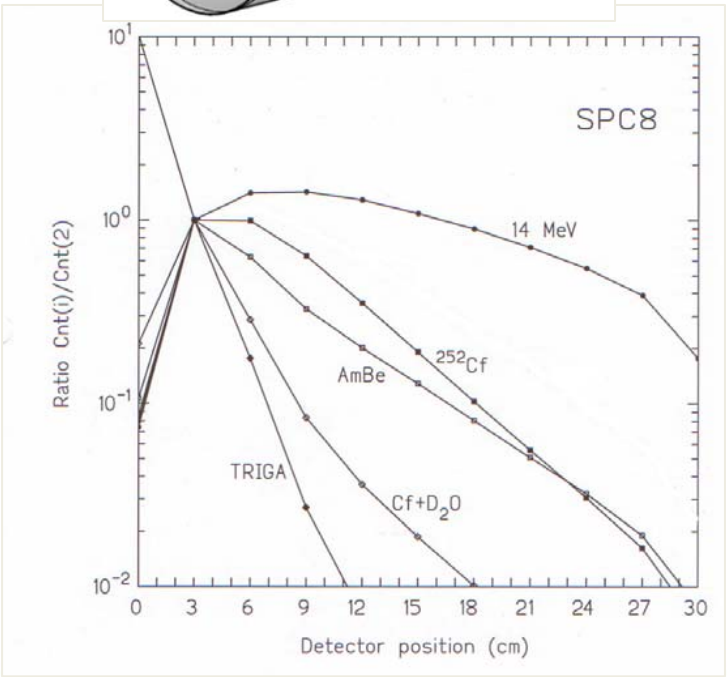

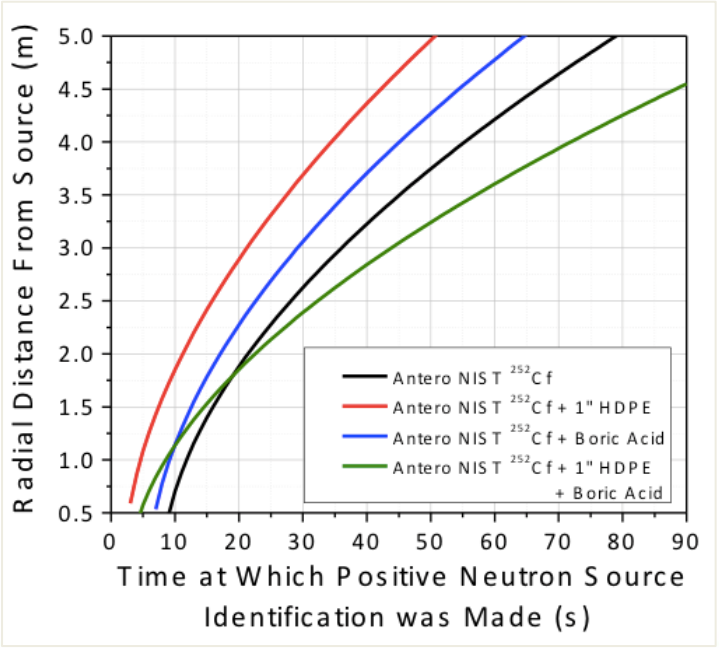

•C.B. Hoshor, et al., Nucl. Instrum. Meth., A803 (2015) pp. 68-81.
•T.M. Oakes, et al., Nucl. Instrum. and Meth., A719 (2013) pp. 6-12.

Modular Neutron Detector (MND) Design and Performance

- 24 1-cm^2 active area MSNDs per MND (6x4 array)
- Enclosed in 3-in x 5-in x 0.6-in HDPE moderator case
  - Approximately 0.25-in outward facing moderator
- Contains bias, pulse amplifying, shaping, discriminating, and TTL-generating electronics
- Programmable bias and LLD threshold
- 3.3 V applied with 1.2 mA current draw
- $\varepsilon_{Cf\text{-}252,bare} = 0.193 \pm 0.002\%$

MGDs and Communications Electronics

•Modular Gamma-Ray Detector (MGD)
- Seven LND Geiger-Müller Counters
- Provides gamma-ray count rate information

•Power Electronics
- Central power board and battery for wired systems
  - 12 hour continuous operation
- On-board power and battery for wireless systems
  - >2 weeks continuous operation

•Communications electronics
- Wired – Controller Area Network or Low Voltage Differential Signal
- Wireless – Bluetooth LE

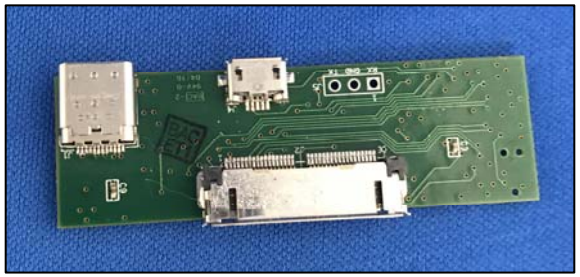

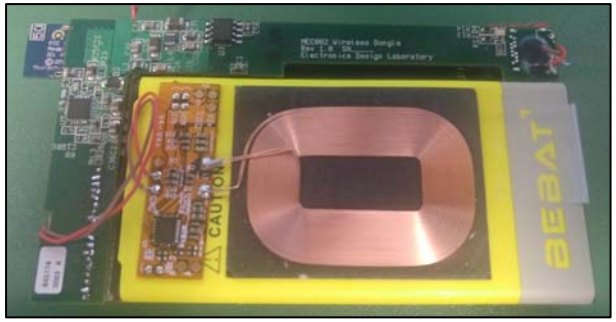

Wearable Detection Device (WDD)

R&D 100 2017 Winner

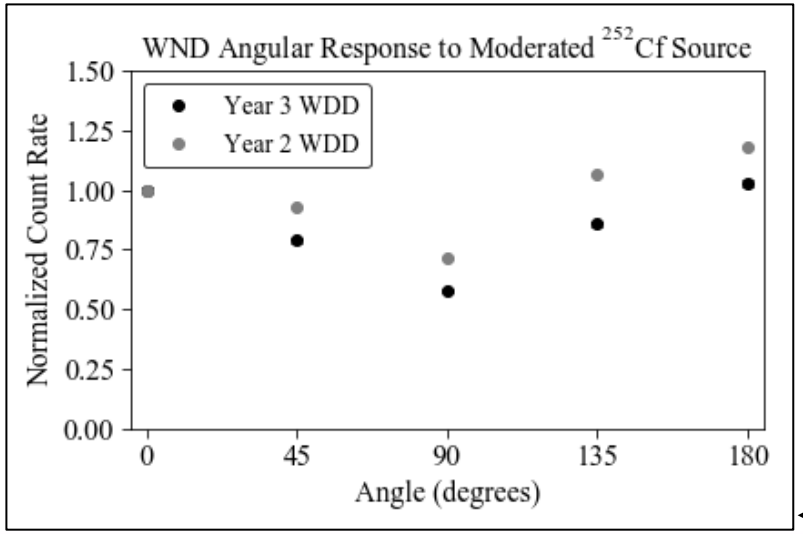

Response from 27.4 ng bare ^{252}Cf at 2 meters.

WDD Design and Layout

- 16 MNDs with communications dongles in specialized prototype garment
  - 8 front and 8 back
- Up to 2 MGDs for complementary gamma-ray detection
- 1 Master Control Board with battery pack (zero-RF, wired versions only)
- Weight – 8 to 11 lbs
- Greater than 12hr Operations Time

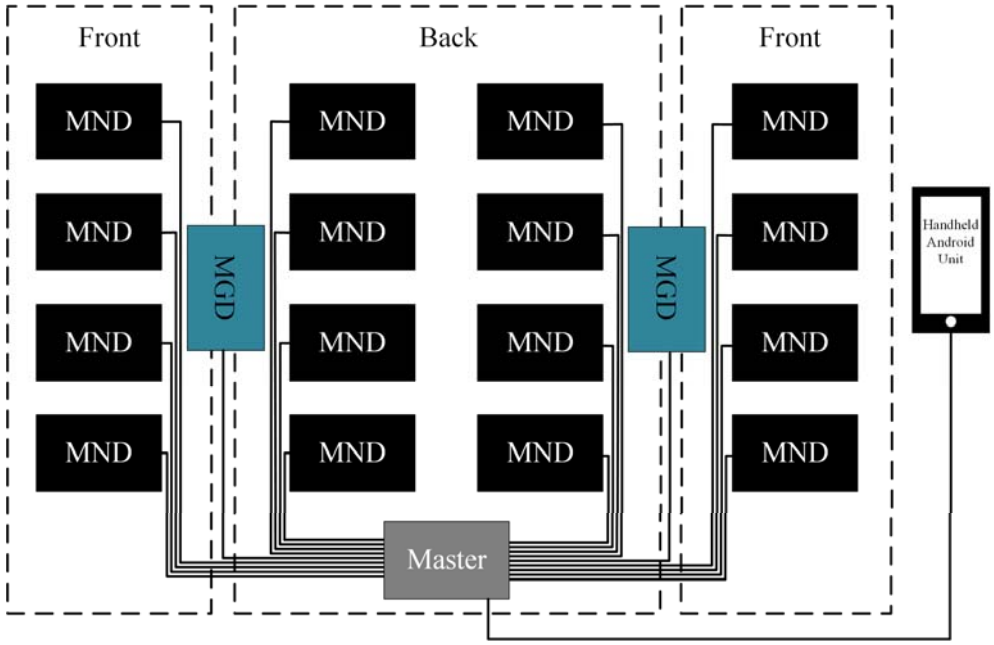

Android Interface

- Real-time count rate updated every second
- Total gross counts during measurement time
- Rolling line graph shows previous minute of count rates
- Individual detector count rate updated every second
- Programmable alarm threshold for neutron count rate
- On-board log file for post processing

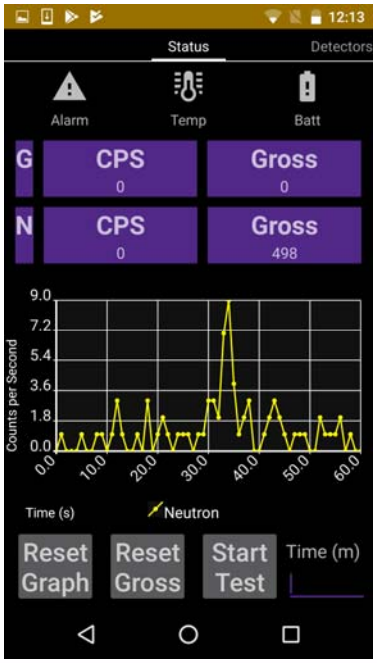

WDD Gamma-Ray Sensitivity and Neutron Moving Source Measurements

^{252}Cf moving 1.2 m/s at 1 meter

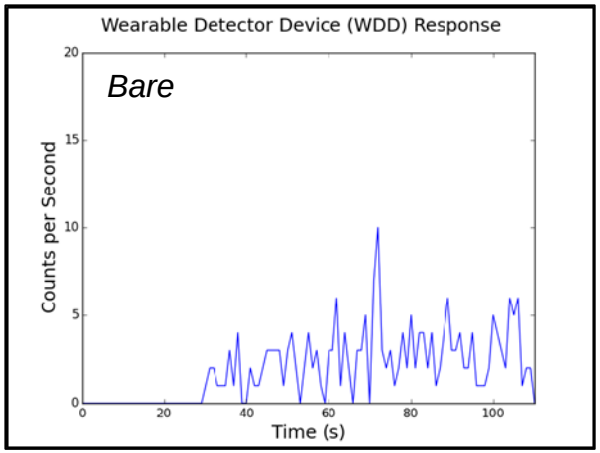

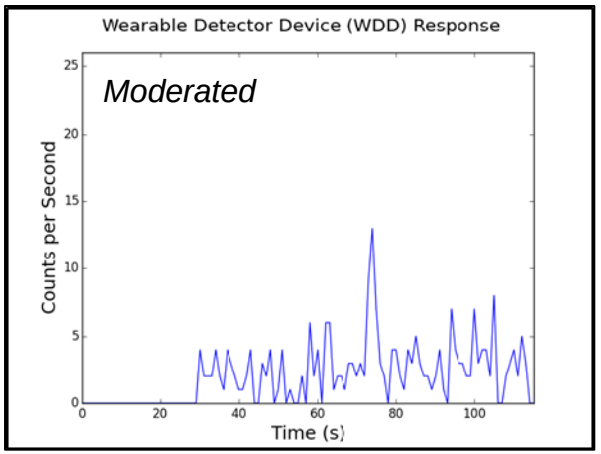

^{252}Cf moving 0.6 m/s at 1 meter

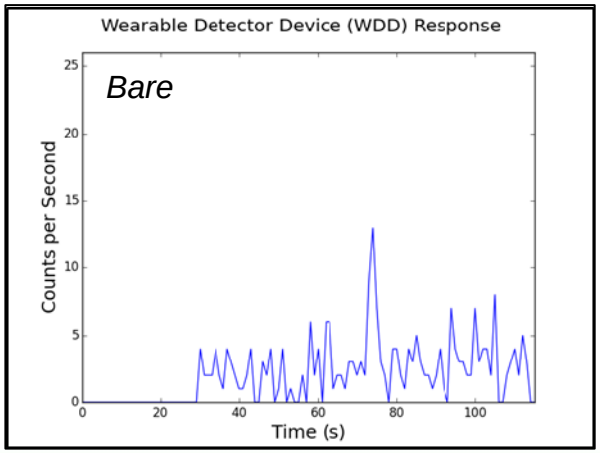

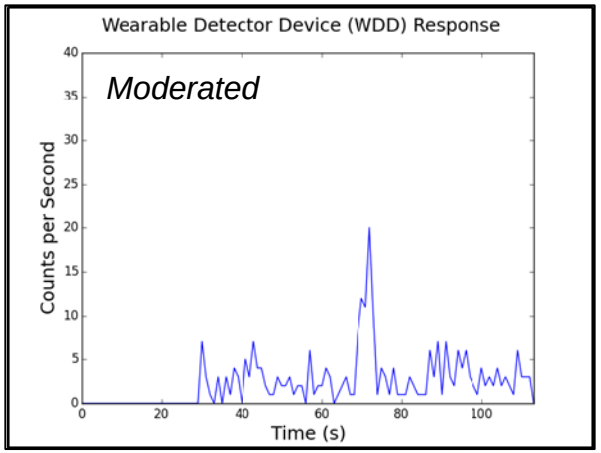

Ambient Dose Equivalent, H*(10)

- For monoenergetic neutrons, H*(10) is calculated with the following

$$H^*(10) = h_{cc,E}\phi_E$$

  - $h_{cc,E}$ is a neutron fluence to ambient dose equivalent conversion coefficient

- For multi-energetic neutron environment,

$$H^*(10) = \int_0^\infty h_{cc}(E)\phi(E)dE$$

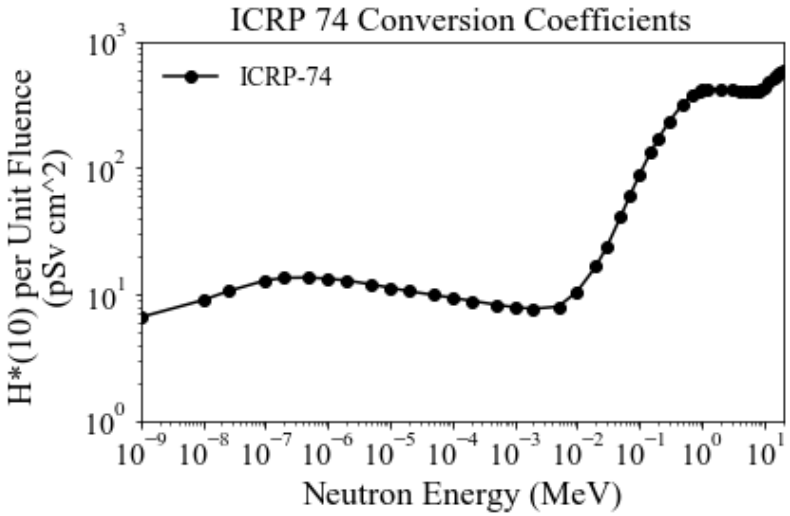

Ambient Dose Equivalent, H*(10)

- Knowledge of the neutron energy fluence is required to determine H*(10)
  - Incident neutron energy is challenging to measure
- Instead, match detector response function to ambient dose equivalent conversion coefficients

$$R = \int_0^\infty C\, d_{cc}(E)\phi(E)dE$$

$$H^*(10) = \int_0^\infty h_{cc}(E)\phi(E)dE$$

- If the fluence is the same and the shape of $d_{cc}(E)$ matches $h_{cc}(E)$, then R can be directly converted to $H^*(10)$ with a calibration coefficient, C, with units of Sv / counts

- The ratio of R to $H^*(10)$ gives an estimate of the accuracy of an instruments reported dose

$$R = \int_0^\infty (C_{th} d_{th}(E) + C_{epi} d_{epi}(E) + C_{fast} d_{fast}(E))\Phi(E)dE$$

Neutron Dosimetry with MNDs – Simulation Results

•Change MND configuration to create thermal, epithermal, and fast neutron bins

•Thermal MND

- 1-mm thick Cd absorber between phantom (moderator) and MND

•Epithermal MND

- 1-mm thick Cd absorber encasing outside of MND away from phantom

•Fast MND

- Replace ^{6}LiF in trenches with paraffin wax
- Use proton recoil to detector fast neutrons

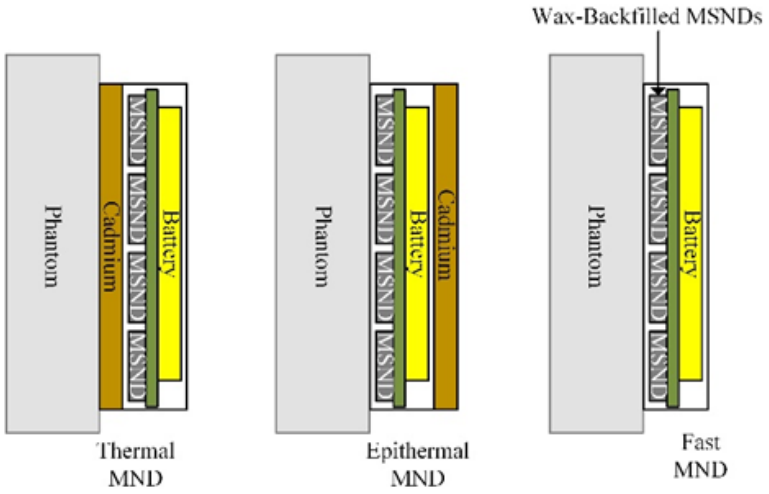

Neutron Dosimetry with MNDs – Simulation Results

- Calibrating each energy channel separately
  - Fast channel normalized at 2 MeV
  - Epithermal channel normalized at 1 eV
  - Thermal channel normalized at 0.01 eV

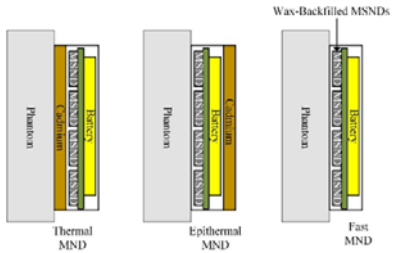

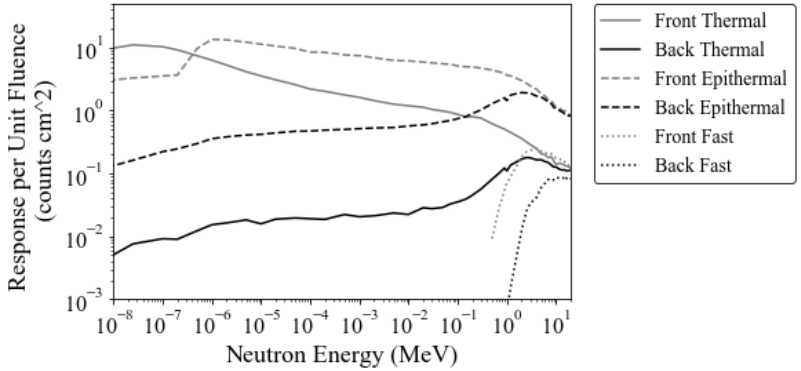

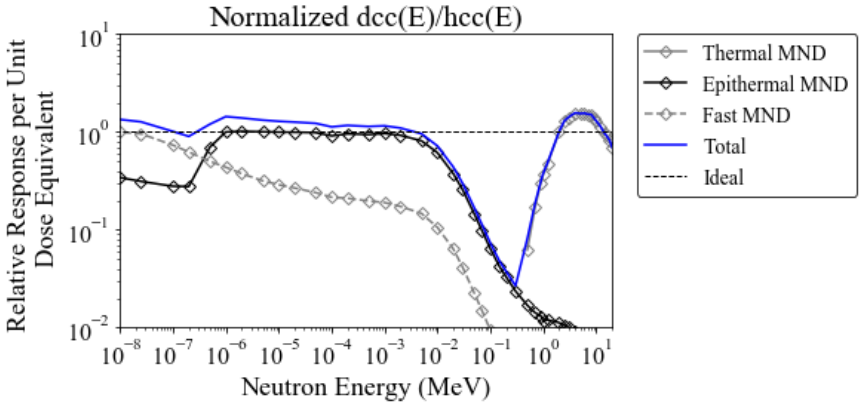

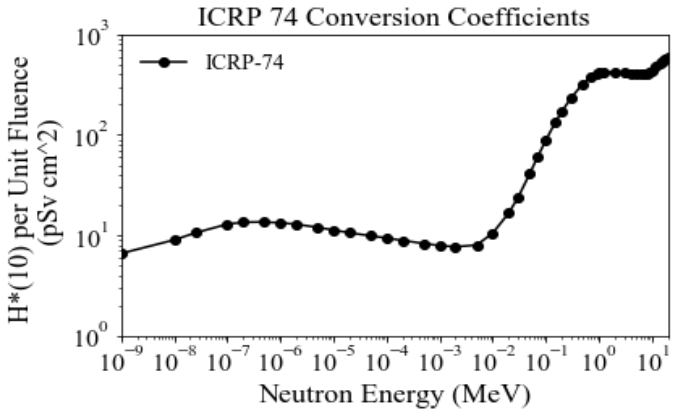

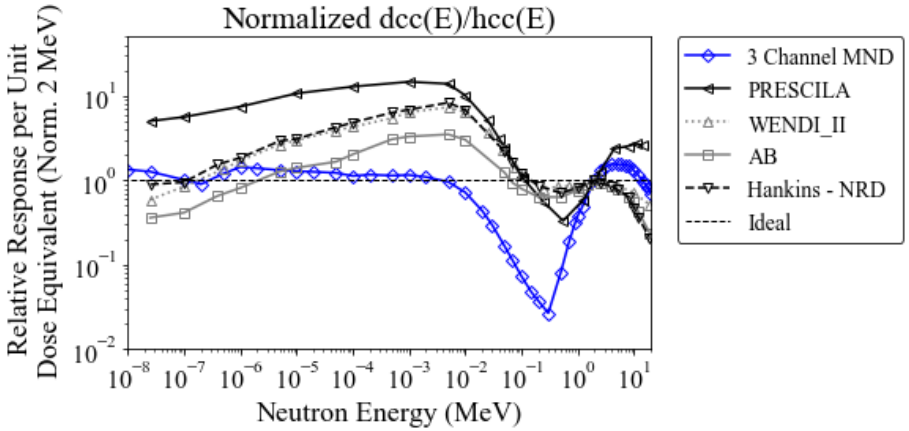

What about nuclear reactor monitoring?

Micro-Pocket Fission Detectors - (MPFD)

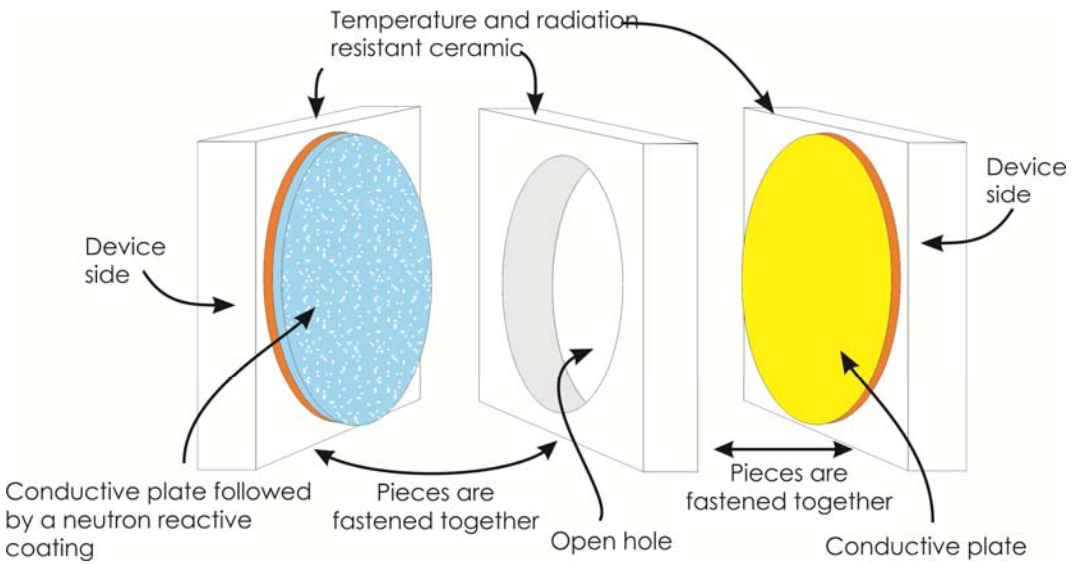

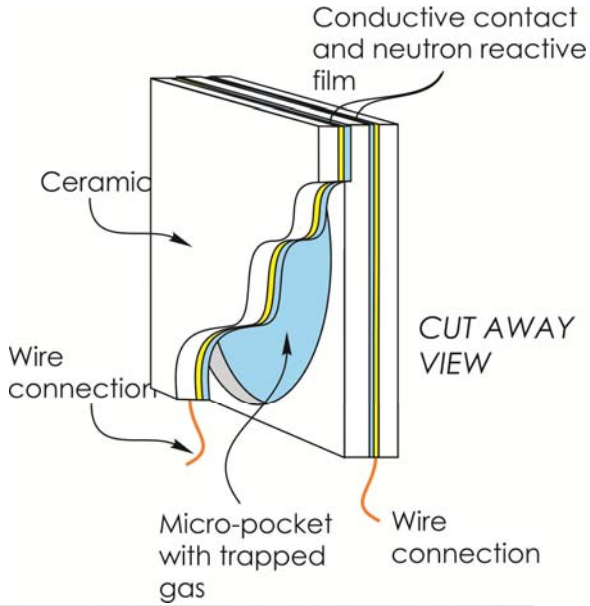

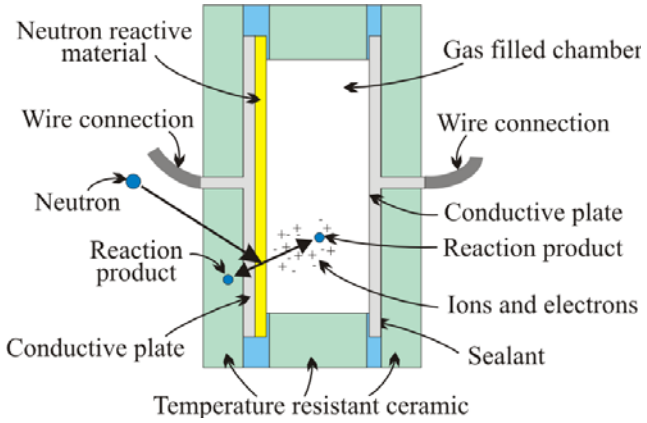

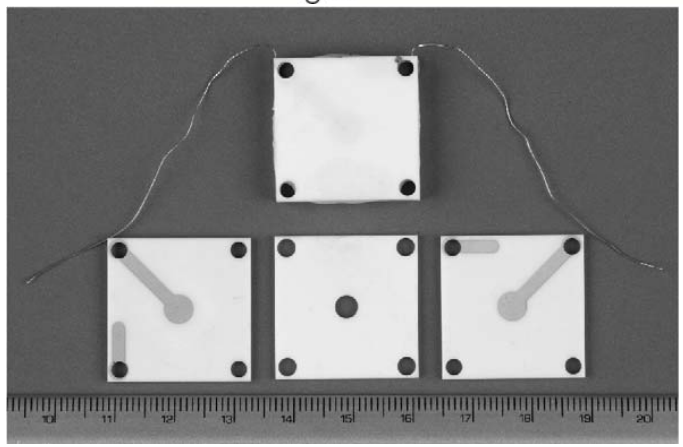

The first micropocket detector.

D.S. McGregor , M.F. Ohmes, R.E. Ortiz, A.S.M.S. Ahmed, J.K. Shultis, Nucl. Instrum. and Meth. A 554(2005) pp. 494-499.

Micro-Pocket Fission Detectors (MPFD)

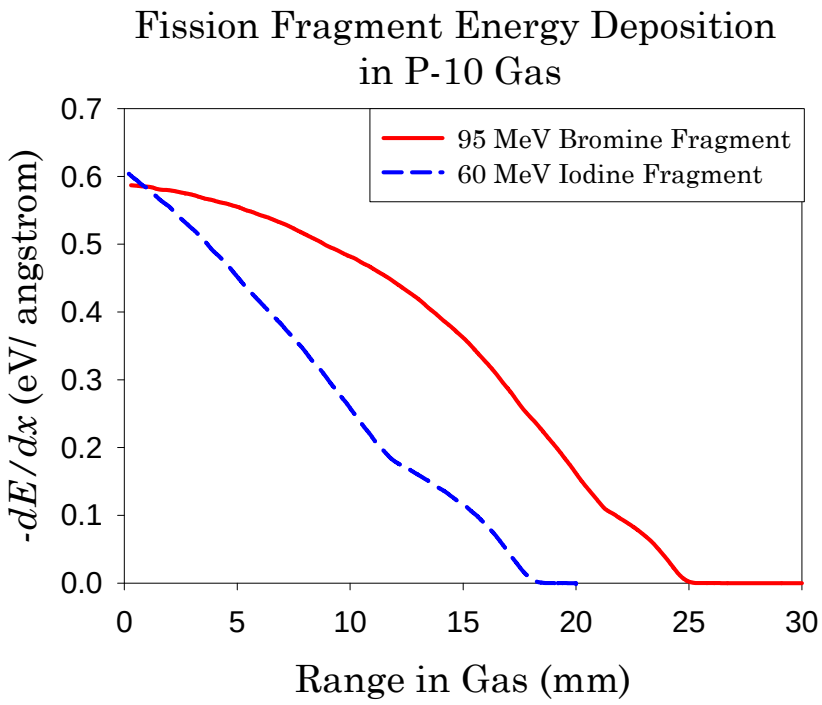

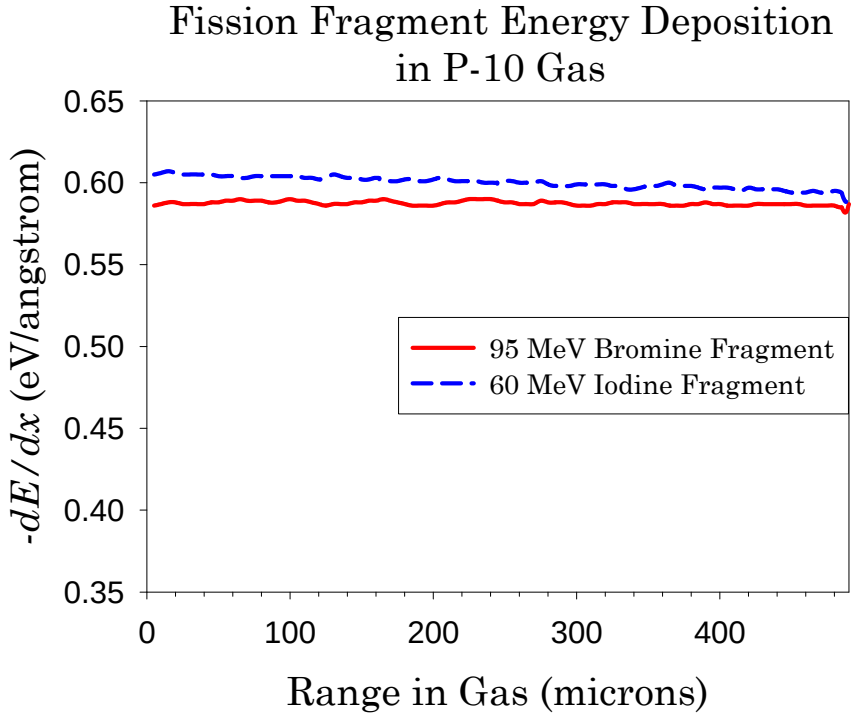

$$\int \frac{dE}{dx} dx \approx 3 \text{ MeV}$$

in a 500 micron wide cavity.

D.S. McGregor , M.F. Ohmes, R.E. Ortiz, A.S.M.S. Ahmed, J.K. Shultis, Nucl. Instrum. and Meth. A 554(2005) pp. 494-499.

Micro-Pocket Fission Detectors (MPFD)

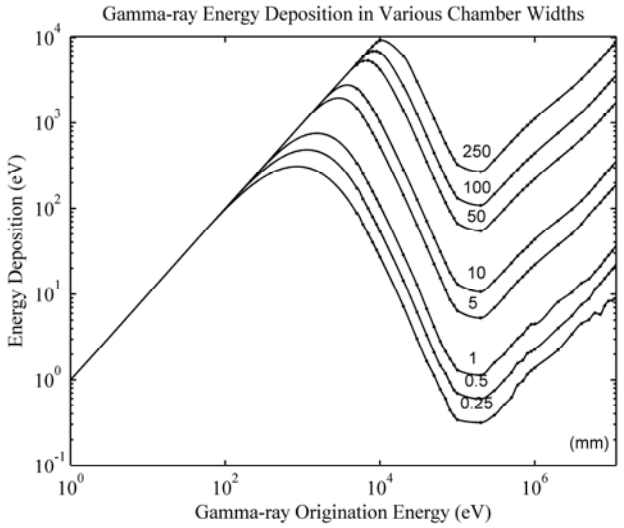

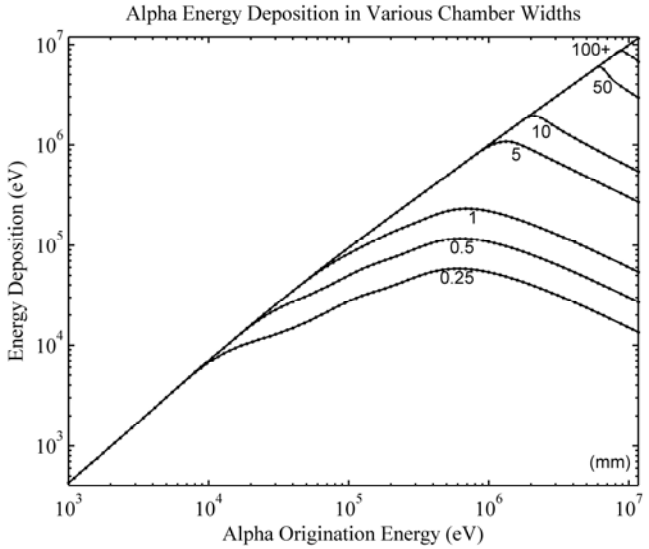

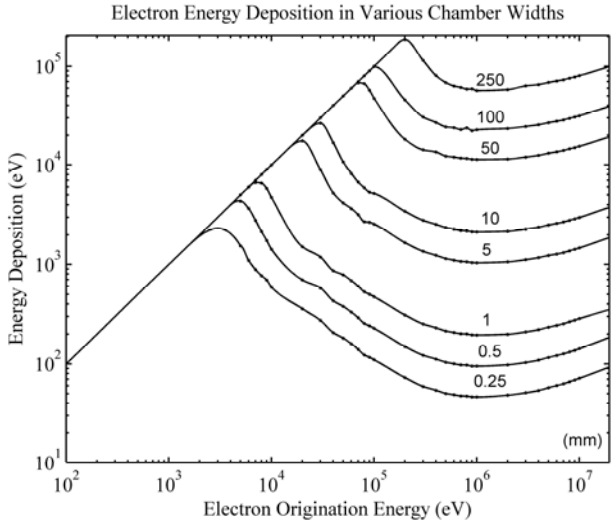

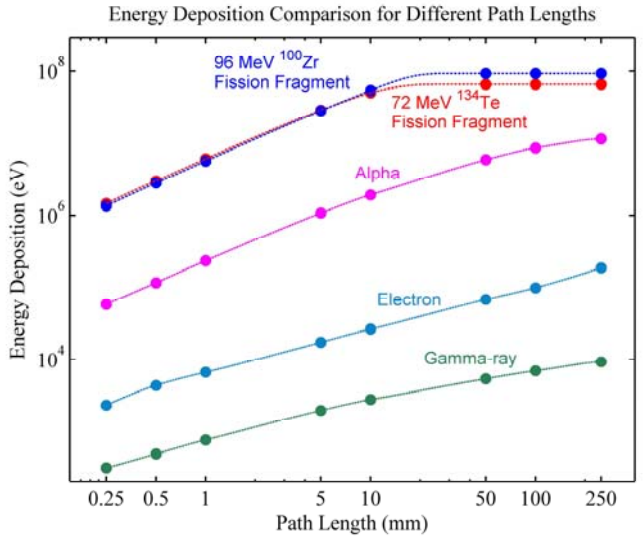

•*M.F. Ohmes, D.S. McGregor, J.K. Shultis, A.S.M.S. Ahmed, R.E. Ortiz, R.W. Olsen, Proc. SPIE, 6319 (2006) pp. P1-P9.*
•*M.F. Ohmes, MS Thesis, 2006.*

KANSAS STATE UNIVERSITY

Semiconductor Materials And Radiological Technologies

MPFDs with Extended Life

Spectrum	Case	232Th	233U	235U	238U	Max. rel. deviation (%)
TRIGA	1	85.7	0	2.7	11.6	0.8
TRIGA	2	85.7	N/A	2.7	11.6	Same
TRIGA	3	N/A	N/A	4.8	95.2	4.6
PWR	1	91.8	4.3	0	3.9	3.8
PWR	2	94.7	N/A	5.2	0	5.1
PWR	3	N/A	N/A	7.6	92.4	22.8

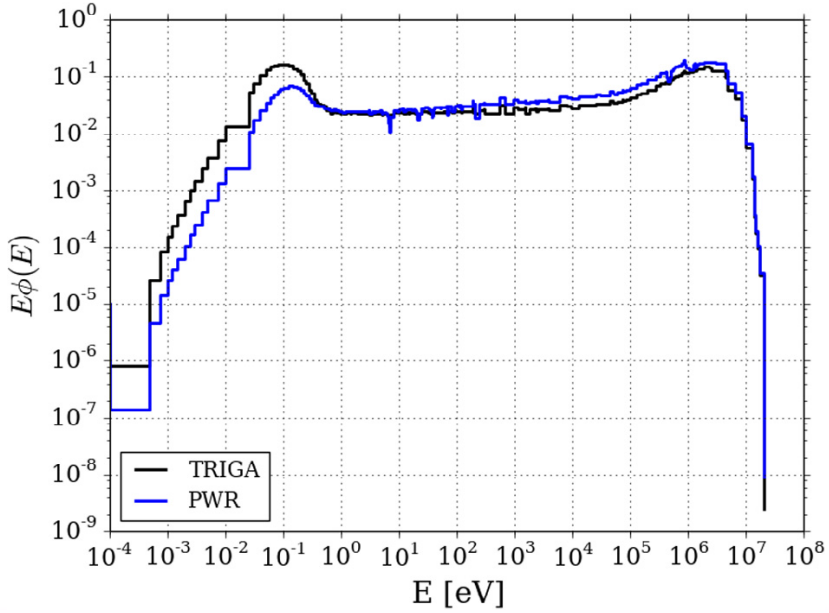

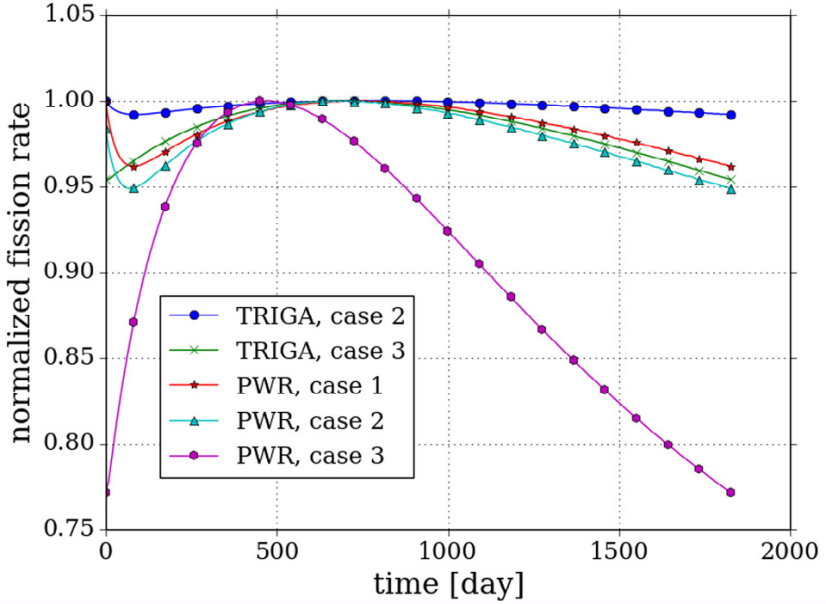

M.A. Reichenberger , T.C. Unruh, P.B. Ugorowski, T. Ito, J.A. Roberts, S.R. Stevenson, D.M. Nichols , D.S. McGregor, An. Nucl. Energy. 87 (2016) pp. 318-323.

Multi-Pocket MPFD Design

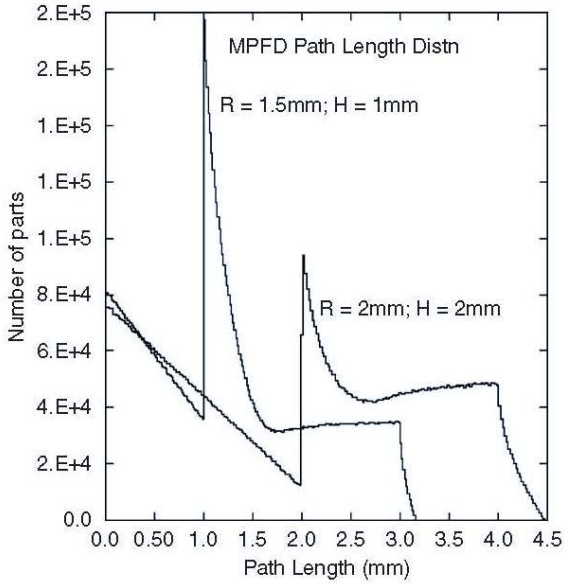

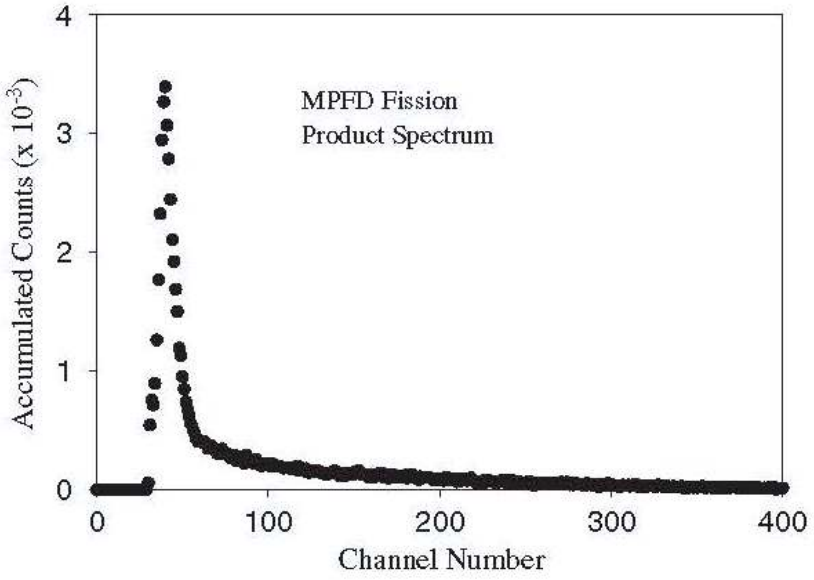

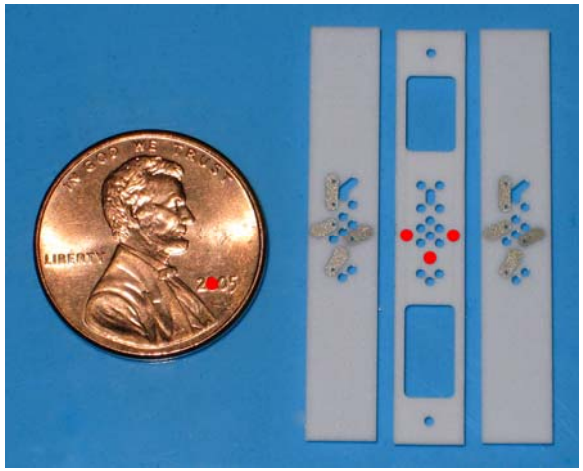

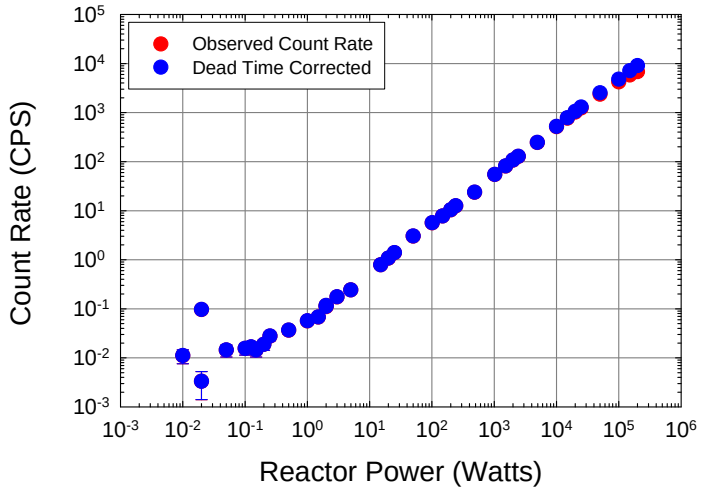

D.S. McGregor , M.F. Ohmes, R.E. Ortiz, A.S.M.S. Ahmed, J.K. Shultis, Nucl. Instrum. and Meth. A 554 (2005) pp. 494-499.

Next Generation MPFDs

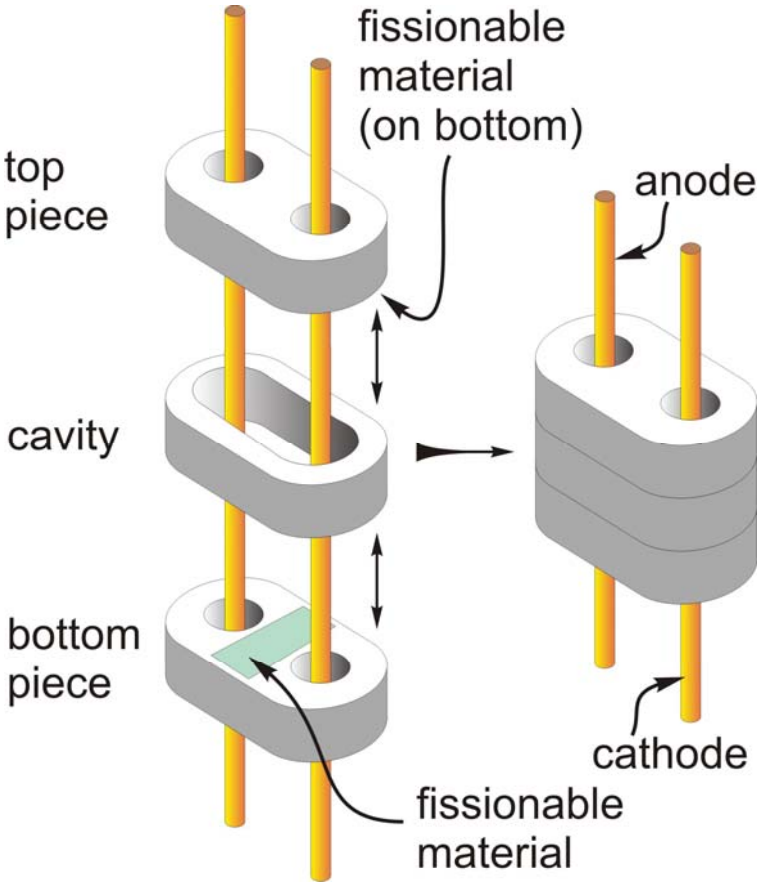

- No bonding adhesives.
- No contact pads.
- No welding of wire bonding.
- Fissionable material not attached to electrode.
- Can be mass produced at low cost.

Micro-Pocket Fission Detectors (MPFD)

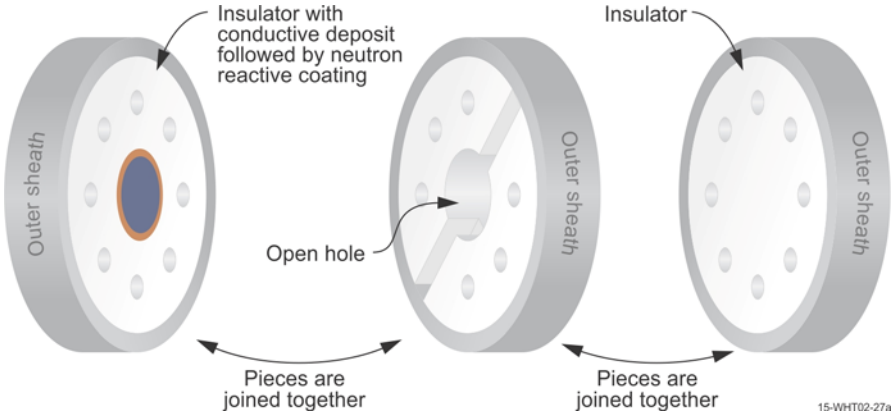

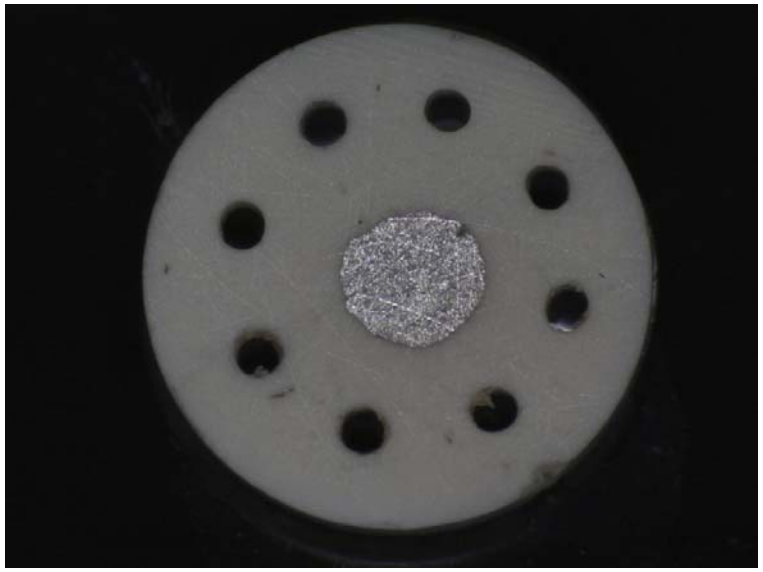

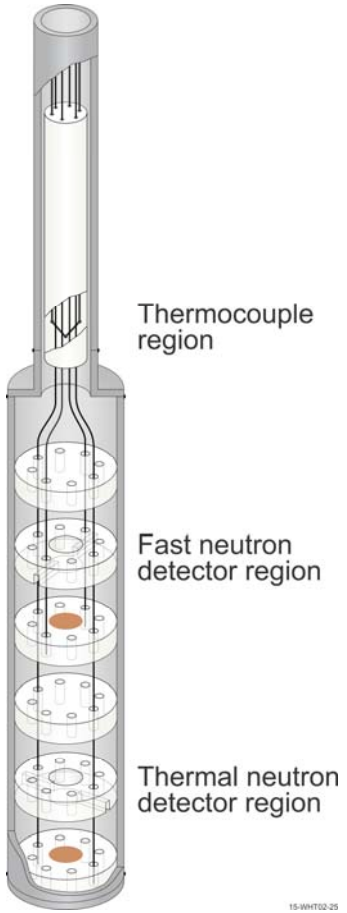

M.A. Reichenberger , T.C. Unruh, P.B. Ugorowski, T. Ito, J.A. Roberts, S.R. Stevenson, D.M. Nichols , D.S. McGregor, An. Nucl. Energy. 87 (2016) pp. 318-323.

Characteristics of tested array:

MPFD Node	Uranium Mass (µg)
1 (top of array)	0.533 ± 0.023
2	0.630 ± 0.026
3	0.548 ± 0.025
4 (bottom of array)	0.619 ± 0.014

Pressure: 30 psi

Gas: Ultra-High Purity Argon

Test facility: Flux wire port

For 250 kWth:

Flux: ~1E13 (thermal) ~1E13 (fast)

Gamma: ~2.5E4 (rad/s)

Location of tested array:

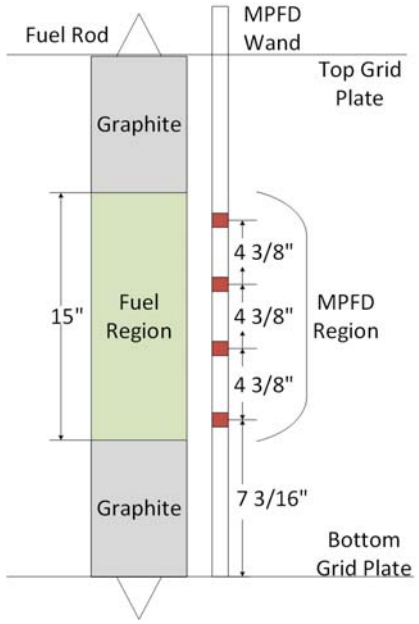

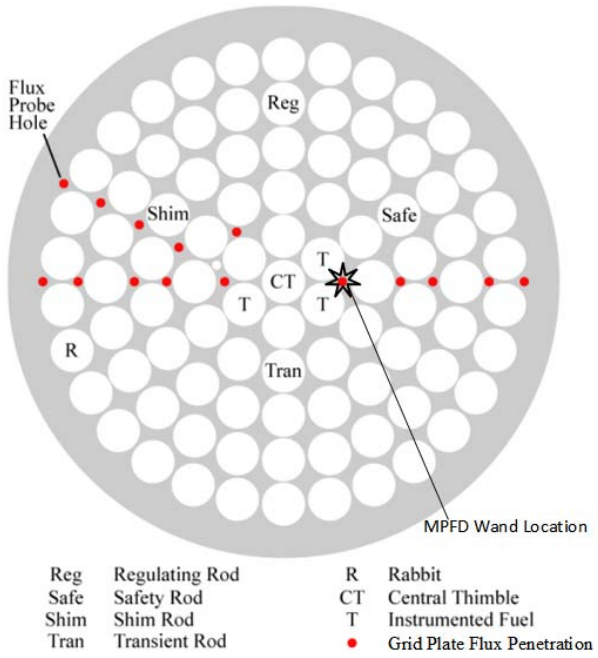

Test Results

Confirmed no cross-talk as evident in the scope trace shown

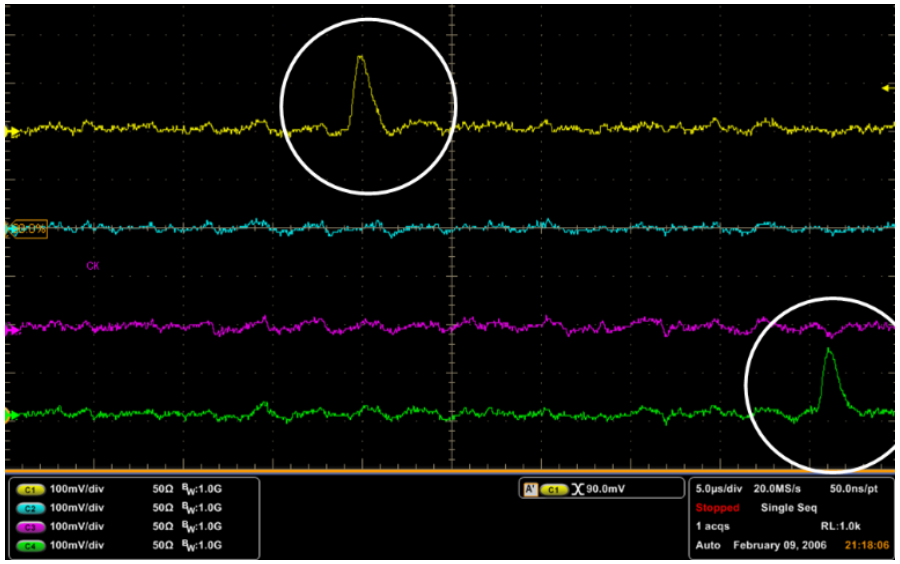

A stability check was conducted with the following conditions.

Power level: 10kWth
Shaping time of 0.5 µs
Gain: 10
Discriminator threshold: 15 of 255
Pulse amplitude: >500mV
Noise amplitude: <100mV

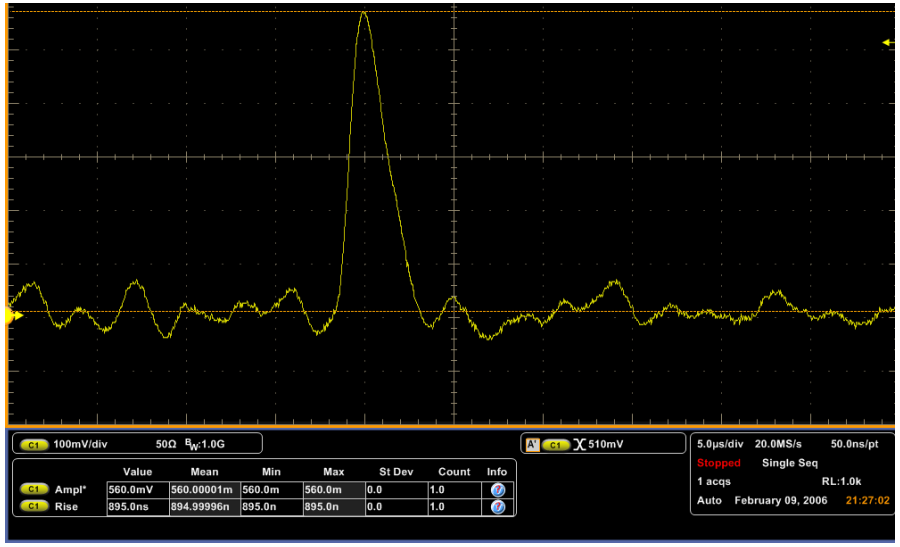

Dynamic Range Tests

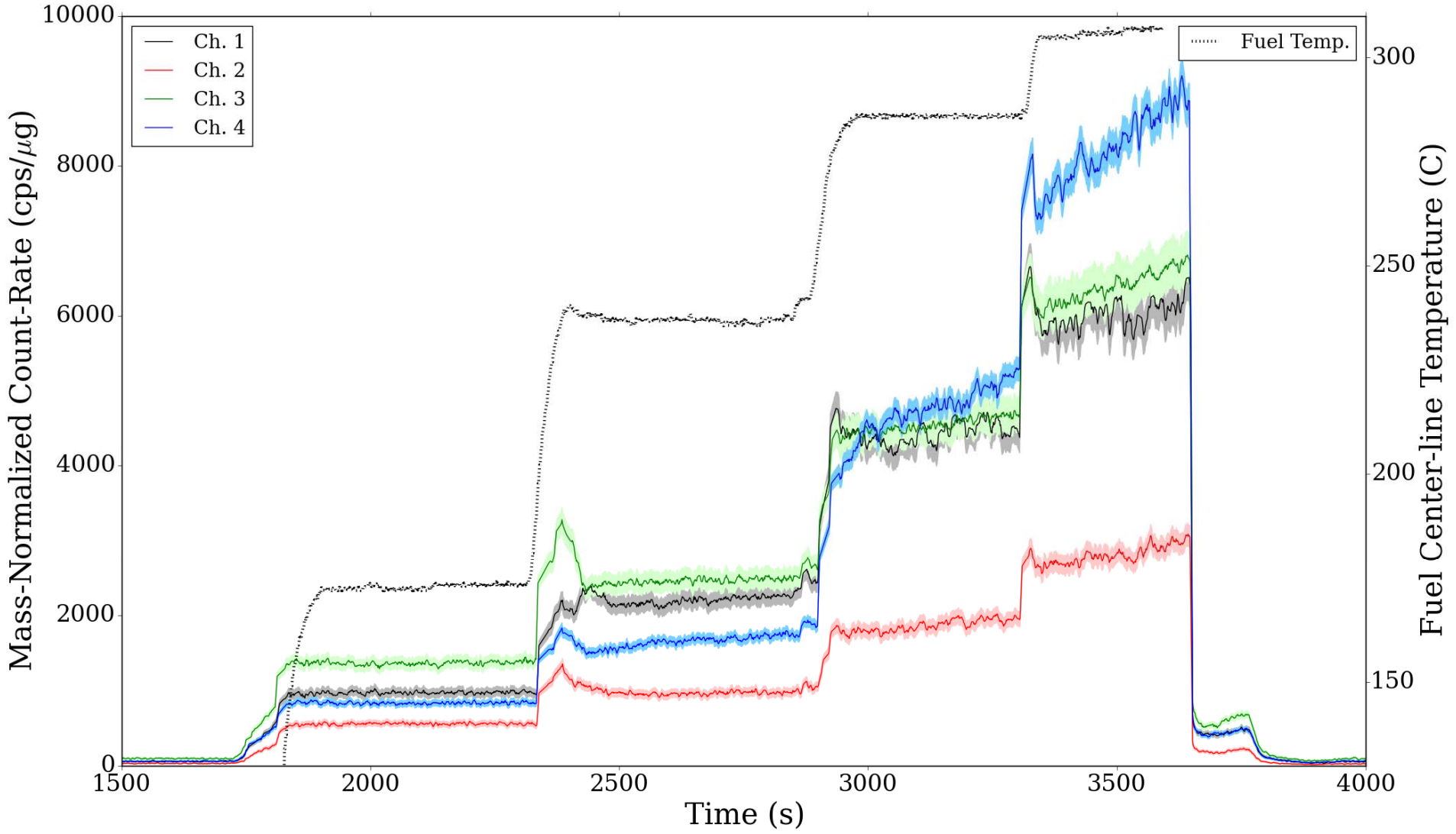

Reactivity Insertion Tests

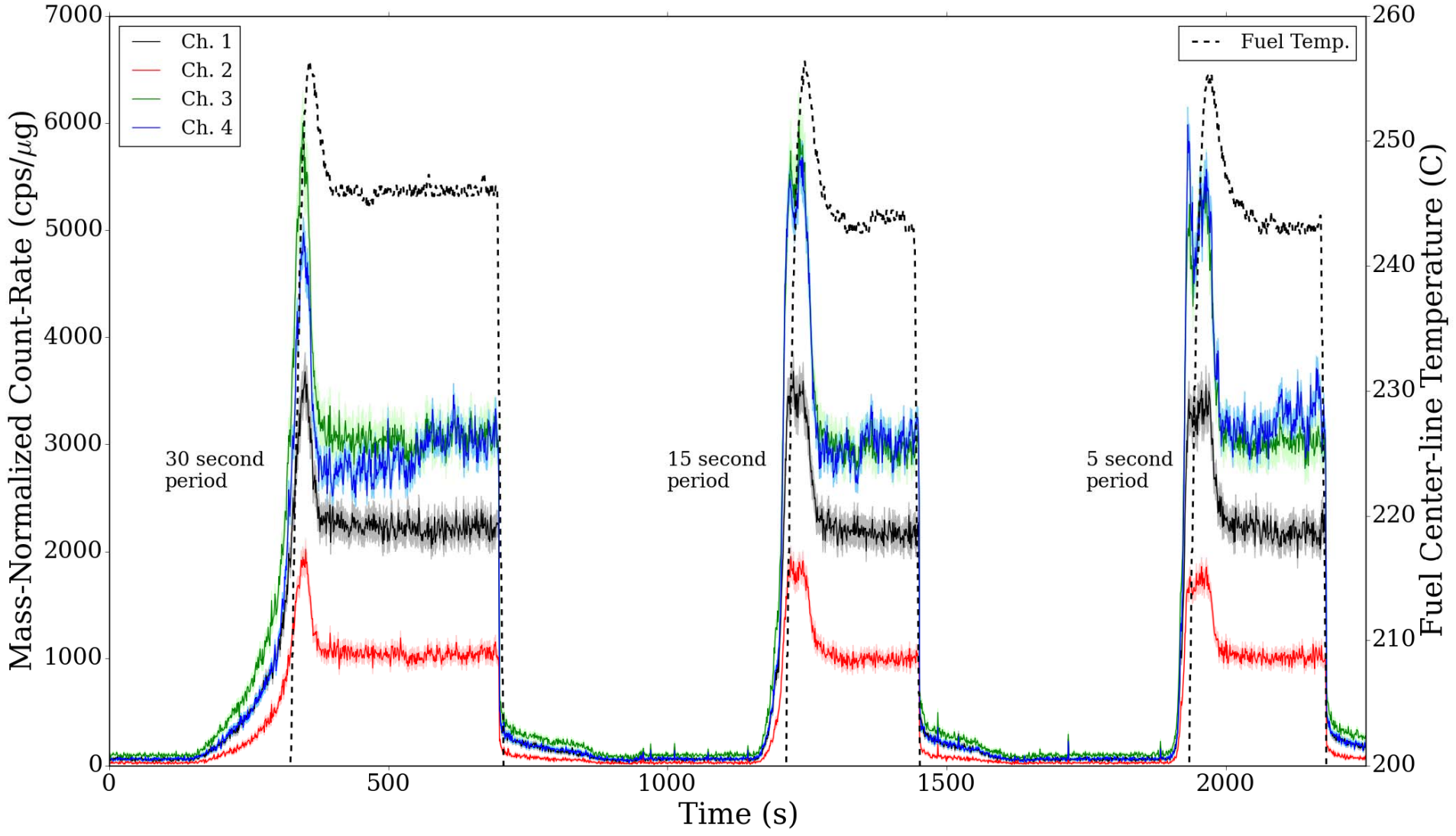

Unique Pair Design

- Parallel wires design
- Disk/Spacer diameter: 4.7 mm
- Pocket volume: ~ 2.0 mm^3

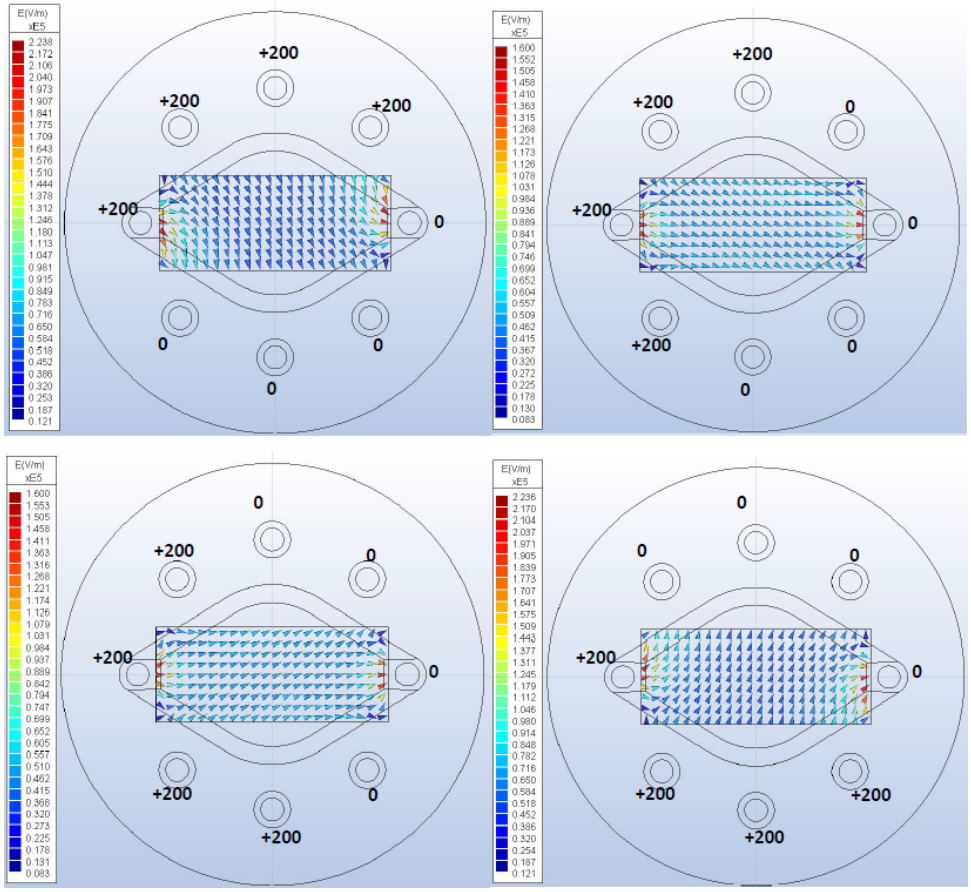

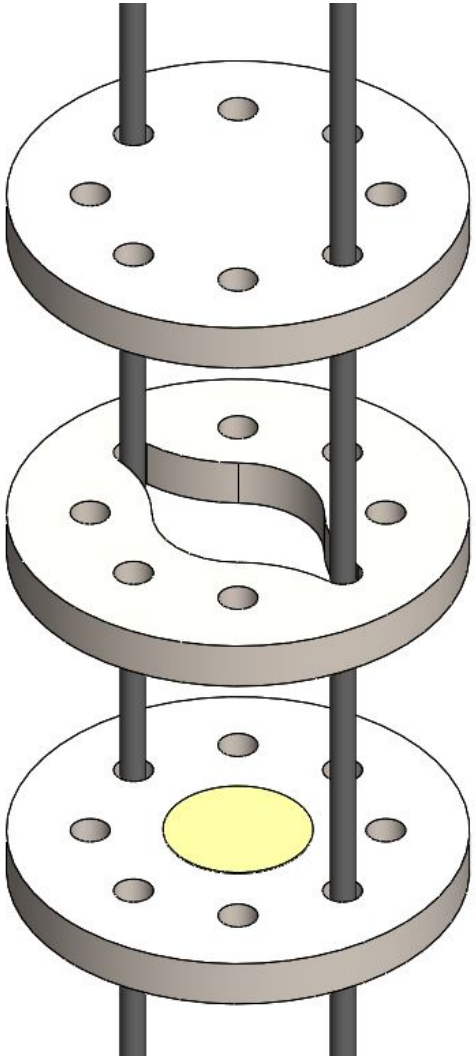

Common Cathode Design (Clover)

- Central shared cathode
- Disk/Spacer diameter: 4.7 mm
- Pocket volume: ~ 0.6 mm^3

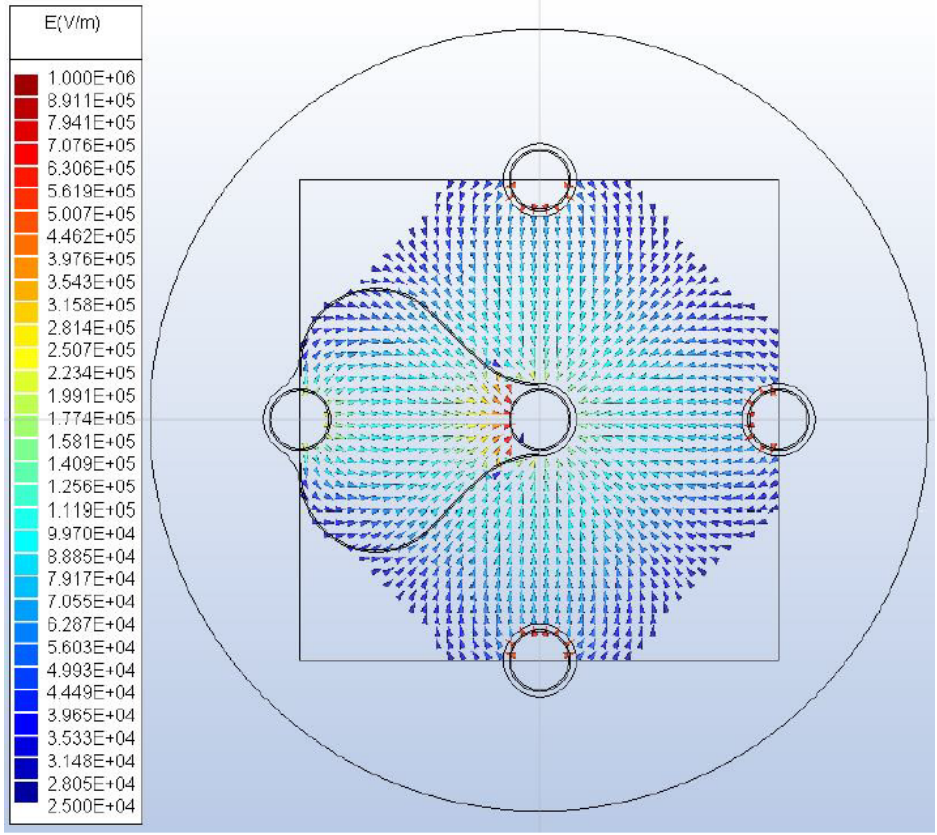

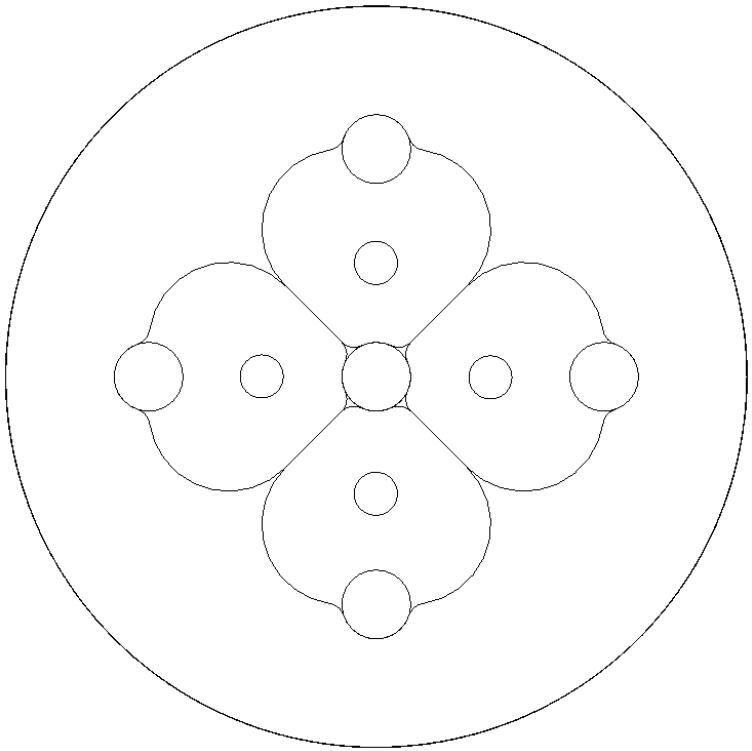

Micro-Pocket Fission Chamber (MPFD)

Micro-Pocket Fission Chamber (MPFD)

- Fission chamber with small form factor
- Real time spatially discrete neutron flux monitor
- Large power bandwidth dependent on fissile coating
- Radiation and temperature resilient materials

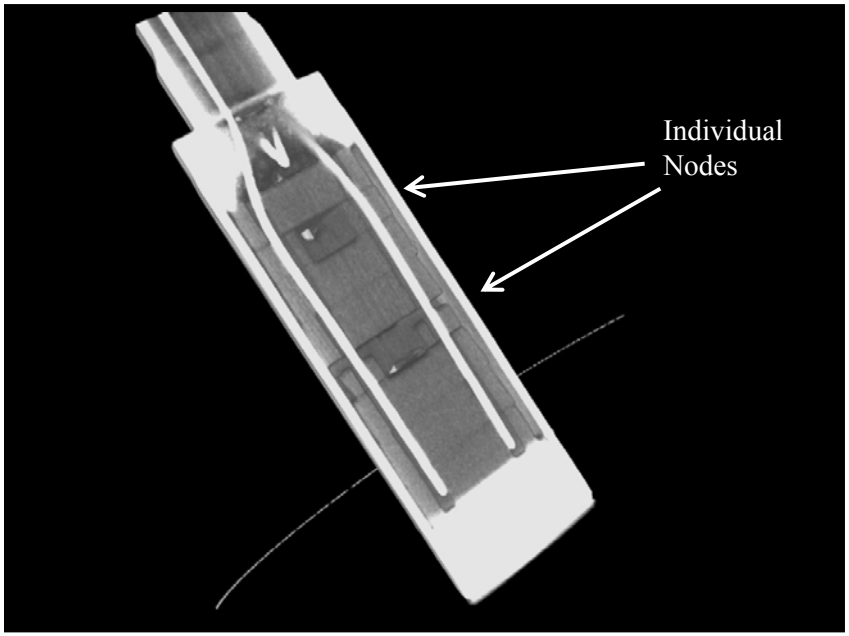

X-ray CT Scan of MPFD
INL-HTTL

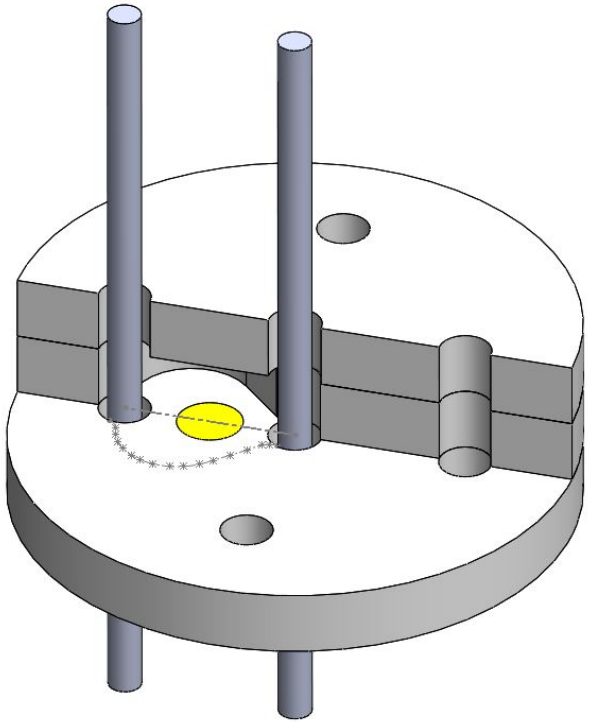

Detector development supports research conducted at:

- *Kansas State University (KSU)*
- *Idaho National Laboratory (INL)*
- *French Alternative Energies and Atomic Energy Commission (CEA)*
- *Massachusetts Institute of Technology (MIT)*

Electrodeposition Process

•Solution based on uranyl nitrate
•Utilizes cyclic voltammetry to deposit fissile coating onto platinum electrode
•Node mass measured with alpha-particle spectrometry

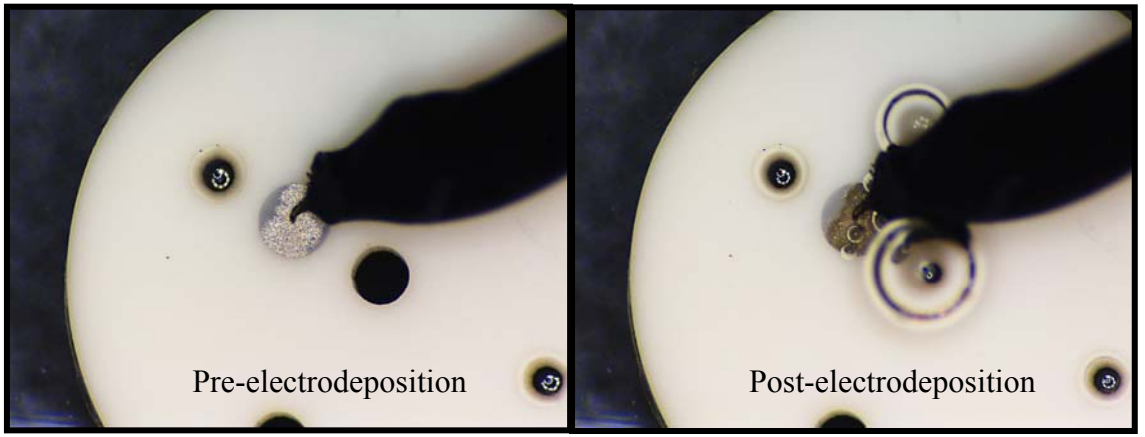

Node Composition

•Loose construction allows for gas to flow into detection chamber
•Two disks
  - One fissile coating
•One spacer

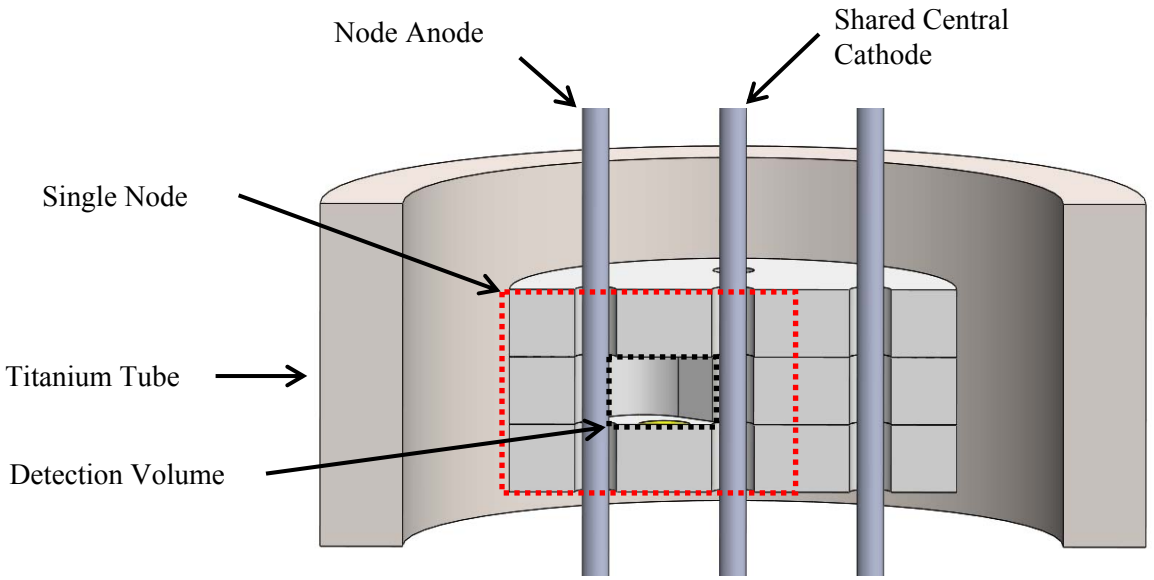

Node Characteristics

•Common cathode design
•Disk/Spacer diameter: 4.7 mm

M.A. Reichenberger, T. Ito, P.B. Ugorowski, B. W. Montag, S.R. Stevenson, D.M. Nichols, D.S. McGregor, Nucl. Instrum. Meth., A812 (2016) pp. 12-16.

Objective of Experiment

•To observe TRIGA pulse tracking using combined signal from all 4 nodes
•Track pulse transient and compare to theoretical pulse shapes
•Test current-mode electronics

Node #	Uranium Mass (ng)	Mass error (ng)	z-distance from core centerline (in)
3 (top)	66.3	1.614	8.4
2	65.2	1.490	11.4
1	65.9	1.503	14.4
0 (bottom)	62.2	1.540	17.4

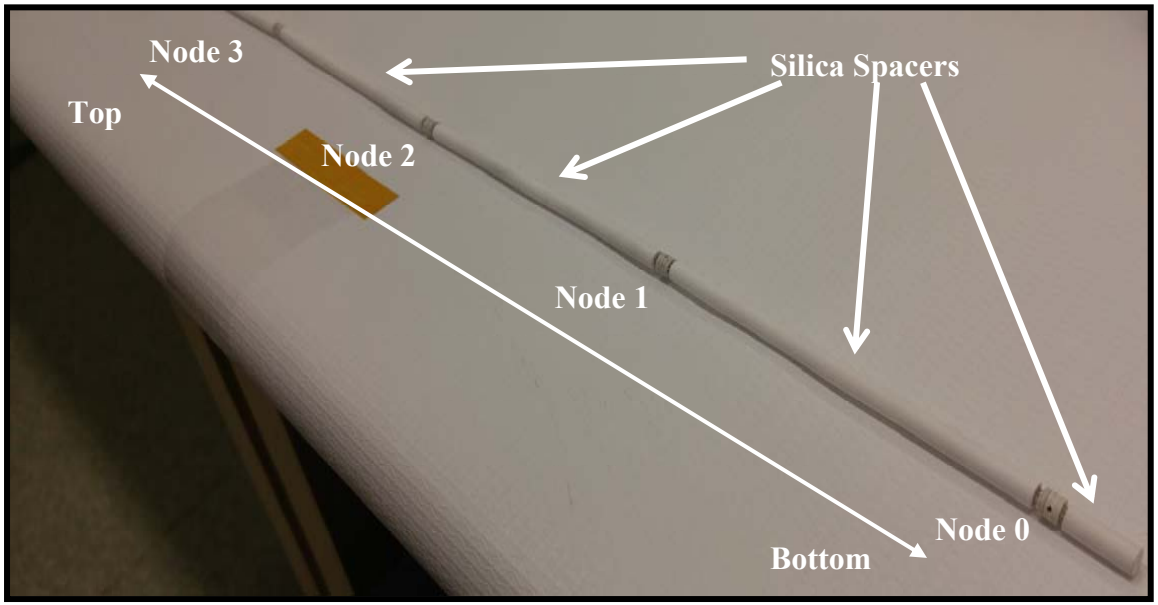

Detector Settings:
•Pressure: 30 psig argon gas
•Current-mode preamplifier

Current mode operation:
•1 cps/10 pC

TRIGA Reactor Pulsing

•Eject most worthy control rod from the core using air pressure

•Large positive reactivity addition to core causes rapid power excursion

•As fuel temperature increases, neutron spectrum hardens and reactor power decreases due to fuel composition

- Cherenkov radiation causes flash of light
- Reactor power increases by a factor of 100 million within fractions of a second

Fuch-Nordheim model used to determine pulse shape

•Based on point reactor kinetics equation (PRKE) with assumptions:

- No delayed neutrons
- Adiabatic fuel heating
- Fuel heat capacity is constant
- Step insertion of reactivity

$$P(t) = \frac{\beta^2 C_p}{2\alpha l'}\left[\frac{\rho_0}{\beta} - 1\right]^2 \operatorname{sech}^2\left(\frac{\frac{\rho_0-\beta}{l'}t}{2}\right)$$

Eq. 1. Power equation

$$t = \frac{\cosh^{-1}\left(\sqrt{2}\right)}{\left[\frac{\rho_0-\beta}{2l'}\right]}$$

Eq. 2. FWHM equation

Constants

TRIGA fuel heat capacity $c_p = 6.648 \cdot 10^{-4}\ \frac{J}{K}$

Fuel temp coefficient $\alpha = 8 \cdot 10^{-5}\ \frac{\Delta k}{K}$

Delayed neutron fraction $\beta = 0.007$

Prompt neutron lifetime $l' = 4.3 \cdot 10^{-5}$ s

Expected Theoretic Pulse Shapes

$2.77 Pulse
- FWHM: 12.2 milliseconds
- Max Power: 1.27 gigawatts
- Pulse peak time: 41.9 milliseconds*

$2.50 Pulse
- FWHM: 14.4 milliseconds
- Max Power: 916 megawatts
- Pulse peak time: 48.9 milliseconds*

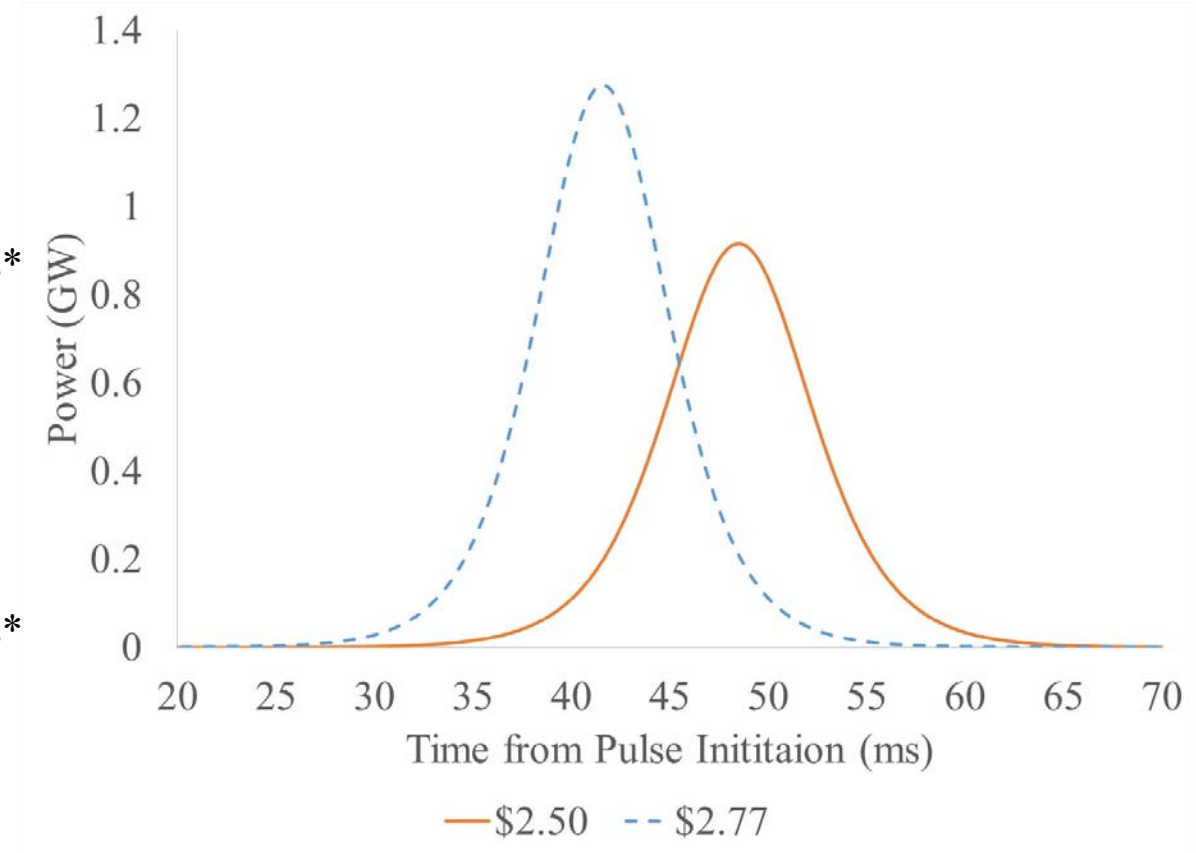

* Pulse peak time can be compared to each pulse by synchronizing the start time to coincide with a power level of 10 W using the Fuchs-Nordheim Model. This is based on the standard procedure of power pulsing at Kansas State University

Experimental Setup – Reactor Deployment

MPFD Wand Positioning

- 4 node array with nodes equally spaced
- Total wand length: 6 feet
- Electrical feedthrough located at the top of the wand, and connected to flexible cable
- Array was located in reflector well
- Thermal flux at 250 kWth expected to be $1.8 \cdot 10^{12} \frac{n}{cm^2 s}$

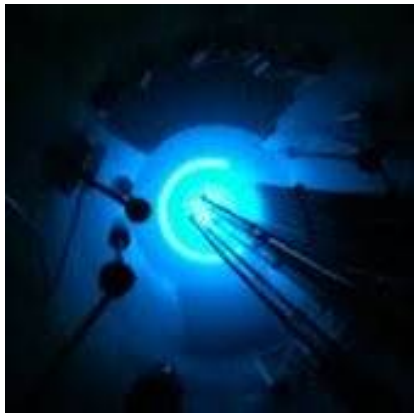

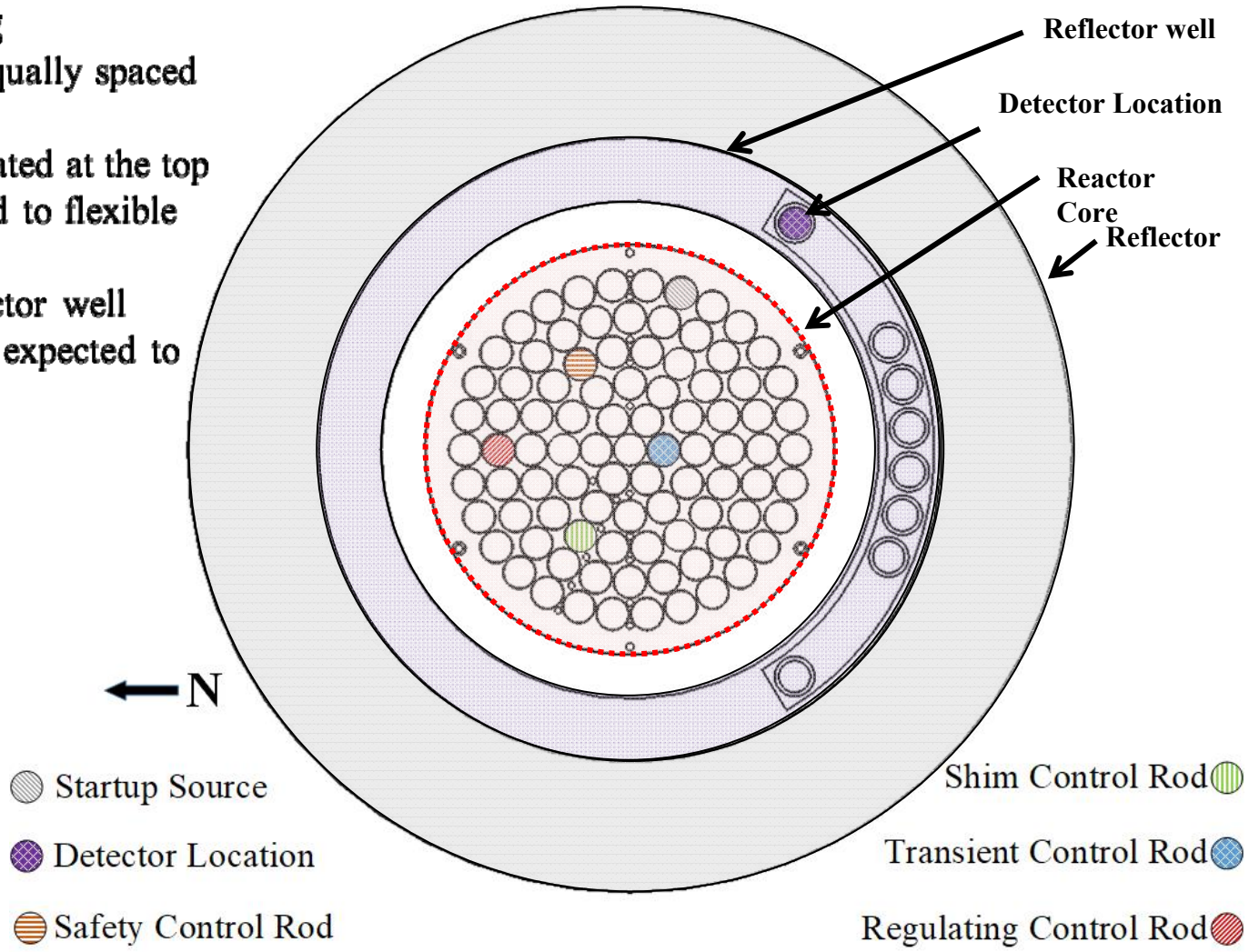

Experimental Results – $2.50 & $2.77 Pulses

$2.50 Pulse Capture Comparison

- 2.0 ms sampling interval
- 100 V applied bias
- Max count rate: 1.14 x 10^6 cps
- FWHM: 16.05 ms

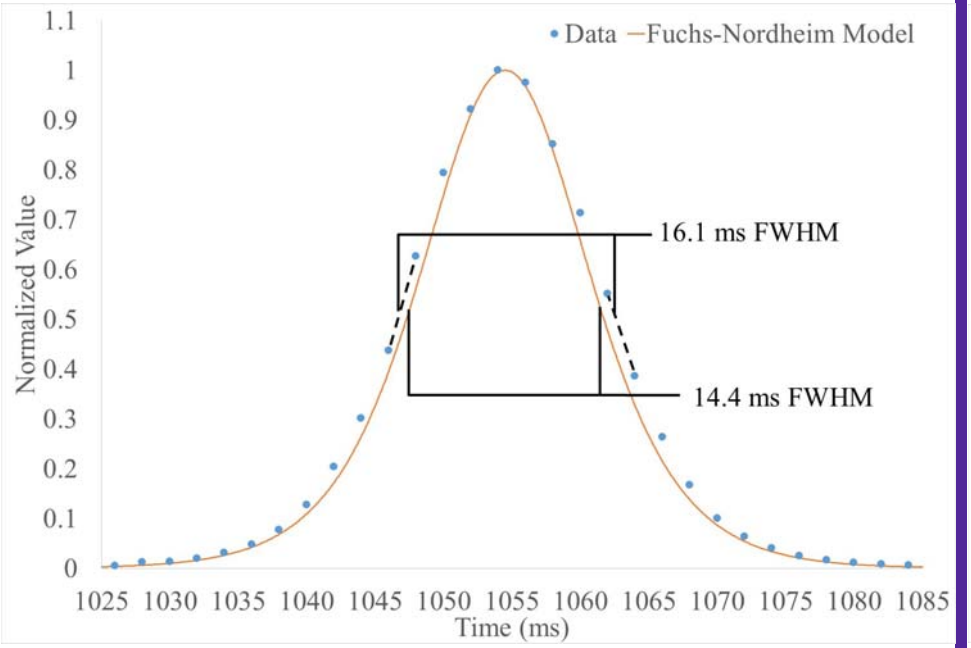

- Theory vs. Experiment FWHM difference is 11.23%

$2.77 Pulse Capture Comparison

- 0.25 ms sampling interval
- 150 V applied bias
- Max count rate: 4.03 x 10^6 cps
- FWHM: 13.25 ms

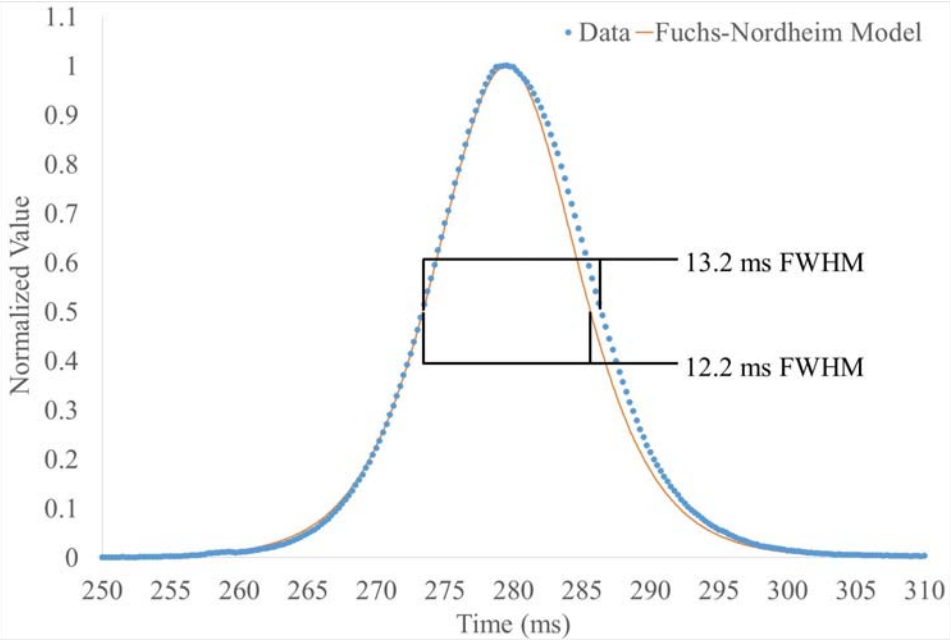

- Theory vs. Experiment FWHM difference is 8.34%

Pulse shape broadening may be a result of summing 4 spatially varying nodes.
(Summing the 4 nodes increases the count rate and allows collection equipment to trigger on pulse rise)

Funding Sponsors

Project Funding provided by:

- *Defense Threat Reduction Agency (DTRA)*
  - DTRA-01-02-B-0067
  - DTRA-01-03-C-0051
  - HDTRA-1-07-1-007
  - HDTRA1-12-C-0002
  - HDTRA1-12-C-0004
  - HDTRA1-14-P-005
  - HDTRA1-14-C-0032
- *Department of Energy (DOE)*
  - DE-FG07-04ID14599
  - NEER DE-00-ID-13919
  - NEER DE- PS07-03ID14540
  - NERI DE-FG07-02SF22611
  - Office of Nuclear Energy/US Department of Energy DE-NE0008305
  - DOE-NE Idaho Operations DE-AC07 05ID14517
  - NNSA DE-FG52-08NA28766
- *National Science Foundation (NSF)*
  - NSF 0412208
- *Office of Naval Research (ONR)*
  - N00014-11-1-0157
  - N00014-13-1-0402

College of Engineering
Mechanical and Nuclear Engineering

Kansas State University
SMART Laboratory

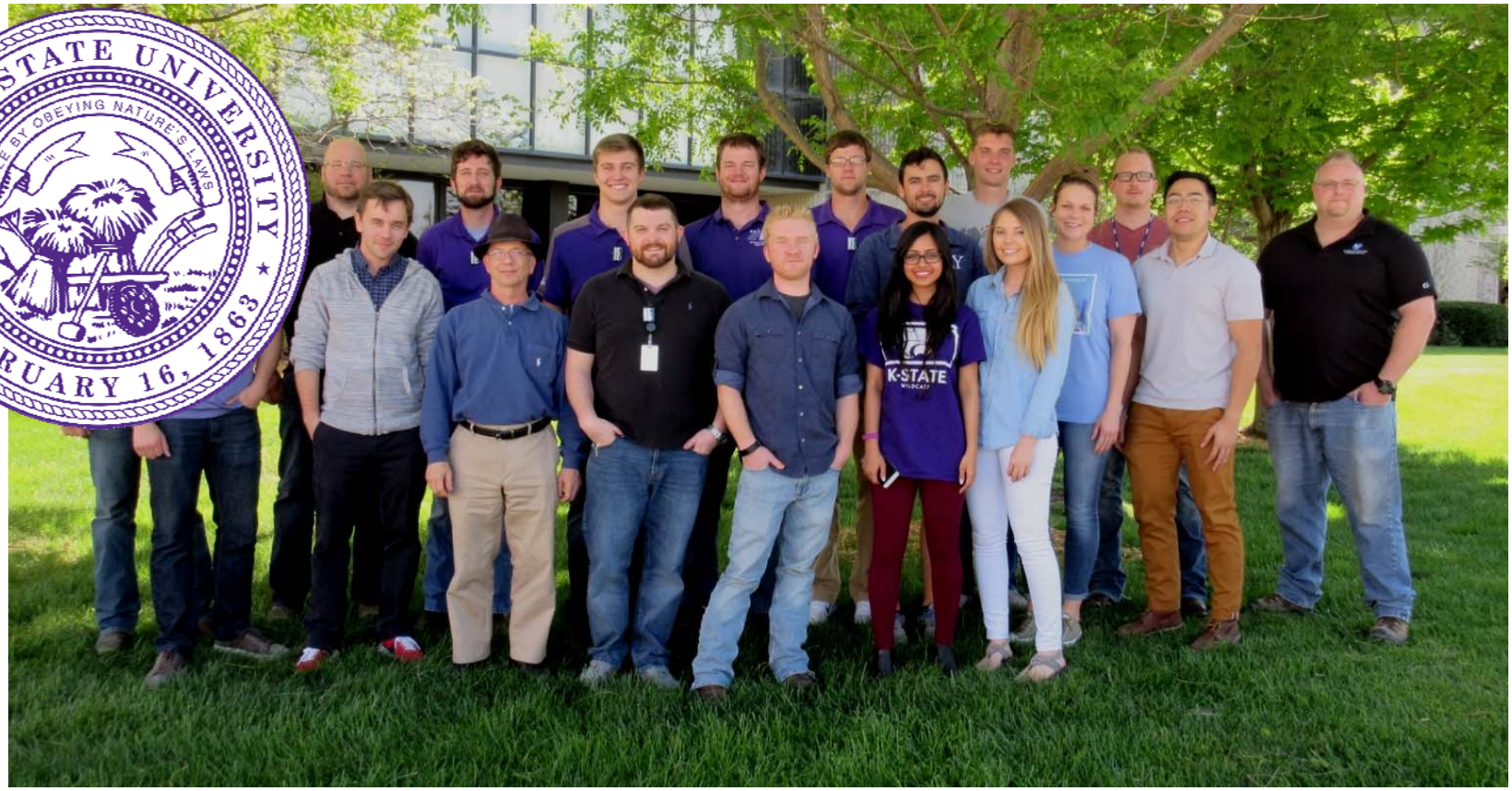

137F Ward Hall
Mechanical and Nuclear Engineering Department
Kansas State University
Manhattan, KS 66531

mcgregor@ksu.edu

http://www.mne.ksu.edu/research/centers/SMARTlab

KANSAS STATE UNIVERSITY

Semiconductor Materials And Radiological Technologies